CHALMERS
UNIVERSITY OF TECHNOLOGY

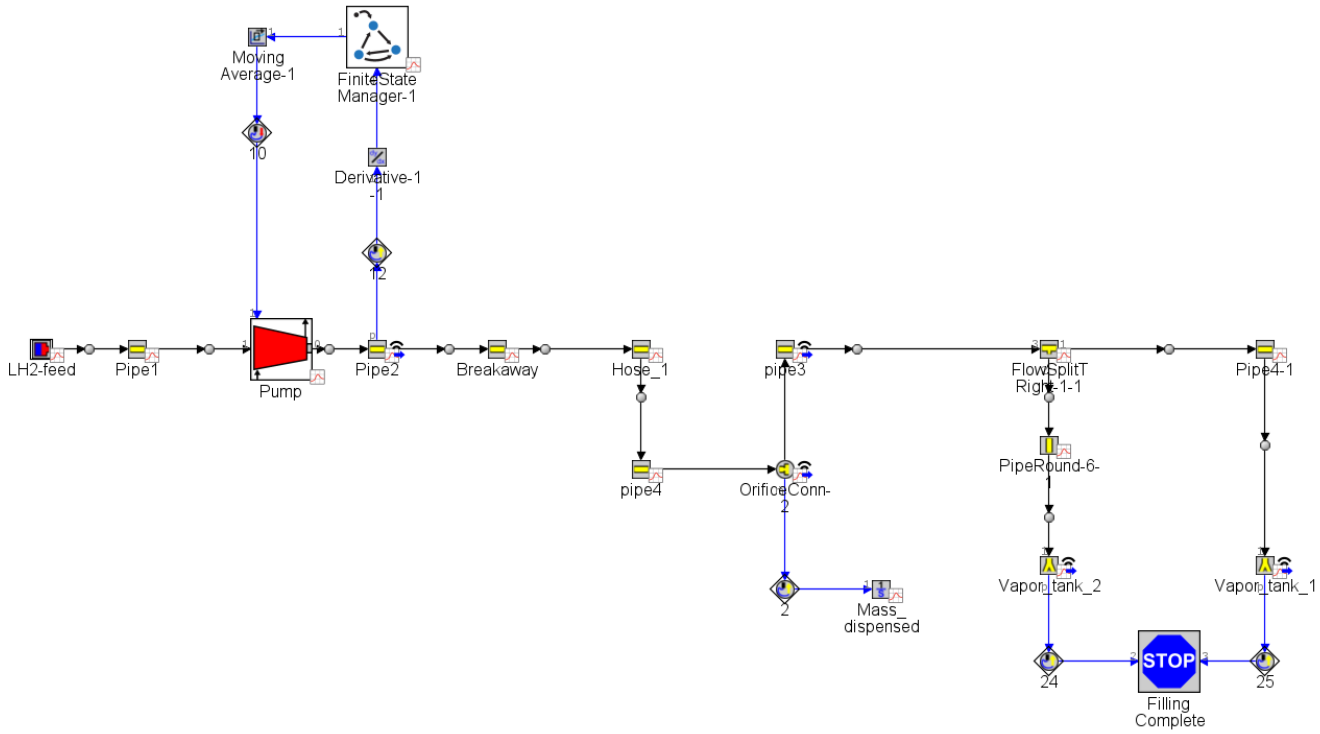

Modelling of subcooled liquid hydrogen fueling system

Master's thesis in Mechanical Engineering

FARZANEH AZIMI
NICCOLO' CANULLO

Department of Mechanics and Maritime Sciences

CHALMERS UNIVERSITY OF TECHNOLOGY
Gothenburg, Sweden 2026
www.chalmers.se

Master's thesis 2026

Modelling of subcooled Liquid Hydrogen Refueling System

FARZANEH AZIMI, NICCOLO' CANULLO

CHALMERS
UNIVERSITY OF TECHNOLOGY

Department of Mechanics and Maritime Sciences
Fluid Dynamics
TechForH2
Chalmers University of Technology
Gothenburg, Sweden 2026

Modeling of subcooled Liquid Hydrogen Refueling System

NICCOLO CANULLO'
FARZANEH AZIMI

Supervisor: Gustavo Hindi, Volvo trucks
Examiner: Tomas Grönstedt, Department of Mechanics and Maritime Sciences Fluid Dynamics

Master's Thesis 2026
Department of Mechanics and Maritime Sciences
Fluid Dynamics
TechForH2
Chalmers University of Technology
SE-412 96 Gothenburg
Telephone +46 31 772 1000

Cover: One-Dimensional model of Subcooled Liquid Hydrogen Refueling

Typeset in LaTeX
Printed by Chalmers Reproservice
Gothenburg, Sweden 2026

Modelling of subcooled Liquid Hydrogen Refuelling System
FARZANEH AZIMI
NICCOLO CANULLO
Department of Mechanics and Maritime Sciences
Chalmers University of Technology

Abstract

In order to reduce greenhouse gas emissions in the transportation sector, hydrogen is recognized as a promising fuel alternative, particularly for heavy-duty applications where high energy density is required. Subcooled Liquid Hydrogen (sLH2) is of significant importance due to its superior volumetric energy density and higher mass flow rates, outperforming compressed gaseous hydrogen in terms of rapid and high-capacity refuelling. However, challenges related to refuelling duration and storage capacity must be addressed, especially for heavy-duty vehicles requiring large hydrogen quantities. The initial thermodynamic state of the tank and the State of Charge (SoC) at the time of refuelling significantly dictate the maximum mass of hydrogen that can be effectively stored. The objectives of this thesis are to investigate the sLH2 refuelling system to determine the optimal initial conditions for truck tanks and to identify other critical factors influencing the process. Furthermore, the thermal behavior and pressure dynamics of sLH2 during refuelling and storage are complex phenomena that require advanced numerical modelling for system optimization. Given its capability for 1D CFD and its reliability in vehicle system simulation, GT-SUITE was selected as the modelling tool to allow for rapid and accurate analysis. Initially, the refuelling system was modeled and validated. Subsequently, the defuelling process was modeled to determine the initial thermodynamic of the tank and SoC. Finally, a sensitivity analysis was performed to identify the key parameters affecting the refuelling system's performance. The results indicate that since the tank pressure must be maintained at a specific level due to fuel cell demand, the initial tank temperature has a predominant impact on the final hydrogen storage mass and the overall system efficiency.

Keywords: SubCooled Liquid Hydrogen, GT-SUITE, Refuelling, Defueling, State of Charge, Heavy Duty Truck.

Acknowledgements

First and foremost, we would like to express our most sincere gratitude to our industrial supervisors: Felix Haberl and Gustavo Hindi at Volvo Trucks, as well as Thomas Walander and Gerhard Kopplin at Manntek. Your invaluable feedback, continuous guidance, and unwavering support throughout this thesis project played a pivotal role in the advancement of this research. Working closely with you was not only an incredibly rewarding learning experience but also left us with wonderful, unforgettable memories.

A big thank you to our Examiner Tomas Grönstedt from Chalmers, for their guidance with both thesis work and report writing.

Valuable support from Gamma Technologies and by GT expert, Doug Petrik, who helped us in providing information, technical details regarding modelling in GT SUITE, which was crucial to obtain reliable results.

Completing our Master's thesis journey within the Volvo Group, Manntek, and Chalmers University of Technology has been an exciting and enriching experience, and we are deeply grateful for this opportunity.

Finally, we would like to thank our families for their love and patience. In particular, I (Farzaneh) wish to express my deepest heartfelt gratitude to my beloved family: to my son, Abtin, who spent days and nights without his mom and showed patience far beyond his years, and to my husband, Ali, without whose unwavering support throughout this entire journey, accomplishing this thesis would have been impossible.

Farzaneh Azimi and Niccolo' Canullo, Gothenburg, 2026

List of Acronyms

Below is the list of acronyms that have been used throughout this thesis, listed in alphabetical order:

CF	Carbon fibre (structural composite overwrap of the shell)
CFD	Computational Fluid Dynamics
CFL	Courant–Friedrichs–Lewy (criterion)
CGH2	Compressed Gaseous Hydrogen
DAE	Differential–Algebraic Equation
EOS	Equation of State
FWD	Forward Discharge Coefficient
GA	Genetic Algorithm
HDV	Heavy-Duty Vehicle
HEM	Homogeneous Equilibrium Model
HRS	Hydrogen Refuelling Station
IAE	Integral of the Absolute (pressure) Error
iHEX	Internal heat exchanger
ISO	International Organization for Standardization
LH2	Liquid Hydrogen
MLI	Multi-Layer Insulation
NIST	National Institute of Standards and Technology
NSGA	Non-dominated Sorting Genetic Algorithm
oHEX	Outer heat exchanger
PCV	Pressure Control Valve
PI	Proportional–Integral (controller)
PID	Proportional–Integral–Derivative (controller)
REFPROP	Reference Fluid Thermodynamic and Transport Properties
sLH2	Subcooled Liquid Hydrogen
SoC	State of Charge
SST	Shear Stress Transport
UDF	User-Defined Function
VD-MLI	Variable-Density Multi-Layer Insulation
VOF	Volume of Fluid

Nomenclature

Below is the nomenclature of the symbols used throughout this thesis.

Latin Symbols

A_{ref}	Reference (orifice) area	m^2
A_s	Heat transfer surface area	m^2
a	Specific Helmholtz free energy	J/kg
C_d	Discharge coefficient	–
C_f	Fanning friction factor	–
c	Local speed of sound	m/s
D	Equivalent diameter	m
e	Specific internal energy	J/kg
H	Total specific enthalpy	J/kg
h	Fluid-side heat transfer coefficient	$W/(m^2 \cdot K)$
K_p	Pressure loss coefficient	–
L	Length	m
m	Mass of hydrogen in the tank	kg
$\dot{m}$	Mass flow rate	kg/s
m_{H_2}	Current hydrogen mass in the tank	kg
m_{max}	Maximum storable hydrogen mass	kg
p	Pressure	bar
p_{min}	Minimum operative pressure	bar
p_{vent}	Venting pressure	bar
$\dot{Q}_{amb}$	Ambient heat leak through the insulation	W

R	Specific gas constant of hydrogen	J/(kg·K)
T	Temperature	K
T_c	Critical temperature	K
T_{fluid}	Fluid temperature	K
T_{wall}	Wall temperature	K
t	Time	s
U	Internal energy	J
u	Flow velocity	m/s
V	Tank volume	m^3
x	Coordinate along the flow direction	m

Greek Symbols

α_o	Ideal-gas contribution to the Helmholtz energy	–
α_r	Residual contribution to the Helmholtz energy	–
δ	Reduced density (ρ/ρ_c)	–
Δp	Pressure drop	bar
Δt	Time step	s
Δx	Discretization length	m
ρ	Density	kg/m^3
ρ_c	Critical density	kg/m^3
τ	Inverse reduced temperature (T_c/T)	–

Subscripts

amb	Ambient
c	Critical
in	Inlet
out	Outlet
max	Maximum
ref	Reference

s	Surface
$wall$	Wall

Contents

List of Figures

List of Tables

1
Introduction

This chapter introduces the application of liquid hydrogen as a fuel for heavy-duty vehicles. It begins by discussing the increasing interest in hydrogen as a sustainable energy carrier and the factors that have motivated its development for transportation applications. The fundamental physical and thermodynamic properties of hydrogen are then presented to establish the necessary background for understanding its behavior. Furthermore, a brief historical overview of hydrogen utilization as a fuel is provided, followed by a description of the different phases of hydrogen and their significance in storage, distribution, and vehicle fuelling systems.

1.1 Background

Reducing greenhouse gas emissions has always been a key priority of the European Union's environmental policy. Transport is responsible for around 31% of total greenhouse gas emissions in the European Union (EU-27) in 2023 [1]. On the other hand, road transport is the largest contributor to greenhouse gas emissions in the transport sector, accounting for around 72.9% of emissions from this sector and 22.6% of total EU greenhouse gas emissions.

Heavy Duty Vehicles (HDVs) are responsible for around one quarter of these emission. In this regard, the European Union introduced CO_2 emission standards for heavy-duty vehicles for the first time in the form of Regulation (EU) 2019/1242 [1]. The law sets targets for reducing carbon dioxide emissions from trucks, and its most recent revision in 2024 set more stringent targets, including a 45% reduction in emissions by 2030, 65% by 2035, and 90% by 2040. The regulations are designed to increase the share of zero-emission vehicles and accelerate the decarbonization of the road transport sector.

One of the solutions proposed for this issue is the use of electric trucks. However, challenges such as long battery charging times, reduced transportable load capacity due to larger batteries required for extended range, the limited driving range of electric trucks, and the high environmental impact of battery production have led truck manufacturers to introduce hydrogen-powered trucks as an innovative addition to

their product portfolios [2].

1.1.1 Physical and Thermodynamic Properties of Hydrogen

Hydrogen is the lightest and the most abundant element in the universe. In terms of energy perspective, hydrogen has one of the highest gravimetric energy densities of any fuel, approximately 120 MJ/kg, which is nearly three times that of conventional diesel fuel.

The key thermodynamic properties of hydrogen that are relevant to this study are summarized in Table 1.1.

Table 1.1: Key thermodynamic properties of hydrogen [3]

Property	**Value**	**Unit**
Molecular weight	2.016	g/mol
Boiling point (at 1 atm)	20.3	K
Critical temperature	33.2	K
Critical pressure	12.96	bar
Triple point temperature	13.8	K
Triple point pressure	0.072	bar
Gravimetric energy density	120	MJ/kg
Volumetric energy density (liquid)	8.5	MJ/L
Density of liquid H_2 (at boiling point)	70.8	kg/m^3
Density of gaseous H_2 (at 1 atm, 300 K)	0.082	kg/m^3

As shown in Table 1.1, the boiling point of hydrogen at atmospheric pressure is only 20.3 K, which means that storing hydrogen in liquid form requires maintaining extremely low temperatures. This places strict demands on the insulation and thermal management of any liquid hydrogen storage system.

1.1.2 History of using hydrogen as a fuel

Utilizing of hydrogen as a fuel dates back to the 19th century, when water was electrolyzed to produce hydrogen for French military airships. Combustion engines were later designed to run on fuels containing hydrogen gas.

In 1988, the Tupolev Tu-155 became the world's first manned aircraft to fly on liquid hydrogen fuel, based on direct combustion [4], and in 2009, the Antares DLR-H2 became the first manned aircraft to fly entirely on fuel cell power, and in recent years, companies such as ZeroAvia and Universal Hydrogen have taken the final steps towards commercializing this clean technology [4].

During the 20th century, the industry's focus transitioned toward fuel cells, which convert hydrogen into electricity through a chemical process without combustion. This innovation prompted General Motors to develop the GM Electrovan, recognized as the world's first recorded fuel cell vehicle [5].

In 2022, the first fleet of hydrogen fuel cell–powered trains was introduced in Germany [6]. Given the significant CO_2 emissions from heavy industry and transportation, hydrogen is now receiving increased attention as a fuel for heavy-duty trucks.

1.1.3 Liquid Hydrogen or Compressed Gas Hydrogen

Hydrogen can be used as a fuel for heavy-duty vehicles in two forms: Compressed Gaseous Hydrogen CGH2 at 700 bar, and Liquid Hydrogen LH2. Although compressed gas is currently the more common technology, liquid hydrogen offers several advantages that make it more attractive. One major advantage of liquid hydrogen is its higher volumetric energy density of 8 MJ/L, compared to 5.6 MJ/L for LH2. This allows trucks to achieve a longer driving range without increasing the size or weight of the fuel tank. In addition to energy density, liquid hydrogen has a storage density of 62 kg/m^3, whereas gaseous hydrogen only reaches about 40 kg/m^3 [7].

Liquid hydrogen can exist in two distinct states depending on the temperature and pressure relative to the saturation curve. When hydrogen is at the saturation temperature corresponding to a given pressure, i.e., on the verge of boiling, it is called saturated liquid hydrogen.

In contrast, subcooled liquid hydrogen (sLH2) is liquid hydrogen that has been cooled to a temperature below the saturation temperature at the higher pressure and therefore remains completely in the liquid phase.

Figure 1.1 shows the different phases of hydrogen on a pressure–temperature diagram. Because the storage tank is a rigid vessel, its volume remains constant. Therefore, thermodynamic state changes associated with heating or cooling at a fixed mass follow constant-volume (isochoric) lines, which are represented by the dashed lines in the figure.

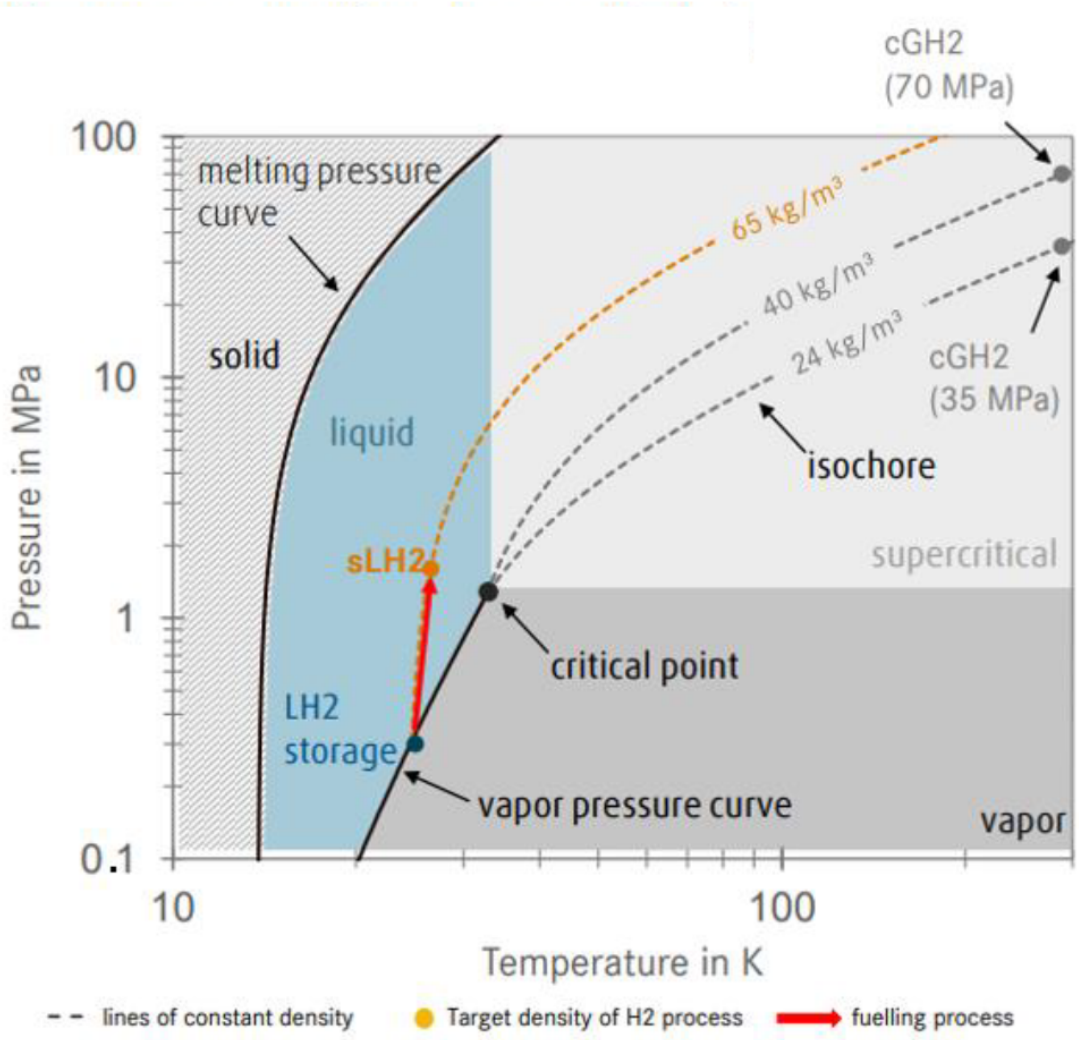

Figure 1.1: Pressure-Temperature diagram of hydrogen [8]

As a result it requires tanks that are cheaper, lighter, and simpler compared to CGH2 [7]. Its fuel delivery system is less complex, completely eliminating the need for the high-pressure compressors used in gaseous hydrogen systems. Furthermore, the refuelling time for liquid hydrogen is approximately half that of CGH2.

1.2 Thesis Structure

This thesis is organized as follows. Chapter 2 provides the theoretical background on the thermodynamic properties of hydrogen and the governing equations used in the 1D model. Chapter 3 describes the validation methodology, model setup. Chapter 4 presents the system description, simulation assumption, initial and boundary con-

ditions, challenges and mitigation strategy for the refuelling validation, defuelling validation, defuelling, and refuelling scenarios. Chapter 5 discusses the result of the simulations. Finally, Chapter 6 summarizes the main conclusions.

2
Theory

In this chapter, properties of hydrogen and governing equations which used in this study will be represented. In order to achieve a one-dimensional model for a sub-cooled liquid hydrogen fuelling system for heavy vehicles, the software GT-SUITE has been used. It is an engineering software which is developed by Gamma Technology and has capabilities and libraries that cover a wide range of applications and industries. This software is very popular and useful for the automotive industry.

2.1 Literature Review

2.1.1 Thermodynamic modelling of Liquid Hydrogen Tanks

The thermodynamic behavior of liquid hydrogen tanks during filling, storage, and discharge has been studied extensively through numerical modelling.

In 2021, Kuroki et al. [9] investigated and simulated the refuelling process of compressed gaseous hydrogen (CGH_2) vehicles, focusing on analyzing the thermal and thermodynamic behavior of hydrogen throughout the entire transfer path, from the station's high-pressure storage tanks (up to 88 MPa) through pipes, control valves, pre-cooling systems, hoses, and nozzles to entering the vehicle tank.

For this purpose, they developed a holistic thermodynamic model based on the simultaneous and transient solution of mass and energy conservation equations, in which the behavior of the gas inside the tank was lumped with one-dimensional wall heat transfer and the behavior of the pressure control valve (PCV) was simulated with an algorithm based on the dichotomy method to apply the standard pressure increase rate (SAE J2601).

Finally, the most important result of this research showed that the developed model is able to predict with very high accuracy the pressure, temperature, and mass flow profiles of hydrogen at any point in the station and at every second of the process, and it was determined that the heating of the gas along the station components (especially the hose and nozzle) has a direct impact on the final temperature of the

vehicle tank, which allows operators to optimize the interaction between the station protocols and the vehicle storage system to increase safety and reduce operating costs.

Wang et al. [10] in 2022, used computational fluid dynamics (CFD) to analyze the thermal and pressure behavior of liquid hydrogen transported in trailer tanks. This study mainly focuses on temperature stratification and the self-pressurization of the stored hydrogen inside the tank.

Abedi et al. [11] have presented a numerical framework for modelling a liquid hydrogen fuelling system in turbofan engines equipped with a thermal management system. This fuelling system is simulated integrally with the operation of the turbofan engine. The coupled heat transfer between the fuelling system and the main engine was a modelling challenge, because in conventional engines the fuel flow is modeled independently, whereas in this study, heat transfer occurs between the air passing through the engine and the hydrogen fuel before the hydrogen is injected into the combustion chamber, which changes the thermodynamic modelling of the entire engine. They were able to directly couple the equations governing the fuel thermal management system to the main engine equations and achieve a stable and fast solution for calculations under all turbofan operating conditions.

Adler and Martins investigated and optimized liquid hydrogen (LH2) tanks for aerospace and transportation applications. Their main focus was on simultaneously reducing the boil-off phenomenon and the total mass of the tank; they developed an analytical model called HyTank, which is specifically designed for fast numerical optimization. Their developed model could perform the simulation and optimization calculations of the tank up to 2000 times faster than traditional and conventional numerical methods, which allows designers to optimize the structure of liquid hydrogen tanks in the early design phases of transportation systems with very high speed and accuracy [12].

2.1.2 Flash Vaporization and Thermal Stratification During Filling

The difference between two types of liquid hydrogen becomes important during the refuelling process. When saturated liquid hydrogen enters the tank, even a small pressure drop or the introduction of a small amount of heat can cause flash vaporization, i.e., part of the liquid vaporizes rapidly and uncontrollably. This phenomenon causes pressure surges and makes the refuelling process difficult to control. In contrast, using subcooled hydrogen at higher pressures of about 20 to 25 bar effectively eliminates this risk and allows for higher flow rates without the problems of two-phase flow at the tank inlet, but it should be noted that flash

vaporization still occurs with this type of liquid hydrogen.

Li et al. in 2025 [13] investigated and simulated the refuelling process of liquid hydrogen (LH2) storage tanks. They analyzed the internal flow and investigated the mass and heat transfer, flash evaporation, and condensation of hydrogen in a vertical tank.

With the aim of providing a theory for the design of liquid hydrogen flow measurement devices, they used the computational fluid dynamics (CFD) method in ANSYS Fluent software along with the volume of fluid (VOF) model to trace the phase boundary and the $k - \epsilon$ turbulence model. By coding user-defined functions (UDF), they upgraded the traditional phase-change model *Lee Model* to accurately predict the flash process and validated it with NASA experimental data.

Finally, the most important result of this research showed that the tank refuelling process includes three distinct stages: the flash phase, the evaporation-condensation phase, and the gas condensation phase of the tank's upper space. It was determined that increasing the inlet mass flow rate causes the collapse of the gas thermal stratification and accelerates the increase in tank pressure, while decreasing the inlet liquid hydrogen temperature (increasing the subcooling degree) due to more severe condensation creates a greater initial pressure drop and increases the efficiency and final filling rate of the tank from 89% to 93%.

In 2019, Melideo et al. [14] investigated and simulated the rapid refuelling process of hydrogen tanks and their main focus on analyzing the phenomenon of thermal stratification, the inhomogeneity of temperature distribution inside the gas and the tank wall, and the effect of three key parameters including the direction of the injection nozzle, the nozzle diameter, and the initial (ambient) temperature.

For this purpose, they used the three-dimensional and time-dependent computational fluid dynamics (CFD) method in ANSYS CFX software along with the Shear Stress Transport (SST) turbulence model to accurately simulate the flow characteristics in compressed hydrogen gas.

Finally, the most important result of this research showed that the direction of the fuelling nozzle has a very decisive effect on the thermal stratification of the tank, so that if the gas injection is not done towards the end of the tank (where the temperature sensor is located), the phenomenon of severe thermal stratification occurs and the sensor may show the temperature lower than the actual limit, which endangers the safety of the tank due to the risk of local heating beyond the permissible limit ($85°C$).

2.1.3 Insulation of Cryogenic Hydrogen Tanks

Thermal insulation plays a critical role in sLH2 storage and refuelling systems. Due to the extremely low boiling point of liquid hydrogen, even a small amount of heat ingress from the surroundings can cause the fluid to vaporize, leading to pressure build-up and boil-off losses. Effective insulation is therefore essential for maintaining the thermodynamic state of the stored hydrogen and ensuring the stability of the system during both storage and refuelling.

There are two general categories of insulation for storing cryogenic fuels such as liquid hydrogen or liquid oxygen: passive and active insulation. Passive insulation involves methods like wrapping multi-layer insulation (MLI) around the tank, while active insulation is used with the goal of completely eliminating the fuel boil-off phenomenon. In an active system, several metallic thermal shields are placed between the MLI layers. A cooling fluid flowing through very fine tubes cools these attached thermal shields, allowing them to intercept and reject the heat absorbed from the environment to the outside of the tank. These systems are primarily used for long-duration space missions [15].

In 2004, Hastings [16] developed, analytically modeled, and experimentally tested a variable density multilayer insulation with a foam underlayer for large liquid hydrogen tanks. Experimental tests with liquid hydrogen showed that the use of VD-MLI insulation halved the heat transfer into the tank compared to standard multilayer insulation, while reducing the weight of the system.

Fesmire et al. [17] experimentally characterized the thermal performance of robust MLI systems for cryogenic applications, reporting effective thermal conductivity values in the range of 0.0009 $\mathrm{W/m \cdot K}$ under practical operating conditions.
In another study, Choi et al. assumed an effective thermal conductivity of 1×10^{-4} $\mathrm{W/(m \cdot K)}$ to simulate the thermal behavior of multilayer insulators (MLI) under high vacuum conditions. The complete agreement of this value with experimental data and NASA technical reports confirms that the thermal conductivity range of insulation systems in modern hydrogen vehicle applications fully overlaps with proven aerospace standards [18]

2.2 Thermodynamic Principle

In this section, governing equations which represent the thermodynamic behavior of the liquid hydrogen tank during refuelling, defuelling, and dormancy will be described.

2.2.1 Conservation of Mass and Energy

Three significant governing equations are fundamental conservation laws: conservation of mass, conservation of energy, and conservation of momentum. These equations produce the base of 1D modelling in GT-SUITE.

The conservation of mass for a control volume, in this case, the tank, states that the rate of change of mass inside the tank is equal to the net mass flow rate across its boundaries:

$$\frac{dm}{dt} = \dot{m}_{in} - \dot{m}_{out} \tag{2.1}$$

where m is the total mass of hydrogen inside the tank, $\dot{m}_{in}$ is the mass flow rate entering the tank, and $\dot{m}_{out}$ is the mass flow rate leaving the tank.

In GT-SUITE, the energy conservation equation is expressed in two different forms depending on the solver type. In the Explicit Solver, the equation is formulated in terms of internal energy, and the main solution variable is the specific internal energy of the fluid (Equation 2.2). In contrast, in the Implicit Solver, the same energy conservation law is written in terms of enthalpy, so that enthalpy includes the effect of pressure work in addition to internal energy $\left(H = e + \frac{p}{\rho}\right)$(Equation 2.3).

Using the enthalpy form in the implicit solver provides a better coupling between pressure, temperature, and energy and improves the numerical stability and convergence of the solution, which is why it is more suitable for simulating compressible flow and heat transfer problems.

$$\frac{d(me)}{dt} = -p\frac{dV}{dt} + \sum_{\text{boundaries}} (\dot{m}H) - hA_s\left(T_{\text{fluid}} - T_{\text{wall}}\right) \tag{2.2}$$

$$\frac{d(\rho HV)}{dt} = \sum_{\text{boundaries}} (\dot{m}H) + V\frac{dp}{dt} - hA_s\left(T_{\text{fluid}} - T_{\text{wall}}\right) \tag{2.3}$$

The momentum equation is represented below:

$$\frac{d\dot{m}}{dt} = \frac{dpA + \sum_{\text{boundaries}}(\dot{m}u) - 4C_f\frac{\rho|u|u}{D}\frac{dxA}{2} - K_p\left(\frac{1}{2}\rho|u|u\right)A}{dx} \tag{2.4}$$

where m is the mass contained in the tank, e is the total specific internal energy, V is the tank volume, ρ is the fluid density, and H is the total specific enthalpy. The parameter A_s represents the heat transfer surface area, which is calculated based on the internal diameter of the tank together with the tank wall and insulation geometry. The parameter h denotes the fluid-side heat transfer coefficient, while T_{fluid} and T_{wall} represent the fluid and wall temperatures, respectively. Furthermore, u denotes the velocity at the boundary, C_f is the Fanning friction factor, K_p is

the pressure loss coefficient, D is the equivalent diameter, and dx represents the discretization length in the flow direction.

2.2.2 Equation of State for Hydrogen

The thermodynamic equation of state (EOS) is needed to relate the pressure, temperature, and density of the hydrogen due to close the system equations. For cryogenic hydrogen, the ideal gas law is not sufficient due to the significant intermolecular interactions at low temperatures and high pressures. Instead, a real gas equation of state is required.

In GT-SUITE, the choice of property method depends on the type of fluid circuit used. Since this study involves subcooled liquid hydrogen with phase change, FluidRefrigerant components are used throughout the model. For this circuit type, GT-SUITE evaluates all thermodynamic and transport properties, including enthalpy, density, and specific heat, using REFPROP (Reference Fluid Thermodynamic and Transport Properties Database), developed by the National Institute of Standards and Technology (NIST) [19].

This applies across all thermodynamic states encountered during the simulation, including subcooled liquid, two-phase, superheated vapor, and supercritical conditions, with no switching to simplified real gas models such as Redlich-Kwong.

REFPROP implements the high-accuracy equation of state developed by Leachman et al. [20] for hydrogen, which expresses the Helmholtz free energy as a function of reduced density $\delta = \rho/\rho_c$ and inverse reduced temperature $\tau = T_c/T$:

$$\frac{a(\rho, T)}{RT} = \alpha^o(\delta, \tau) + \alpha^r(\delta, \tau) \tag{2.5}$$

where a is the specific Helmholtz free energy, R is the specific gas constant for hydrogen, α^o is the ideal gas contribution, and α^r is the residual contribution that accounts for real gas behavior. All other thermodynamic properties are derived from this relation through standard thermodynamic identities.

2.2.3 State of Charge (SoC) Definition

The State of Charge (SoC) is a key parameter in this study, as it describes how much hydrogen is available in the tank at any given point relative to its maximum capacity.

$$\text{SoC} = \frac{m_{H_2}}{m_{max}} \times 100\% \tag{2.6}$$

where m_{H_2} is the current mass of hydrogen in the tank and m_{max} is the maximum hydrogen mass that can be stored under the reference filling conditions.

The two-phase flow behavior and phase change phenomena that occur during the refuelling process, including flash vaporization, are discussed in detail in Chapter 3.

The governing equations introduced in this chapter serve as the theoretical foundation for the models developed in this thesis. In the following chapters, these equations are applied and adapted for each specific process, refuelling, defuelling, and dormancy, according to the corresponding boundary conditions and modelling assumptions.

2.3 GT-SUITE as a 1D CFD Tool

GT-SUITE is built around a 1D fluid dynamics framework, in which pipes, valves, heat exchangers, and other components are connected in order to produce a fluid network. The governing equations of mass, momentum, and energy conservation are solved simultaneously across the entire network at each time step. GT-SUITE allows to model the transient behavior of complex systems to be captured efficiently.

In GT-SUITE, flow network discreticized in one direction. Direction is defined based on the discretization length by user per each component. For instance, pipe components are divided with series of sub-volumes, while flow splits and tanks are treated as single elements.

Sub-volumes are connected through their interfaces, where vector quantities such as heat flux and velocity are calculated. However, scalar quantities (pressure, temperature, density, and enthalpy) are assumed to be uniform within each sub-volume and are evaluated at its centroid (Figure 2.1) [21].

The variables are evaluated by the numerical core by solving the one-dimensional Navier-Stokes equations, the laws of conservation of mass and energy determine the thermodynamic state of each sub-volume, and the momentum equation solves the vector quantities at the boundaries. As a result, all the calculated variables represent cross-sectional averages along the flow path.

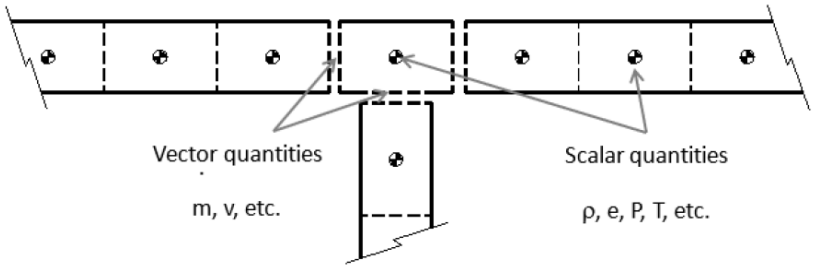

Figure 2.1: Component discretization [21]

2.3.1 Implicit vs. Explicit Solver Formulation

To advance the governing equations in time, the numerical framework offers a choice between an explicit and an implicit time-integration solver.

The explicit solver fundamentally treats mass flow rate, density, and internal energy as primary variables. In that, the state of the system at time step t+(Δt) is calculated only based on the information available at time step t, and no iterative process is performed to arrive at the final answer. This feature makes the calculations relatively simple and fast; however, in order to ensure numerical stability, it is necessary to choose a very small time step. The maximum allowable time step (Δt) is strictly bounded by the Courant-Friedrichs-Lewy (CFL) stability criterion:

$$\Delta t \leq \frac{\Delta x}{|u| + c} \tag{2.7}$$

where Δx is the discretization length, u is the local fluid velocity, and c is the local speed of sound. Due to the high speed of sound in cryogenic domains and the small discretization lengths required for accuracy, the explicit method restricts Δt to extremely small values (10^{-6} to 10^{-4} seconds). This makes the explicit solver highly suitable for high-frequency wave dynamics and severe pressure pulsations, which is not the primary focus of long-term system behavior.

In a refuelling process there are three factors that limits to using explicit solver:

- *Defuelling time:* defuelling takes about 9 hours, using very small time steps can increase the number of computational steps to tens of millions, resulting in significant computational cost.
- *Flowsplit:* In this case, the time step must be chosen small enough that only a fraction of the mass in the Flowsplit control volume can escape during a time step; otherwise, the probability of numerical instability and unrealistic results increases.
- *Heat transfer limitation:* In becomes active when the mass of the fluid inside the control volume is too small, or the heat transfer coefficient is too large. In

this situation, if the time step is chosen too large, the fluid temperature may exceed the wall temperature in a time step, which is physically unrealistic.

For the transient simulation of the subcooled liquid hydrogen fuelling system, the implicit solver is highly efficient and mathematically advantageous. While the refuelling and defuelling phases involve rapid mass transfer, the overall system timescales, particularly during the extended dormancy (holding) phase, are relatively long and governed by thermal inertia. Therefore, to optimize computational efficiency while ensuring robust convergence across the multi-phase transitions, the implicit solver formulation is adopted for this study.

Conversely, the implicit solver selects mass flow rate, pressure, and total enthalpy as its primary coupled variables. It solves a non-linear system of equations simultaneously for all subvolumes at the current time step using an iterative Newton-Raphson procedure. Although the computational effort per iteration is higher, the implicit scheme is unconditionally stable, allowing for significantly larger time steps ($\Delta t \approx 0.01$ to 0.1 seconds).

3

Methods

This chapter describes the numerical modelling framework adopted in the present thesis for the simulation of a subcooled liquid hydrogen (sLH_2) fuelling system for heavy-duty trucks. The overall modelling workflow consists of two main sub-systems:

- a *Refuelling* model,
- a *Defuelling* model.

In this study, the modelling approach began with the development of an initial refuelling system model, followed by verification of its numerical convergence and stability. Subsequently, a relevant research study investigating liquid hydrogen refuelling using a 3D-CFD approach was utilised for validation and comparison of the simulation results [22].

To further improve the accuracy of the refuelling system model, the nozzle was modelled based on technical data and specifications provided by the nozzle supplier.

In order to determine the initial conditions prior to the refuelling process, a defuelling (fuel consumption) model was developed. For this purpose, data from a relevant research study based on a lumped-parameter modelling approach was used for validation, and the simulation results demonstrated good agreement with the reference data [23].

The primary objective of the defuelling model was to predict the thermodynamic state of the onboard tank before the start of the refuelling process.

After obtaining different initial tank conditions, a sensitivity analysis was conducted to identify the optimum initial conditions for the beginning of the refuelling process.

In order to model the refuelling process and identify the main system components and their control strategies, the final draft of the international standard ISO/FDIS 13984, titled *Liquid Hydrogen - Land Vehicle Fuelling Protocol* [24], was used as the primary reference throughout the model development phase.

3.1 Simulation Framework: GT-SUITE

To accomplish the defined objectives, a one-dimensional (1D) computational modelling tool was used to develop a simulation model of the sLH_2 refuelling system. The selected software was GT-SUITE (version 2025), a commercial multi-physics simulation platform developed by Gamma Technologies LLC. GT-SUITE is widely adopted in the automotive and energy sectors for the modelling of thermal-fluid systems, powertrains, and energy storage components, offering a robust and validated environment for 1D thermodynamic and fluid dynamic analyses.

3.1.1 Rationale for the Choice of a 1D Modelling Approach

The physical phenomena governing a sLH_2 fuelling system (for instance, the transient thermodynamic evolution of a cryogenic fluid within pressurised tanks, the heat exchange with the surrounding tank wall, and the two-phase flow dynamics during refuelling and defuelling) can in principle be investigated using high-fidelity three-dimensional Computational Fluid Dynamics (3D CFD) methods.

However, such approaches entail significant computational costs: a single transient simulation of a full refuelling event, typically lasting several hundred seconds of physical time, would require on the order of several days (up to two weeks in high-fidelity configurations [22]) even on high-performance computing clusters, due to the fine spatial and temporal resolution required to resolve cryogenic phase-change phenomena. This makes 3D CFD unsuitable for the iterative design, parametric studies, and sensitivity analyses that constitute a substantial part of the present work.

A 1D lumped-parameter approach, as implemented in GT-SUITE, overcomes this limitation by representing the system as a network of interconnected control volumes, pipes, valves, and boundary conditions, each governed by the conservation equations of mass, momentum, and energy integrated over the respective volume.

This reduction in spatial dimensionality allows full transient simulations of the entire fuelling cycle to be completed in less than 10 minutes on a standard engineering workstation, while still capturing the dominant thermodynamic and fluid dynamic behaviour of the system with sufficient fidelity for engineering purposes. The computational efficiency of the 1D approach is particularly valuable in the context of this thesis, where multiple operating scenarios must be analysed under a range of initial conditions and control strategies.

Moreover, the short execution time facilitates an iterative model development process, enabling rapid identification and correction of modelling errors across successive

simulation runs.

Beyond computational speed, GT-SUITE offers several practical advantages that further justified its selection:

- **Modularity and reconfigurability**: the model topology is defined through a graphical interface in which individual components (tanks, pipes, orifices, heat exchangers, and controllers) are represented as discrete objects connected by fluid paths. This architecture makes it straightforward to modify the system configuration without restructuring the underlying equations, thereby accelerating the model development cycle.
- **Built-in cryogenic fluid properties**: GT-SUITE incorporates thermophysical property databases sourced from the National Institute of Standards and Technology (NIST) for hydrogen in both its gaseous and liquid phases, enabling accurate evaluation of density, enthalpy, entropy, specific heat, and transport properties as functions of temperature and pressure across the cryogenic operating range relevant to sLH_2.
- **Multi-case execution**: the platform natively supports the definition and execution of parametric sweep studies in which a large number of simulations with systematically varied input parameters can be launched and post-processed in a single automated workflow. This capability is particularly valuable when the influence of a given parameter on the system response is not known a priori, as it allows the analyst to efficiently explore the input space and quantify each parameter's effect without requiring a separate, manually configured simulation for each case. This feature was exploited in the sensitivity analysis presented in Chapter 5.
- **Control-system integration**: dedicated control blocks together with support for PID-based and logic-based controllers are available directly within the modelling environment, enabling the implementation of realistic system control strategies without requiring external software.
- **Advanced post-processing and data visualization**: integrated tools for automated result visualization, signal analysis, and comparison between simulation cases simplify the interpretation of the large datasets generated during transient and parametric analyses.
- **Validated industrial track record**: GT-SUITE has been extensively validated and applied in the literature for the simulation of thermal management systems, cryogenic storage tanks, and hydrogen-related components [25, 26, 27], providing confidence in the reliability of the simulation results obtained in the present work.

3.1.2 Limitations of the 1D Modelling Approach

Despite its practical advantages, the 1D modelling framework implemented in GT-SUITE is subject to a number of inherent limitations that must be acknowledged when interpreting the simulation results.

- **Homogeneous equilibrium assumption:** As described in Section 3.2.1.2, GT-SUITE handles two-phase mixtures through a Homogeneous Equilibrium Model, in which the liquid and vapour phases within each control volume are assumed to share a common pressure and temperature at all times. This assumption precludes the representation or the accuracy of non-equilibrium phase-change phenomena such as flash vaporisation, which may occur at the onset of refuelling when subcooled liquid hydrogen is suddenly exposed to the lower pressure of the warm onboard piping.
- **Absence of stratification:** The lumped-parameter nature of the 1D approach implies that each control volume is characterised by a single, spatially uniform thermodynamic state. As a consequence, thermal stratification (the development of temperature gradients within the liquid phase of a cryogenic tank over time) cannot be captured by the model.
- **Two-phase convergence:** The implicit solver in GT-SUITE can exhibit convergence difficulties during rapid two-phase transients, particularly when the thermodynamic state crosses the saturation boundary within a single time step. In such cases, manual adjustment of solver tolerances or time-step constraints may be required to maintain numerical stability.
- **Fixed solver architecture:** As a commercial simulation platform, GT-SUITE does not provide direct access to the underlying conservation equations or solver source code. Modifications to the mathematical formulation of specific components (such as the introduction of custom phase-change correlations or non-standard constitutive relations in the tanks) are only possible through user-coded subroutines, the development of which falls outside the scope of the present thesis. Accordingly, all models were constructed exclusively using the standard component library provided by the software.

These limitations are inherent to the 1D modelling philosophy and do not compromise the validity of the results for the engineering objectives of this thesis. Their potential impact on specific simulation outcomes is discussed in the context of the respective validation exercises presented in Chapter 5.

3.2 Refuelling

The refuelling model developed in this study was validated against the three-dimensional, two-phase CFD modelling framework proposed by Molkov et al. [22], *"Liquid Hydrogen Refuelling at HRS: Description of SLH2 Concept, Modelling Approach and Results of Numerical Simulations"*, adopted as the primary validation reference.

In the present context, refuelling denotes the filling phase, that is, the stage in which hydrogen is transferred from the station storage tank to the onboard vehicle tank while the truck is stationary at the dispensing station. The model thus reproduces the thermodynamic evolution occurring inside the receiving tank as hydrogen is delivered during the filling operation.

The referenced work employed a coupled thermodynamic and transient three-dimensional CFD approach to simulate the transfer of liquid hydrogen from the station storage tank to the onboard vehicle tanks, providing a detailed and physically grounded benchmark against which the present model could be assessed.

3.2.1 Modelling Approach and System Configuration

The reference study [22] presents a comprehensive modelling framework for LH2 refuelling through the entire equipment of a hydrogen refuelling station (HRS). The modelling approach comprises two coupled models: a thermodynamic model for the LH2 transfer from the HRS storage tank to the pump exit, and a three-dimensional two-phase CFD model from the pump exit through all HRS equipment down to the onboard storage tanks. The HRS equipment modelled includes pipes with bends, an automatic pressure control valve (PCV), a breakaway, a hose, a nozzle, and a three-way manifold connected to two onboard storage tanks which are shown in the PID diagram of the conceptual LH2 refueiling system Figure 3.1.

The HRS storage tank has a volume of 61.36 m^3 and holds 4 tonnes of LH2 at a pressure of 0.3 MPa (abs) and a saturation temperature of 24.68 K. Each of the two onboard storage tanks has a volume of 0.71 m^3 and a capacity of 44 kg of LH2 at 100% state of charge (SoC). The tanks are cylindrical with hemispherical end caps, an internal length of 2.3 m, and an internal diameter of 0.66 m. All pipes, the breakaway coupling, the hose, and the nozzle have an inner diameter of 25.4 mm and are fabricated from stainless steel 316L with a wall thickness of 2 mm.

Breakaway coupling is a safety device installed in the transfer line to prevent hydrogen spillage and equipment damage in the event of an unintended drive-away or pull-away incident. The coupling is designed to act as the weakest point in the transfer system, separating in a controlled manner when excessive tensile loads are

applied to the hose.

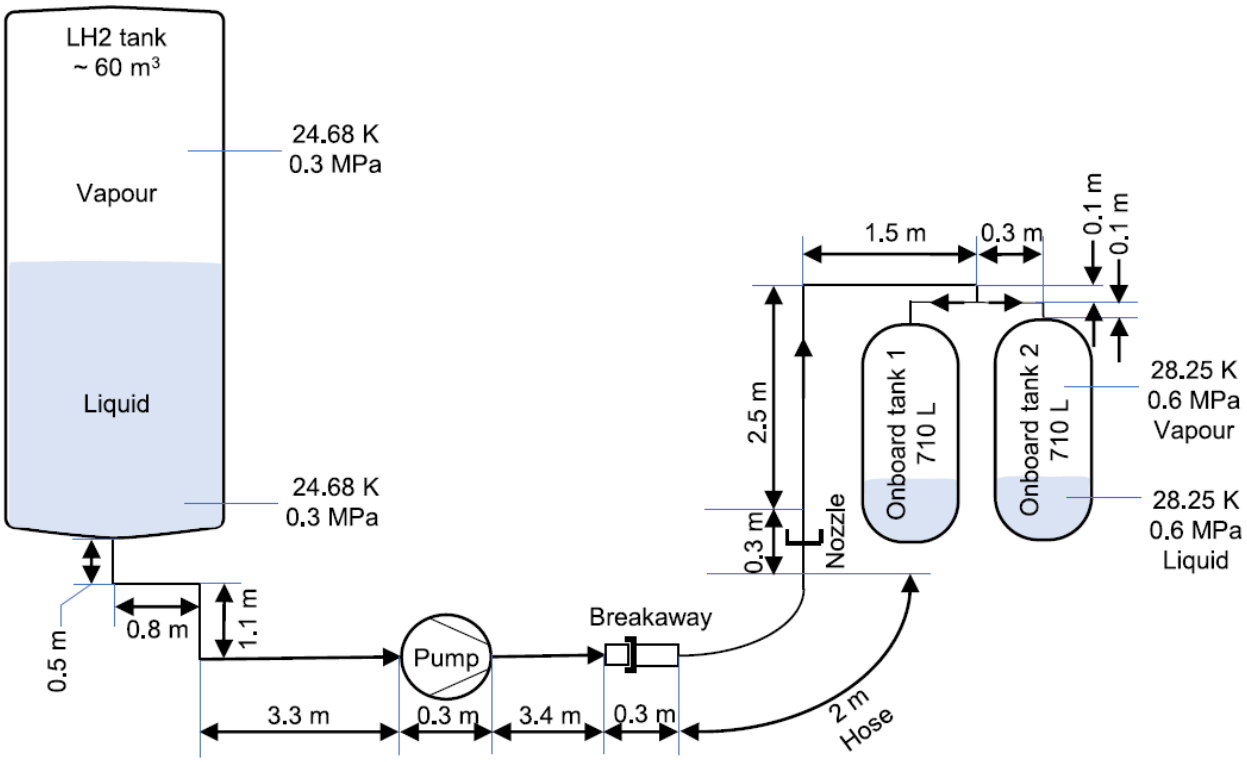

Figure 3.1: P&ID diagram of the LH_2 refuelling station in [22].

3.2.1.1 Governing Equations

In current project, the temporal evolution of the thermodynamic state inside each onboard storage tank is governed by the conservation of mass and energy. The total mass conservation equation is:

$$\frac{dm_{\text{tank}}}{dt} = \dot{m}_{\text{in}} \tag{3.1}$$

where $\dot{m}_{\text{in}}$ is the incoming LH2 mass flow rate. The energy conservation equation for the tank control volume is:

$$\frac{dU_{\text{tank}}}{dt} = \dot{m}_{\text{in}}\, h_{\text{in}} + \dot{Q}_{\text{wall}} \tag{3.2}$$

where U_{tank} is the total internal energy of the two-phase mixture, h_{in} is the specific enthalpy of the incoming hydrogen flow, and $\dot{Q}_{\text{wall}}$ is the heat transfer rate through the tank walls. The total internal energy of the two-phase mixture is:

$$U_{\text{tank}} = m_l\, u_l + m_g\, u_g \tag{3.3}$$

where u_l and u_g are the specific internal energies of the saturated liquid and vapour phases respectively. Although the energy conservation equation governing the tank is expressed in a form that distinguishes between the liquid and vapor phases, as shown in Equations 3.2 and 3.3, it is important to clarify how this formulation relates to the modelling approach employed in GT-SUITE.

GT-SUITE does not track the liquid and vapor phases as separate, independent variables. Instead, it adopts a Homogeneous Equilibrium Model (HEM), in which the two-phase mixture is treated as a single unified fluid characterized by a vapor quality parameter, x. Under this assumption, thermodynamic equilibrium between the phases is enforced at all times, and the thermophysical properties of the mixture are evaluated from fluid property tables, such as those provided by REFPROP, as functions of pressure and temperature.

Within this framework, Equation (3.3) can be rewritten as:

$$U_{\text{tank}} = m_{\text{total}} \left[(1 - x)\, u_l + x\, u_g \right] \tag{3.4}$$

which GT-SUITE evaluates implicitly using the equilibrium vapor quality x and the saturation properties u_l and u_g retrieved from the property tables. Consequently, while the individual phase masses m_l and m_g are not stored as explicit state variables within the solver, they can be recovered as post-processed quantities through the relations:

$$m_l = (1 - x)\, m_{\text{total}}, \qquad m_g = x\, m_{\text{total}} \tag{3.5}$$

The two-phase formulation presented in Equations (3.2)–(3.5) therefore remains physically consistent with the GT-SUITE implementation; the distinction is that the phase-separated representation is an analytical decomposition of the mixture state, whereas the software resolves the energy equation in terms of the aggregate mixture properties.

3.2.1.2 Phase Change Model

In GT-SUITE two-phase behaviour inside the tanks is governed by the thermodynamic equilibrium assumption, whereby the liquid and vapour phases are assumed to coexist in mutual thermodynamic equilibrium at all times. Under this assumption, the saturation temperature T_{sat} corresponds uniquely to the instantaneous tank pressure through the real-gas equation of state for hydrogen:

$$T_{\text{sat}} = f(P_{\text{sat}}) \tag{3.6}$$

evaluated using the NIST REFPROP database [28].

3.2.1.3 Pressure Control Valve and Pump Modelling

In the three-dimensional CFD model of Molkov et al. [22], in order to change the mass flow rate through the refuelling time, the automatic pressure control valve (PCV) is used and the resistance coefficients are dynamically adjusted through a User Defined Function (UDF) so that the resulting mass flow rate reproduces the profile prescribed by the refuelling protocol. Heat transfer at the PCV is disabled in the reference model, and the expansion across the valve is treated as an isenthalpic.

In the present one-dimensional GT-SUITE model, the cryogenic liquid hydrogen pump is represented using the `ImposedFlowRefrig` template, which prescribes the refrigerant mass flow rate as a time-varying external input. This modelling approach is appropriate when the delivered mass flow rate is determined by the system-level refuelling strategy rather than by the internal hydraulic characteristics of the pump itself, which is the case in the present study.

The pump element includes an isentropic efficiency parameter η_{is}, which accounts for the irreversibilities in the compression process.

$$\eta_{\text{is}} = \frac{h_{2s} - h_1}{h_2 - h_1}, \tag{3.7}$$

where h_1 is the inlet (suction) enthalpy, h_2 is the actual outlet (discharge) enthalpy, and h_{2s} is the outlet enthalpy corresponding to an isentropic process.

The outlet thermodynamic state is therefore determined from the combination of the imposed mass flow rate, the pressure rise, and the specified isentropic efficiency. Since the objective of the present study is to reproduce the prescribed refuelling protocol rather than to analyse pump performance in isolation, the pump is treated as an idealised flow-delivery device. The time-dependent mass flow rate profile imposed at the pump boundary is entirely governed by the State Manager element described in Section 3.2.1.4, which implements the phase logic of the refuelling protocol. The physical rationale behind the flow rate values at each phase is discussed there.

Table 3.1 summarises the key modelling choices of the reference CFD model [22] alongside the corresponding approaches adopted in the present GT-SUITE model.

3.2.1.4 State Manager Configuration for LH_2 Refuelling

To replicate the transient behavior of the liquid hydrogen refuelling process, a State Manager element was implemented in GT-SUITE as the supervisory control unit of the simulation. The State Manager monitors user-defined system variables, such as nozzle outlet temperature, and tank pressure, at every time step, and triggers automatic transitions between predefined operating states when the specified logical

Table 3.1: Comparison of the reference CFD methodology [22] and the present GT-SUITE model.

Aspect	**Reference CFD [22]**	**Present GT-SUITE Model**
Dimensionality	3D transient	1D lumped-parameter
Pump representation	Thermodynamic (isentropic)	Imposed mass flow rate
PCV representation	Porous medium (UDF)	State Manager boundary condition
Spatial discretisation	239,111 control volumes	Pipe element length steps
Computational cost	∼14 days (72-core CPU)	Minutes

conditions are met. Within each state, the mass flow rate delivered by the pump is prescribed as a fixed or ramped value, effectively emulating the flow control actions carried out by the fuelling station dispenser during a real refuelling event.

The state sequence implemented in the State Manager follows the single-hose, target-pressure-based fuelling protocol defined in ISO/FDIS 13984:2025 [24]. According to this standard, the main fuelling phase consists of three successive sub-phases, each associated with a specific flow rate range and a defined transition criterion. The standard additionally requires that the fuelling station shall terminate the flow as soon as possible but within 5 s in the event that either the maximum fuelling pressure of 1.5 MPa(g) or the minimum pressure of 0.1 MPa(g) is exceeded at any point during the process [24]. The three sub-phases are described in the following paragraphs and shown in figure 3.2 .

- **Phase 1 - Start of Fuelling (Cool-down):** The first phase is initiated when the main fuelling valve opens and the cryogenic pump begins delivering liquid hydrogen at a deliberately reduced flow rate. The two primary objectives of this phase are: (i) to progressively cool the warm components along the supply line, including the hose and nozzle, from their initial near-ambient temperature toward cryogenic operating conditions, and (ii) to condense the gaseous hydrogen already present inside the vehicle storage tank, thereby reducing the tank pressure sufficiently to avoid prematurely reaching the maximum fuelling pressure during the subsequent steady-state phase. ISO/FDIS 13984:2025 specifies that the minimum flow rate during this phase shall not be less than 5 % of the station's maximum average flow rate, in order to compensate for the heat ingress from the warm components along the supply line [24].

  In the present model, a flow rate of approximately 20 g/s was prescribed for this phase, roughly 18 % of the nominal flow rate, consistent with the conceptual refuelling protocol of Molkov et al. [22]. This value was also found to provide adequate thermal margin against excessive flash vaporisation during

the initial cool-down period.

The State Manager uses the nozzle outlet temperature as the primary transition criterion for this phase. The transition to Phase 2 is triggered when the nozzle outlet temperature drops below the cool-down threshold temperature T_{cool}, indicating that subcooled liquid hydrogen is being delivered to the tank inlet and that the supply line has reached a sufficiently cryogenic condition. This criterion reflects the temperature control requirement of ISO/FDIS 13984:2025, which specifies that the fuelling station should target a mass-averaged hydrogen supply temperature below 26.5 K at the nozzle before the steady-state fuelling phase begins [24].

- **Phase 2 - Steady-State Fuelling** Once the cool-down criterion is satisfied, the State Manager commands the pump to ramp up the mass flow rate to the nominal target value of 400 kg/h (approximately 111 g/s), which is then maintained approximately constant for the remainder of this phase. This value was adopted from the conceptual protocol of Molkov et al. [22] and lies comfortably within the maximum average flow rate of 220 g/s defined for the protocol range specified in ISO/FDIS 13984:2025 [24]. During this phase, the majority of the hydrogen inventory is transferred to the vehicle storage tank, and the tank pressure is expected to remain within the steady-state pressure corridor defined by the protocol, generally rising gradually as the liquid level increases.

  The transition from Phase 2 to Phase 3 is triggered when the tank pressure reaches the threshold $P_{\text{target}} - 0.6\,\text{MPa}$ (while in ISO standard, it is Ptarget-0.2 MPa), at which point the rate of pressure rise begins to accelerate as the tank transitions toward the fully liquid state. The standard requires that the fuelling station shall begin reducing the flow rate as soon as possible, but within 5 s of the pressure reaching this threshold [24].

- **Phase 3 - End of Fuelling (Ramp-down)**

  During the end-of-fuelling phase, the State Manager commands the pump to reduce the flow rate to below 30 % of the nominal value. This reduction provides the station control system with sufficient time to terminate the hydrogen flow before the tank pressure overshoots the target value. ISO/FDIS 13984:2025 specifies that the fuelling station shall maintain this reduced flow rate until the target pressure P_{target} is reached, and then terminate the fuelling event within 5 s [24]. In the present model, the fuelling is terminated when the simulated tank pressure reaches 1.6 MPa, corresponding to the LH2-15(0) protocol designation defined in ISO/FDIS 13984:2025 and consistent with the reference scenario of Molkov et al. [22].

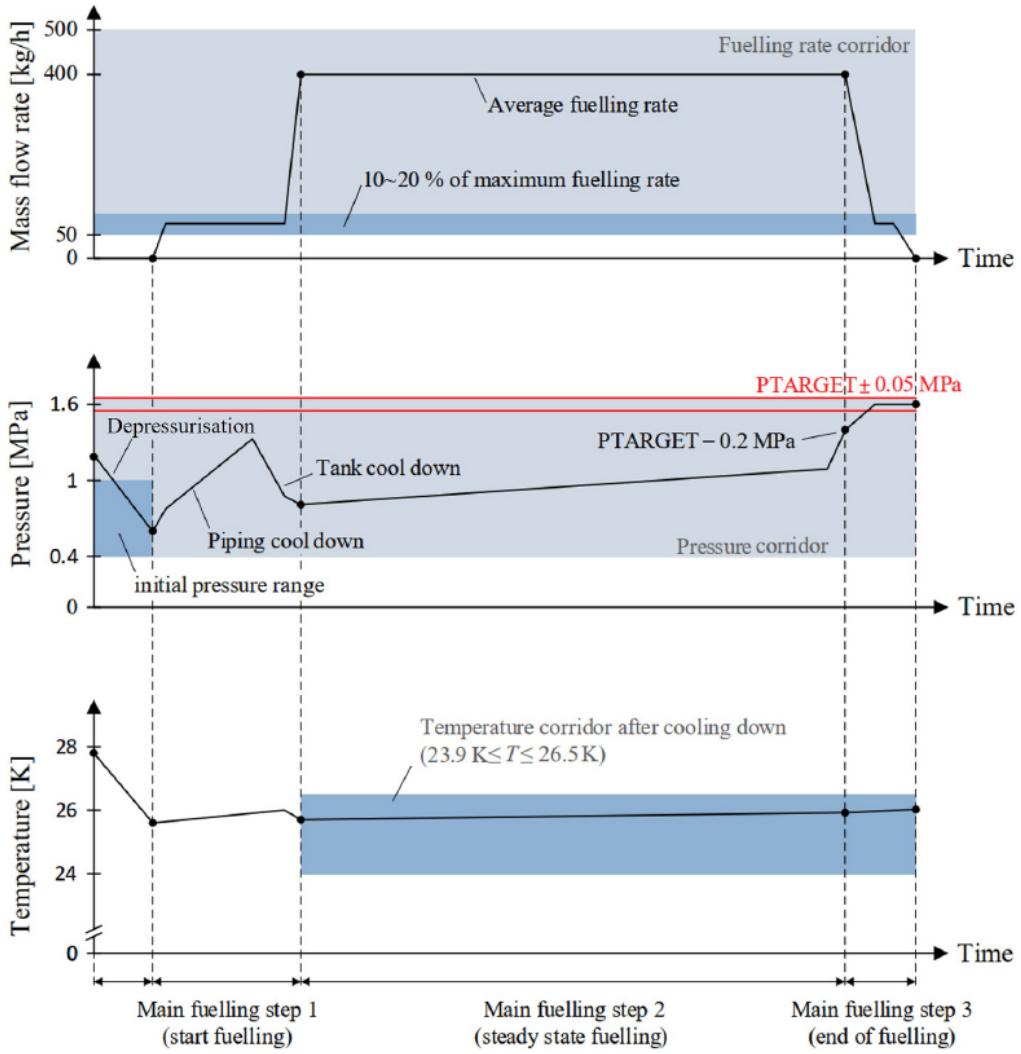

Figure 3.2: Conceptual mass flow rate, pressure, and temperature patterns during LH2 refuelling [22]

Table 3.2 summarises the three operating states implemented in the GT-SUITE State Manager, together with the prescribed flow rate and the logical condition governing the transition to the next state.

This three-state structure provides a physically consistent and protocol-compliant representation of the LH2 refuelling process within the one-dimensional simulation framework, and ensures that the predicted flow rate, pressure, and temperature profiles can be compared directly against the reference results of Molkov et al. [22].

Table 3.2: GT-SUITE State Manager: prescribed mass flow rates and transition criteria for each phase of the LH_2 refuelling simulation, based on [24].

State	Phase	Flow rate	Transition criterion
1	Cool-down (start of fuelling)	≈20 g/s	$T_{\text{nozzle}} \leq T_{\text{cool}}$
2	Steady-state fuelling	111 g/s (400 kg/h)	$p_{\text{tank}} \geq P_{\text{target}} - 0.6\,\text{MPa}$
3	End-of-fuelling (ramp-down)	≈20 g/s	$p_{\text{tank}} \geq P_{\text{target}} = 1.6\,\text{MPa}$

3.3 Defuelling

The defuelling model was developed based on the scientific publication by L. Stops et al. [23], *"Generalized thermodynamic modelling of hydrogen storage tanks for truck application"*, used as a first validation reference. In the present context, defuelling denotes the in-operation phase, that is, the stage in which hydrogen is gradually withdrawn from the truck's tank while the vehicle is being driven, for instance to supply the fuel cell stack. The model therefore reproduces the thermodynamic evolution occurring inside the on-board tank as hydrogen is consumed during normal vehicle operation.

Unlike the refuelling phase, for which a 3D CFD simulation was available, the defuelling process suffers from a significant knowledge gap in the literature, with relatively few publications addressing this specific operating scenario. For this reason, a 0D thermodynamic model for subcooled liquid hydrogen (sLH2) in truck applications was adopted, which, despite its simplicity, provides a physically consistent and computationally efficient framework suitable for the goals of this thesis.

3.3.1 Reference Models for the defuelling Validation

The defuelling model developed in this thesis is validated against the thermodynamic framework presented by Stops et al. [23], which itself builds upon the foundational implicit DAE model by Hamacher et al. [29]. Both models adopt a 0D lumped-parameter approach and are briefly described hereafter, as they represent the reference against which the GT-SUITE implementation is validated.

3.3.1.1 Modelling the thermodynamic behavior of cryo-compressed hydrogen tanks for trucks

Hamacher et al. [29] developed a single set of differential-algebraic equations to model the thermodynamic behavior of a cryo-compressed hydrogen (CcH2) onboard

storage tank for heavy duty trucks. The key design objective was to derive one unified equation system valid across all three operating scenarios, *refuelling*, *discharge*, and *dormancy*, without requiring a change of model equations at phase boundaries or scenario transitions.

The model is built on the following core assumptions:

- Hydrogen temperature T and pressure p are spatially uniform within the tank (perfectly mixed hypothesis).
- The solid tank structure (aluminum liner and carbon fiber overwrap) is at the same temperature as the hydrogen at all times.
- Thermodynamic properties of para-hydrogen are computed via REFPROP [28].
- Temperature-dependent heat capacities of aluminum (c_{Alu}) and carbon fiber (c_{CF}) are taken from the NIST webbook.

The model consists of two differential equations and nine algebraic equations. The first is the mass balance:

$$\frac{\mathrm{d}M}{\mathrm{d}t} = \dot{M}_{\mathrm{fuel}} - \dot{M}_{\mathrm{disch}} - \dot{M}_{\mathrm{vent}} \tag{3.8}$$

where M is the total hydrogen mass stored in the tank, $\dot{M}_{\mathrm{fuel}}$ is the mass flow rate supplied during refuelling, $\dot{M}_{\mathrm{disch}}$ is the mass flow rate extracted to feed the fuel cell during discharge, and $\dot{M}_{\mathrm{vent}}$ is the mass flow rate released through the relief valve during dormancy, whenever the maximum allowable pressure is reached.
The second is the energy balance, formulated in terms of the total internal energy $U_{\mathrm{tot}} = U_S + M \cdot u$, which includes both the hydrogen and the solid structure:

$$\frac{\mathrm{d}U_{\mathrm{tot}}}{\mathrm{d}t} = \dot{M}_{\mathrm{fuel}} \cdot h_{\mathrm{fuel}} - \dot{M}_{\mathrm{disch}} \cdot h - \dot{M}_{\mathrm{vent}} \cdot h + \dot{Q}_{\mathrm{disch}} + \dot{Q}_{\mathrm{amb}} \tag{3.9}$$

where U_S is the internal energy of the solid tank structure (aluminium liner and carbon fibre overwrap) and u is the specific internal energy of the hydrogen, both evaluated as a function of the tank temperature. On the right-hand side, h_{fuel} is the specific enthalpy of the incoming hydrogen during refuelling, while h is the specific enthalpy of the hydrogen stored in the tank, which, consistently with the perfectly mixed hypothesis, is also taken as the enthalpy of both the discharged and the vented flows. The term $\dot{Q}_{\mathrm{disch}}$ represents the heat supplied by the internal heat exchanger (iHEX) during discharge to sustain the minimum operative pressure, and $\dot{Q}_{\mathrm{amb}}$ is the heat leak from the environment through the tank insulation.

The use of internal energy U in Equation (3.9) makes the formulation inherently phase-independent: no distinction between single-phase and two-phase regions is required in the differential equations themselves. Phase changes are handled transparently through the REFPROP evaluation of $u(T, \varrho)$.

The remaining algebraic equations define:

- the solid internal energy U_S via numerical integration of $c_i(T)$
- the hydrogen density $\varrho = M/V_{\text{tank}}$
- the ambient heat leak $\dot{Q}_{\text{amb}} = k_{\text{tank}} A_{\text{tank}} (T_{\text{amb}} - T)$
- the thermodynamic state (u, h, p) from REFPROP

Two scenario-dependent boundary conditions complete the system, defining the values of $\dot{Q}_{\text{disch}}$ and $\dot{M}_{\text{vent}}$ depending on whether the tank is in standard, minimum-pressure (defuelling), or maximum-pressure mode (dormancy).

During the discharge scenario, as hydrogen is extracted from the tank, both the density and the pressure drop. If the pressure falls to the minimum allowed value p_{min}, an internal heat exchanger (iHEX) is activated to prevent further pressure decrease. The iHEX recirculates warm hydrogen (previously heated by the outer heat exchanger (oHEX) after leaving the tank) back into the tank, adding heat $\dot{Q}_{\text{disch}}$ to the stored hydrogen. This heating raises the hydrogen temperature and, consequently, its pressure, maintaining it at p_{min}. The minimum pressure requirement arises from two practical constraints: the minimum inlet pressure required by the **fuel cell**, and the pressure drops across valves, regulators, and heat exchangers in the downstream circuit.

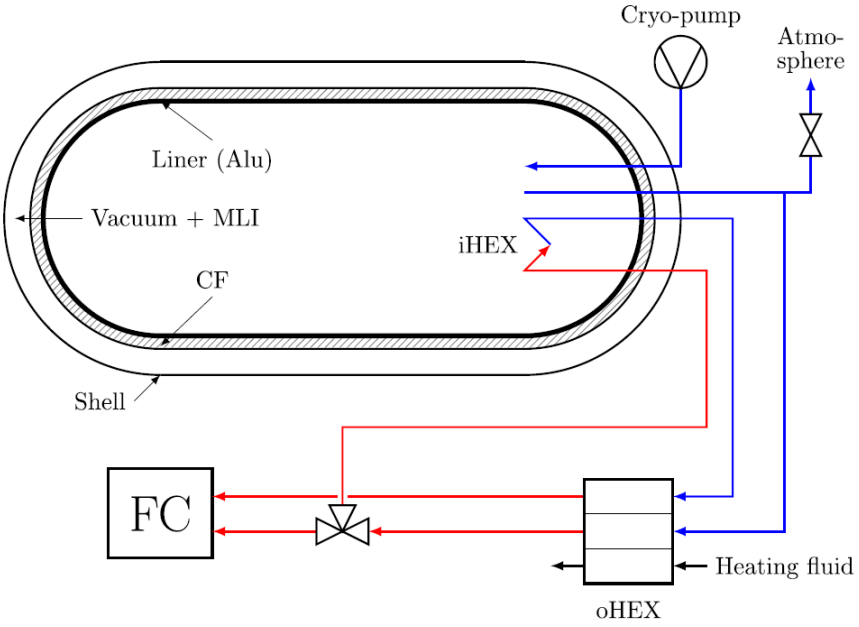

Figure 3.3: CcH2 hydrogen storage tank system. iHEX: internal heat exchanger; oHEX: outer heat exchanger; CF: carbon fibre (structural composite overwrap of the shell).

Despite its generality, the implicit formulation of Hamacher et al. [29] presents two

main limitations. First, expressing the energy balance in terms of U_{tot} rather than T provides limited thermodynamic insight, as the individual contributions of mass flows and heat exchanges to the temperature evolution are not directly readable from the equations. Second, the algebraic expressions for $\dot{Q}_{\mathrm{disch}}$ and $\dot{M}_{\mathrm{vent}}$, derived for the isobaric boundary conditions at $p = p_{\mathrm{min}}$ and $p = p_{\mathrm{vent}}$ respectively, involve the partial derivatives $(\partial T/\partial \varrho)_p$ and $(\partial h/\partial \varrho)_p$, which are not well-defined in the two-phase region, restricting the model to single-phase conditions and making it unsuitable for sLH2 tank simulations.

Both limitations are addressed by Stops et al. [23]. The energy balance is reformulated explicitly for the hydrogen temperature T, making each term physically interpretable. Furthermore, the two-phase region is handled by replacing the single-phase properties c_v and $(\partial p/\partial T)_\varrho$ with their two-phase equivalents: the specific isochoric two-phase heat capacity c_{v2P} and the saturation pressure derivative $\mathrm{d}p_{\mathrm{sat}}/\mathrm{d}T$, both available from REFPROP [28]. This substitution preserves the structure of the equation system across all phases without requiring any change of equations at phase boundaries, resulting in a generalized model applicable to CH2, sLH2, and CcH2 storage technologies.

3.3.1.2 Generalized thermodynamic modelling of hydrogen storage tanks for truck application

To overcome the limitations of Hamacher et al. [29], Stops et al. [23] introduced an explicit and generalized reformulation applicable to all three physical hydrogen storage technologies: compressed gaseous hydrogen (CH2), subcooled liquid hydrogen (sLH2), and cryo-compressed hydrogen (CcH2). The operating logic retains the same three scenarios (discharge, refuelling, dormancy):

- **Mode A: Standard**: $p_{\mathrm{min}} < p < p_{\mathrm{vent}}$, no heating or venting required (during refuelling).
- **Mode B: Minimum pressure**: $p = p_{\mathrm{min}}$, heat exchanger activated; occurs only during discharge.
- **Mode C: Maximum pressure**: $p = p_{\mathrm{vent}}$, venting activated; occurs only during dormancy.

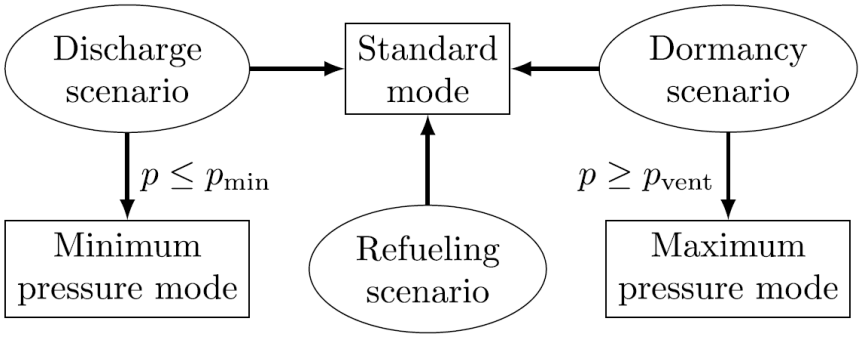

Figure 3.4: Visualization of the relationship between the three operating scenarios and the three operational modes

With respect to Hamacher et al. [29], three main advancements are introduced. First, the solid tank structure and the hydrogen are no longer assumed to share the same temperature. Instead, a separate energy balance governs the solid temperature T_s, which exchanges heat with the hydrogen via natural convection:

$$\dot{Q}_s = \alpha_s \cdot A_i \cdot (T_s - T) \tag{3.10}$$

Second, the specific enthalpy of the extracted mass flows is refined in the two-phase region. Rather than assuming all streams carry the enthalpy h of the ideally mixed tank content, it is assumed that only saturated liquid leaves during discharge (h_{disch}) and only saturated vapor is vented during dormancy (h_{vent}). In the single-phase region, both reduce to h, recovering the assumption of Hamacher [29].

Third, the energy balance is reformulated explicitly for the hydrogen temperature T, making each contributing term physically interpretable:

$$\begin{aligned} Mc_v \frac{\mathrm{d}T}{\mathrm{d}t} = &\dot{M}_{\text{fuel}}(h_{\text{fuel}} - h) - \dot{M}_{\text{vent}}(h_{\text{vent}} - h) - \dot{M}_{\text{disch}}(h_{\text{disch}} - h) + \\ &+ \frac{T}{\varrho}\left(\frac{\partial p}{\partial T}\right)_{\varrho}\left(\dot{M}_{\text{fuel}} - \dot{M}_{\text{disch}} - \dot{M}_{\text{vent}}\right) + \dot{Q}_s + \dot{Q}_{\text{disch}} \end{aligned} \tag{3.11}$$

In the two-phase region, c_v and $(\partial p/\partial T)_{\varrho}$ are replaced by the specific isochoric two-phase heat capacity c_{v2P} and the saturation pressure derivative $\mathrm{d}p_{\text{sat}}/\mathrm{d}T$ from REFPROP [28], preserving the equation structure across all phases without switching.

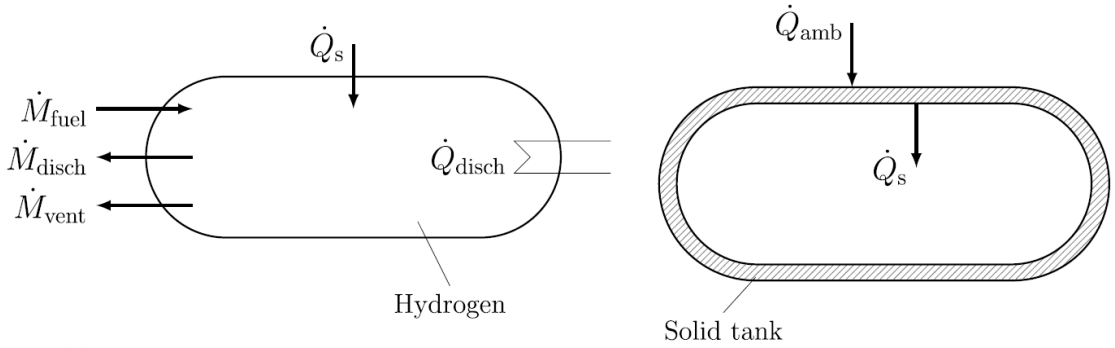

(a) Hydrogen system control volume

(b) Solid system control volume

Figure 3.5: System control volumes of hydrogen and the solid tank

Having established the theoretical framework of both reference models, the following discussion focuses on the **discharge scenario**, which represents the core of the defuelling validation carried out in this thesis. Table 3.3 summarizes the parameters used by Stops et al. [23] for the sLH2 discharge case and the corresponding values adopted in the GT-SUITE model. The two setups are largely equivalent, with the main difference lying in the thermal boundary conditions.

Table 3.3: Parameters used for the sLH2 tank system: comparison between Stops et al. [23] and the GT-SUITE model.

Parameter	**Stops et al.**	**GT-SUITE**
Hydrogen type	para	para
Tank volume V_{tank} in m^3	0.5	0.5
Inner tank area A_i in m^2	4.0	4.0
Aluminum mass M_{alu} in kg	50	adiabatic
Ambient temperature T_{amb} in K	298.15	298.15
Minimum pressure p_{min} in bar	6	6
Ideal stop density ϱ_{stop} in kg/m^3	2.4	2.4
Discharge mass flow $\dot{M}_{disch}$ in g/s	1	1

Regarding the thermal boundary conditions, a direct replication of the heat transfer coefficient approach used by Stops et al. was not straightforward in GT-SUITE, as the reference model computes the heat leak through a single lumped coefficient k_{amb} applied to the outer tank area, without explicitly modelling internal convection or radiation. The reference paper reports a typical heat leak of approximately 5 W for the sLH2 tank, consistent with:

$$\dot{Q}_{amb} = k_{amb} \cdot A_o \cdot (T_{amb} - T) = 0.005 \cdot 4.1 \cdot \Delta T \approx 5\,\mathrm{W} \tag{3.12}$$

To replicate this condition in GT-SUITE, the tank was configured as **adiabatic** with a constant heat leak of $\dot{Q}_{amb} = 5\,\mathrm{W}$ applied directly to the hydrogen, avoiding the

need to model natural convection (and radiation) explicitly, which would introduce additional unknowns not reported in the reference paper.

During the discharge scenario for sLH2, the tank pressure drops rapidly as hydrogen is extracted, reaching the minimum operative pressure $p_{\min} = 6\,\text{bar}$ relatively quickly. At this point, the internal heat exchanger is activated to maintain the pressure at $p_{\min}$. As the hydrogen subsequently enters the two-phase region, both pressure and temperature remain nearly constant, and the heat requirement drops to a lower, roughly constant value, as only the evaporation enthalpy needs to be supplied to sustain the phase change. Once all liquid hydrogen has evaporated and the tank returns to a single-phase gaseous state, the heat requirement rises again as the hydrogen must be heated further to maintain the minimum pressure.

In the reference model of Stops et al. [23], the required heat flow $\dot{Q}_{\text{disch}}$ is computed analytically from the energy balance at each time step. In the GT-SUITE implementation, a **PID controller** was adopted instead to regulate the heat input from the internal heat exchanger, targeting $p_{\min}$ as the controlled variable. This approach does not reproduce the exact instantaneous heat flow values of the reference model, but provides a more physically realistic and flexible representation of the heat exchanger behavior, closer to how an actual system would operate in practice. Furthermore, it makes the model readily extensible to future analyses involving variable discharge rates or more complex drive cycles, where a fixed analytical heat flow would no longer be applicable.

3.4 Nozzle

The fuelling nozzle is the terminal component of the HRS dispensing line and constitutes the physical interface between the stationary fuelling infrastructure and the onboard liquid hydrogen (LH2) storage system of the vehicle. Its primary function is to establish a secure, leak-tight, and thermally conditioned flow path through which cryogenic liquid hydrogen is transferred from the station dispenser into the vehicle tank during the refuelling event [30].

In the context of liquid hydrogen fuelling for heavy-duty trucks, the nozzle and its associated receptacle on the vehicle side collectively form the *fuelling interface*, which must satisfy simultaneous requirements of hydraulic efficiency, thermal integrity, mechanical robustness, and operational safety.

Because liquid hydrogen is stored at a temperature of approximately only a few degrees above absolute zero, $-253\,^{\circ}\mathrm{C}$ (20 K), the nozzle operates under the most extreme cryogenic conditions of any component in the refuelling circuit [30]. Any inadequacy in the hydraulic or thermal design of the nozzle propagates directly into the thermodynamic state of the fluid delivered to the tank, thereby affecting the achievable fill mass, fill time, and the extent of flash evaporation within the storage vessel.

3.4.1 Key Design Parameters of a Cryogenic LH_2 Nozzle

The performance of a liquid hydrogen fuelling nozzle is governed by four principal categories of parameters: hydraulic resistance, thermal insulation and heat leak, coupling and sealing integrity, and material compatibility with cryogenic hydrogen. Each is discussed in turn below.

3.4.1.1 Hydraulic Resistance and Pressure Drop

As the fluid flows through the internal passages, valves, and restrictions of the nozzle body, it experiences a pressure drop $\Delta p_{\mathrm{nozzle}}$ that scales with the square of the volumetric flow rate. This relationship is governed by:

$$\Delta p_{\mathrm{nozzle}} = \frac{1}{2\rho}\left(\frac{\dot{m}}{C_d\, A_{\mathrm{ref}}}\right)^2 + \sum_k f_k \frac{L_k}{D_k}\frac{\rho u_k^2}{2} \tag{3.13}$$

where the first term captures the concentrated losses at any orifice-like restriction (governed by the discharge coefficient C_d and reference area A_{ref}), and the second term accounts for distributed frictional losses along the internal flow passages of hydraulic diameter D_k, length L_k, and mean velocity u_k, with f_k denoting the Darcy–Weisbach friction factor [31]. The net pressure drop across the nozzle reduces the available driving pressure at the tank inlet and can, if excessive, limit the

achievable mass flow rate during refuelling. Accurate characterization of Δp_{nozzle} as a function of $\dot{m}$ is therefore a prerequisite for correct system-level simulation.

It should be noted that the effective discharge coefficient of a cryogenic nozzle may exhibit a dependence on the mass flow rate, owing to Reynolds-number-dependent variations in the internal flow regime and the degree of flow separation at internal restrictions. This flow-rate dependence must be accounted for when constructing a look-up map of $C_d(\dot{m})$ for use in one-dimensional simulations.

3.4.1.2 Thermal Insulation and Heat Leak

The large temperature difference between the liquid hydrogen inside the nozzle (around 20 K) and the surrounding environment (around 293 K) creates a significant driving force for heat leak. Without adequate thermal insulation, this unwanted heat gain can partially or fully vaporize the liquid hydrogen before it even reaches the tank, compromising the quality of the delivered fluid and potentially triggering two-phase flow instabilities in the upstream line. Several insulation techniques are commonly used to address this challenge, and these are introduced below.

- **Vacuum-jacketed construction**: The inner fluid-wetted passage is enclosed within an outer jacket, with the annular space evacuated to pressures below 10^{-3} mbar. Vacuum insulation suppresses all three modes of heat transfer simultaneously; a 25 mm thick vacuum jacket provides thermal performance approximately 40 times superior to an equivalent thickness of foam insulation [32]. Modeled nozzle has vacuum-jacketed insulation in its construction.
- **Multi-layer insulation (MLI)**: Alternating layers of aluminized Mylar and low-conductivity spacer material are installed within the vacuum annulus to further suppress radiative heat transfer between the warm outer jacket and the cold inner pipe [15].

Due to the presence of insulation, a certain amount of heat leak $\dot{Q}_{\text{nozzle}}$ persists through the nozzle body, which can affect the enthalpy and hydrogen quality at the nozzle outlet. In this study, constant heat input which was provided by Manntek, is implemented in the model.

3.4.2 The Manntek LH2 Fuelling Nozzle

Manntek is one of the collaborating partners in this project and provided the nozzle used for system modelling in the refuelling simulations. The company is a globally recognized supplier of coupling solutions for cryogenic, gas, and chemical fluid handling applications, with over a decade of specialized expertise in cryogenic gas couplings [33].

Manntek also played a central role in the development of the world's first sub-

cooled liquid hydrogen (sLH2) refuelling station, and has been an active contributor to international standardization efforts for LH_2 truck fuelling interfaces under ISO auspices [34].

The Manntek LH2 is a pneumatically operated dry-disconnect coupling with a nominal diameter of DN20, designed for liquid hydrogen refuelling in cryogenic conditions on the vehicle side [34]. This nozzle has vacuum insulation in the fluid passageway and connection area, which minimizes heat transfer to the refuelling system and prevents the formation of condensation on external surfaces. Also, the operation of its internal valves is done pneumatically and under the control of the PLC of the fuelling station, so that it is possible to establish a connection with just one simple movement by the driver, and there is no need for specialized training of the operator [33]. In addition, the nozzle is stored in a heated enclosure when not in use, which prevents ice formation and keeps it at the proper temperature for refuelling operations [34].

In order to use this equipment in the 1D model of the refuelling system in GT-SUITE, Manntek provided two dedicated datasets for this nozzle to the project. The first dataset includes a pressure drop versus mass flow rate map obtained through experimental nozzle characterization, and the second dataset is an estimate of the steady-state thermal leakage calculated based on a dedicated thermal analysis of the nozzle assembly. The method of using this dataset in developing a 1D equivalent model for the nozzle in GT-SUITE, as well as the optimization process used to determine the equivalent discharge coefficient in the forward flow direction, will be presented in detail in the following sections.

3.4.2.1 Geometric Simplification of the Nozzle

The three-dimensional geometry of the Manntek nozzle was initially made available as a detailed CAD model. Directly resolving the internal flow field of such a complex geometry within a one-dimensional system simulation framework is not feasible; GT-SUITE operates on a network of lumped and one-dimensional flow elements rather than discretized three-dimensional volumes. Accordingly, an equivalent one-dimensional representation of the nozzle was developed through a two-step simplification procedure.

In the first step, the three-dimensional geometry was simplified with a straight pipe segment, and an orifice element. In the second step, a GT-SUITE sub-model was assembled, consisting of an inlet flow boundary condition, a pipe element connected in series to an orifice element, and an outlet flow boundary condition, as illustrated schematically in Figure 3.6 which is the standard model for optimization.

Figure 3.6: Schematic of the one-dimensional GT-SUITE sub-model for Manntek nozzle characterization

3.4.2.2 GT-SUITE Optimization Framework

In this study, model calibration is performed using the integrated optimization framework of GT-SUITE. The objective is to tune a set of uncertain model parameters, referred to as factors, such that the simulation outputs (responses) match experimental or reference data.
The calibration problem is formulated as an optimization problem in which model parameters are adjusted to minimize the discrepancy between simulated and target responses.

In this study, the GT-SUITE Integrated Design Optimizer was used to calibrate the discharge coefficient of the nozzle in the 1D model. The optimization was set up as a Single Objective problem, where the goal was to match the simulated pressure drop across the nozzle to the values provided by the supplier. Since the supplier data consists of pressure drop values at discrete mass flow rates, each mass flow rate was treated as a separate case and optimized independently.

The only factor varied during the optimization was the forward discharge coefficient of the nozzle. This parameter controls the effective flow area of the nozzle and has a direct influence on the pressure drop. By adjusting this coefficient, the optimizer was able to tune the model so that the simulated pressure drop matches the supplier data at each mass flow rate.

The response RLT was the pressure drop across the nozzle, and the objective was set to Target. This means the optimizer minimized the following objective function at each case:

$$f = (R - R_{\text{target}})^2 \tag{3.14}$$

where R is the simulated pressure drop and R_{target} is the corresponding target value from the supplier data. The optimizer iteratively adjusted the forward discharge coefficient until f was driven as close to zero as possible, meaning the simulated and supplier pressure drops were in good agreement.

The search algorithm used was the Accelerated Genetic Algorithm (Accelerated GA), which is a modified version of the standard Genetic Algorithm (NSGA-III). Compared to the standard version, the Accelerated GA uses fast metamodelling between generations to find better solutions in fewer iterations, making it a more efficient choice for non-linear calibration problems such as this one. The population size was left at the default value (`def`), which is automatically set based on the number of factors, and the number of generations was set to 15. As a result, the total number of designs evaluated by the optimizer was equal to the population size multiplied by 15.

Two additional settings were enabled to improve computational efficiency. The Faster Runtime option was turned on, which runs all optimization designs within a single solver process instead of launching a new process for each design, reducing the computational overhead considerably. The Automatic Data Suppression option was also activated, which suppresses all unnecessary output data, such as Time RLTs, plots, and animation files, during the optimization, keeping file sizes small and improving the overall speed of the process.

3.4.3 Calibration of the Equivalent Forward Discharge Coefficient

The pressure drop across the orifice element in GT-SUITE is governed by the standard orifice flow relation [35]:

$$\Delta p = \frac{1}{2\rho}\left(\frac{\dot{m}}{C_{d,\mathrm{fwd}}\, A_{\mathrm{ref}}}\right)^2 \tag{3.15}$$

where Δp is the pressure drop across the orifice, ρ is the local fluid density, $\dot{m}$ is the mass flow rate, A_{ref} is the reference cross-sectional area of the orifice, and $C_{d,\mathrm{fwd}}$ is the forward discharge coefficient. This dimensionless parameter accounts for the contraction of the flow stream and the viscous losses at the orifice restriction; it ranges from zero to unity, with higher values corresponding to lower hydraulic resistance.

Because the simplified one-dimensional model does not resolve the three-dimensional internal geometry of the Manntek nozzle in detail, $C_{d,\mathrm{fwd}}$ was treated as an unknown calibration parameter whose value was determined by matching the simulated pressure drop to the reference data provided by Manntek. To account for the possible flow-rate dependence of the effective discharge coefficient, due to changes in the internal flow regime and separation patterns within the nozzle, the calibration was performed independently at multiple operating points spanning the expected mass flow rate range of the fuelling process. These mass flow rates were provided by the manufacturer and made available for use in this study.

The calibration procedure was automated using the GT-SUITE integrated optimizer. For each target mass flow rate $\dot{m}_i$, the optimizer was tasked with finding the value of $C_{d,\mathrm{fwd}}$ that minimized the following scalar objective function:

$$\mathcal{F}(C_{d,\mathrm{fwd}}) = |\, \Delta p_{\mathrm{sim}}(C_{d,\mathrm{fwd}},\, \dot{m}_i) - \Delta p_{\mathrm{ref},i}\,| \tag{3.16}$$

where Δp_{sim} is the pressure drop predicted by the GT-SUITE nozzle sub-model and $\Delta p_{\mathrm{ref},i}$ is the corresponding reference pressure drop from the Manntek dataset at the same operating point. The optimization was carried out for each mass flow rate point independently, yielding a discrete map of $C_{d,\mathrm{fwd}}$ as a function of $\dot{m}$. This map was subsequently incorporated into the full-system GT-SUITE model as a look-up table, enabling the nozzle pressure drop to be predicted accurately across the entire operating range without altering the physical geometry representation.

3.5 Tank Properties

This section describes the geometry and material properties adopted for the onboard storage tank in the models that reproduce real operating conditions, namely the refuelling and the (two-tank) defuelling models. These properties were chosen to make the tank model as realistic as possible. The validation models, by contrast, follow the geometry and thermal treatment of their respective reference studies, as described in the corresponding sections.

The onboard storage tank geometry consists of a cylindrical section with hemispherical ends on both sides. Based on the assumed length-to-diameter ratio of $L/D = 3.5$, the internal tank length and diameter are estimated to be 2.3 m and 0.66 m, respectively. Each tank has a volume of 0.71 m^3 and can carry 44 kg of $\mathrm{LH_2}$ at 100% SoC. The volume was determined from the designed capacity of 44 kg of $\mathrm{sLH_2}$ at a density of 62 $\mathrm{kg/m^3}$, corresponding to a pressure of 16 Bar and a temperature of 29 K. The tanks are installed horizontally, consistent with the configuration used on the truck.

The heat transfer between the hydrogen, the tank wall and the surrounding environment has a significant influence on the thermodynamic behavior of the stored fluid, and therefore on both the defuelling and the refuelling processes. For this reason, in the models that aim to reproduce real operating conditions (Sections 4.3 and 4.4), the tank wall and the insulation layer are modelled explicitly through their physical properties, rather than relying on an adiabatic assumption or a prescribed heat-flux boundary condition.

An adiabatic assumption would be unrealistic and would lead to unreliable predictions of the pressure and temperature evolution inside the tank.

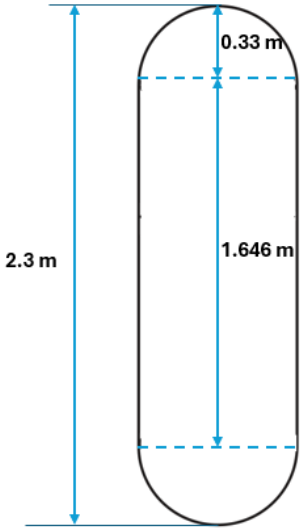

Figure 3.7: Tank geometry

Obtaining suitable material properties for a real sLH2 truck tank proved challenging. The tank manufacturers were contacted directly, but exact specifications were not available. Reliable data specific to liquid hydrogen truck tanks are also extremely scarce in the open literature. For this reason, the wall and insulation were modelled on the basis of aerospace cryogenic hydrogen tank data, in particular from NASA experimental liquid hydrogen storage tanks, which represent one of the few well-documented references for this type of system. This choice was further supported by a review of the literature on cryogenic hydrogen storage, discussed in Section 2.1.3.

The resulting material assumptions are summarised below:

- **Tank shell:** aluminium, selected for its combination of high structural strength, low density and good performance at cryogenic temperatures.
- **Insulation layer:** multilayer insulation (MLI) with a thickness of 20 mm and an effective thermal conductivity $k_{\text{eff}} = 9 \times 10^{-4}$ W/m $\cdot$ K, consistent with values reported in the literature for cryogenic hydrogen storage systems and in line with typical insulation standards used in heavy-duty truck applications [18, 16].

While modelling the tank on the basis of an aerospace reference is a simplifying assumption, it provides a physically reasonable basis for capturing the thermal behavior of the system within the scope of a 1D modelling approach.

4

Simulation

This chapter presents the implementation of the two simulation models developed in this thesis: a defuelling model and a refuelling model. The two models are closely linked: the defuelling model is run first to determine the thermodynamic state of the onboard tank at the end of a driving cycle, and its output is then used as the initial condition for the refuelling model. This sequential approach allows the refuelling process to be simulated under physically consistent starting conditions, rather than arbitrary assumptions.

Since the minimum operative pressure is fixed at 6 bar (the minimum inlet pressure required for proper fuel cell operation), the only parameter that varies at the start of refuelling is the state of charge of the onboard tank, which is directly determined by the hydrogen density and, consequently, by the tank temperature at the end of the defuelling process. The ultimate objective is therefore to identify the initial temperature condition that maximises the amount of liquid hydrogen transferred into the onboard tank during refuelling, thereby maximising the usable hydrogen available for the subsequent driving cycle and extending the effective range of the vehicle.

For each model, the system architecture, component configuration, boundary conditions, and control strategies are described, followed by the validation results and a discussion of the agreement with the reference data.

4.1 Refuelling validation

Two different refuelling models are considered in this work. The first model is developed for validation purposes, while the second is the in-house refuelling model implemented after completion of the defuelling analysis.

For the validation study, the refuelling system presented by Molkov et al. [22] is implemented. The validation is carried out by comparing the predicted pressure and temperature profiles with the results reported in the reference study.

4.1.1 System Description

Based on the reference article which is explained in Chapter 3, the refuelling system consists of an LH_2 station tank, pump, breakaway coupling, hose, nozzle, pipes, and two on-board storage tanks.

The onboard storage tank geometry is the same as described in Section 3.5, with an internal length of 2.3 m, a diameter of 0.66 m and a volume of 0.71 m^3. In this validation model, however, the tank walls are modelled as stainless steel with a thickness of 3 mm, following the reference study [22], rather than the aluminium shell and MLI insulation adopted for the real-operation models. The other elements are described in the methods chapter.

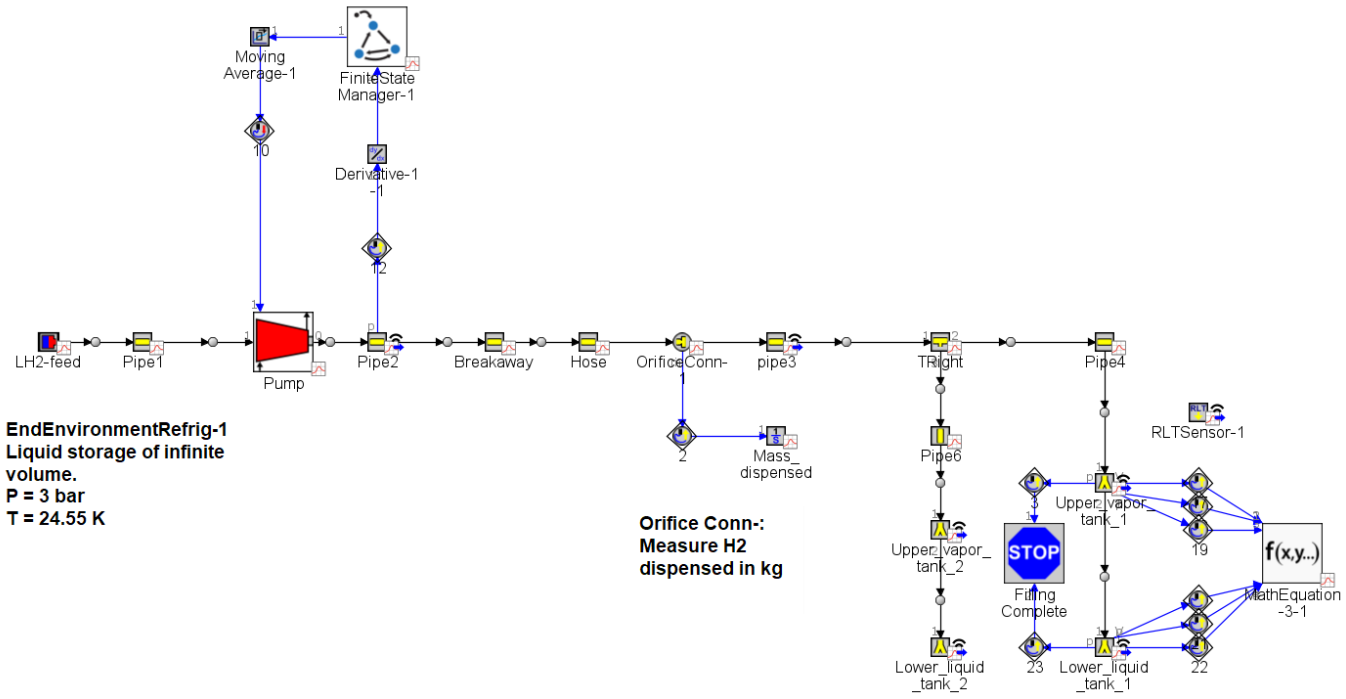

Figure 4.1: Sub-liquid hydrogen refuelling system layout in GT-SUITE.

The dimensions of the system components are presented as in Table 4.1.

Table 4.1: Geometrical dimensions and thermal boundary conditions of the liquid hydrogen fueling line components used in the GT-SUITE model.

	HRS Reservoir	**Pipe 1**	**Pipe 2**	**Breakaway**	**Hose**	**Pipe 3**	**Pipe 4**	**Pipe 5**	**Tanks**
Length [m]	–	5.7	3.4	0.3	2.0	3.7	0.7	0.1	2.3
Diameter [m]	–	0.025	0.025	0.025	0.025	0.025	0.025	0.025	0.6
Thickness [mm]	–	2	2	2	2	2	2	2	3
Pressure [bar]	3	3	6	6	6	6	6	6	6
Temperature [K]	24.55	24.55	88	88	88	88	88	88	28.25
Heat Flux [W/m^2]	–	0.6	0.6	636.6	0.6	0.6	0.6	0.6	1
Discretization Length [cm]	–	10	10	10	10	10	10	10	–

4.1.2 Modelling Assumptions

Due to a limitation of 1D modelling, several assumptions are made and presented in this section.

- **Refuelling station condition**
  In the current simulation the refuelling station is modeled as a boundary condition with pressure and temperature. The initial conditions of the fluid upstream of the pump are also assumed to be nearly identical to those reported in the reference study. However, the inlet temperature is set to 24.55 K instead of 24.68 K because GT-SUITE cannot initiate a simulation at the exact saturated condition.

  Also there is another possibility to define boundary condition with pressure or temperature and enthalpy. This adjustment does not significantly affect the simulation results, as the reference study neither modeled the flow upstream of the pump nor included the pump itself in their 3D CFD analysis. Therefore, this assumption is not expected to introduce any meaningful deviation in the overall modelling results.

- **Material properties and wall heat transfer**
  The reference article provides information only about the metallic components of the tank and does not report the thermal properties or conductivity of the insulation layer, and implemented the heat input for each component.

  Therefore, several assumptions were made in the present study to consider the heat transfer. Specifically, external convective and radiative heat-transfer effects were neglected by setting both the convection heat-transfer coefficient and radiative heat-transfer rate to zero. Instead, the heat flux reported in the reference article was directly applied as a heat input to the system. Under these assumptions, the model accounts for conductive heat transfer through the tank wall and convective heat transfer within the fluid inside the tank.

This approach allows the thermal behavior of the system to be represented while remaining consistent with the information available in the reference study. Also, the pipes and tanks were modeled with a stainless steel layer, allowing their thermal mass and cooling behavior to be captured during the refuelling process.

- **Nozzle**
  In the validation model, the nozzle was modeled as an orifice with a forward discharge coefficient equal to 1.0 and a reverse discharge coefficient equal to 0.0 to avoid revere flow in the nozzle.

- **Pump**
  In the reference study, liquid hydrogen is pressurized by a pump to approximately 20 bar and then expands through the downstream piping until it reaches the pressure level set by the vehicle tank conditions. Replicating this exact pressure behaviour was not the objective of the present work; instead, the pump is modelled through the `ImposedFlowRefrig` component, which prescribes the mass flow rate as an external input.

  The mass flow rate is controlled by the State Manager according to the active refuelling phase, while the isentropic efficiency is set to the reference value of 0.65. Based on the imposed flow rate, the inlet conditions and this efficiency, the component computes the corresponding pump outlet state, providing a more realistic representation of the pump behaviour while ensuring consistency with the mass transfer rates reported in the reference study.

- **Mass Flow rate**
  In the present simulation, the mass flow rate in different phases of the refuelling is mentioned in the Table 3.2. The refuelling process was assumed to start with a mass flow rate of 20 g/s, rather than 0 g/s as specified in the reference study. Similarly, at the end of the refuelling process, the mass flow rate was reduced to 20 g/s, and the simulation was terminated once the tank pressure reached 1.6 MPa (16 bar).

  These modifications were introduced for the implementation of the simulation and are not expected to significantly affect the overall results. Any discrepancies compared with the reference study are therefore expected to be minor.

4.1.3 Initial and Boundary Conditions

The initial and boundary conditions used in the present model are derived from reference CFD study by [22] and can be summarized as Table 4.2. The components

lying between the pump and the onboard storage tanks are first seeded with gaseous hydrogen at 88 K, which is significantly higher than the critical temperature of hydrogen (33.2 K). This condition represents the pre-heated state of the piping system prior to the commencement of the refuelling process.

Heat transfer through the insulated walls is modeled using prescribed heat flux boundary conditions, as summarized in Table 4.1.

Table 4.2: Initial and boundary conditions of the LH2 refuelling system [22]

Parameter	Value	Unit
HRS pressure	0.3	MPa (abs)
HRS temperature	24.5	K
Initial pipe temperature	88.0	K
Initial pipe pressure	0.6	MPa (abs)
Initial onboard tank pressure	0.6	MPa (abs)
Initial onboard tank temperature	28.25	K
Initial LH2 fill level (volumetric)	35	%
Target final pressure	1.6 ± 0.05	MPa

4.1.4 Solver

The numerical solver settings employed in the GT-SUITE simulation were configured to ensure both physical accuracy and computational stability for the two-phase cryogenic hydrogen refuelling process.
Table 4.3 presents the key solver setting.

4.1.4.1 Time Control

The simulation was run in continuous transient mode with the automatic steady-state shut-off disabled, since the refuelling process is inherently transient and does not converge to a steady state. A fixed time step of 0.05 s was selected, which was found to provide a satisfactory balance between temporal resolution and computational efficiency for the flow rates and pressure dynamics encountered in the LH_2 refuelling process.

4.1.4.2 Flow Solver Settings

The flow loss model was set to Automatic, allowing GT-SUITE to select the appropriate friction and heat transfer correlations based on the local flow regime. The time step and solution control were set to `implicit_user`, activating the implicit solver with user-defined tolerances. This is particularly important for cryogenic two-phase flows, where strong coupling between the pressure and enthalpy fields

can cause numerical stiffness.

The implicit solver was configured in Standard mode, with both Compressible Flow Enhancement and Additional Relaxation for Stiff Fluids enabled. These options improve convergence stability when large density gradients are present, as is the case near the liquid–vapour saturation boundary of hydrogen.

4.1.4.3 Thermal Solver

The thermal wall solver was set to transient mode, which computes the time-dependent temperature distribution within the pipe and tank walls. This is essential for correctly capturing the cool-down of the warm transfer line components during the start-of-fueling phase, where the thermal mass of the nozzle, hose, and piping significantly influences the pressure and temperature evolution in the vehicle tank.

4.1.4.4 Convergence Tolerances

The convergence tolerances were set as follows: pressure residual tolerance 1×10^{-4}, energy residual tolerance 1×10^{-4}, Continuity residual tolerance 1×10^{-4}, absolute pressure tolerance 5 Pa, absolute flow rate tolerance 1×10^{-3} kg/s, and absolute temperature tolerance 5×10^{-3} K. The maximum number of iterations per time step was set to 1000, and the linear equation solver convergence criterion was set to 1×10^{-10}. The tolerance values mentioned were used in the initial stage of development and validation of the refuelling model. Since the duration of the refuelling simulation was about 12 minutes, no significant mass imbalance was observed during the simulation, therefore, a comprehensive sensitivity study on the residual tolerance of the continuity equation was not deemed necessary at this stage.

Next, a more detailed assessment of the effect of the residual tolerance of the continuity equation was performed using the defuelling model, which is described in Section 4.2.1. Unlike the refuelling case, the defuelling simulation had a much longer physical duration (about 9 hours) and was therefore more sensitive to the accumulation of numerical errors related to mass conservation.

Table 4.3: Summary of GT-SUITE solver settings for the LH2 refuelling validation simulation.

Parameter	**Value**
Time Control	
Time control mode	Continuous transient
Time step	0.05 s
Maximum iterations/step	1000
Steady-state auto shut-off	Off
Flow Solver	
Flow loss model	Automatic
Solution control	Implicit (user-defined)
Implicit solver method	Standard
Compressible flow enhancement	On
Relaxation for stiff fluids	On
Thermophysical Model	
Mixture viscosity weighting	Mass-weighted
Energy equation conduction	Enabled
Thermal wall solver	Transient
Convergence Tolerances	
Pressure residual	1×10^{-4}
Energy residual	1×10^{-4}
Continuity residual	1×10^{-4}
Pressure (absolute)	5 Pa
Flow rate (absolute)	1×10^{-3} kg/s
Temperature (absolute)	5×10^{-3} K
Linear solver criterion	1×10^{-10}

4.1.5 Challenges and mitigation strategy

As noted in the methodology section, GT-SUITE does not support separate thermodynamic property calculations for the liquid and vapor phases when modelling a two-phase fluid. This creates a challenge when comparing simulation results against the reference study, which reports distinct temperature profiles for each phase.

modelling the tank as a single flow-split element is not sufficient to resolve this, since the temperature and pressure outputs from a single element represent mixture-averaged values rather than phase-specific ones. Other tank modelling approaches available in GT-SUITE, including the three-dimensional tank element, were also tested, but none produced any meaningful difference in the results.
To work around this limitation, the tank was represented using two separate flow-split elements: one for the liquid phase and one for the vapor phase which is shown

in Figure 4.2.

The volume of the liquid flow-split was set to match the actual liquid volume inside the tank, which is approximately 35% of the total tank volume, while the remaining 65% was assigned to the vapor flow-split. Each element was given appropriate initial conditions: a vapor quality of zero for the liquid flow-split, representing saturated liquid, and a vapor quality of one for the vapor flow-split, representing saturated vapor.

In the liquid region, the fluid remains in a purely liquid state throughout the refuelling process, so no phase change occurs there. In the vapor region, flash vaporization takes place during the early stages of refuelling, as the sudden introduction of cold liquid causes a rapid drop in temperature and pressure within the vapor space. As refuelling continues, the rising liquid level gradually occupies the volume initially assigned to the vapor flow-split, which is consistent with the physical behavior of the tank during filling. While this two-element approach carries certain inherent limitations, it provides a reasonable approximation for the purposes of this study. These limitations are discussed further in the results section.

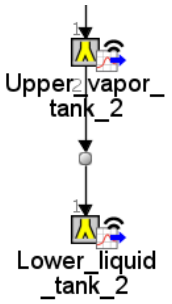

Figure 4.2: Two flow-split tanks for modelling the two phase flow tank in GT-SUITE

4.2 Defuelling validation

As explained in the Methods chapter 3.3, the defuelling model is validated against the 0D lumped-parameter framework by Stops et al. [23], adopted as a reference since detailed numerical or experimental data for sLH2 discharge are scarce in the literature. From that work, the discharge scenario is used to determine the thermodynamic state of the hydrogen in the onboard tank at the end of a driving cycle, which in turn provides the initial condition for the subsequent refuelling simulation. The validation is carried out by comparing the density-temperature evolution of the tank, together with the heat input required to sustain the minimum operative pressure, against the values reported by Stops et al. [23] for the sLH2 case.

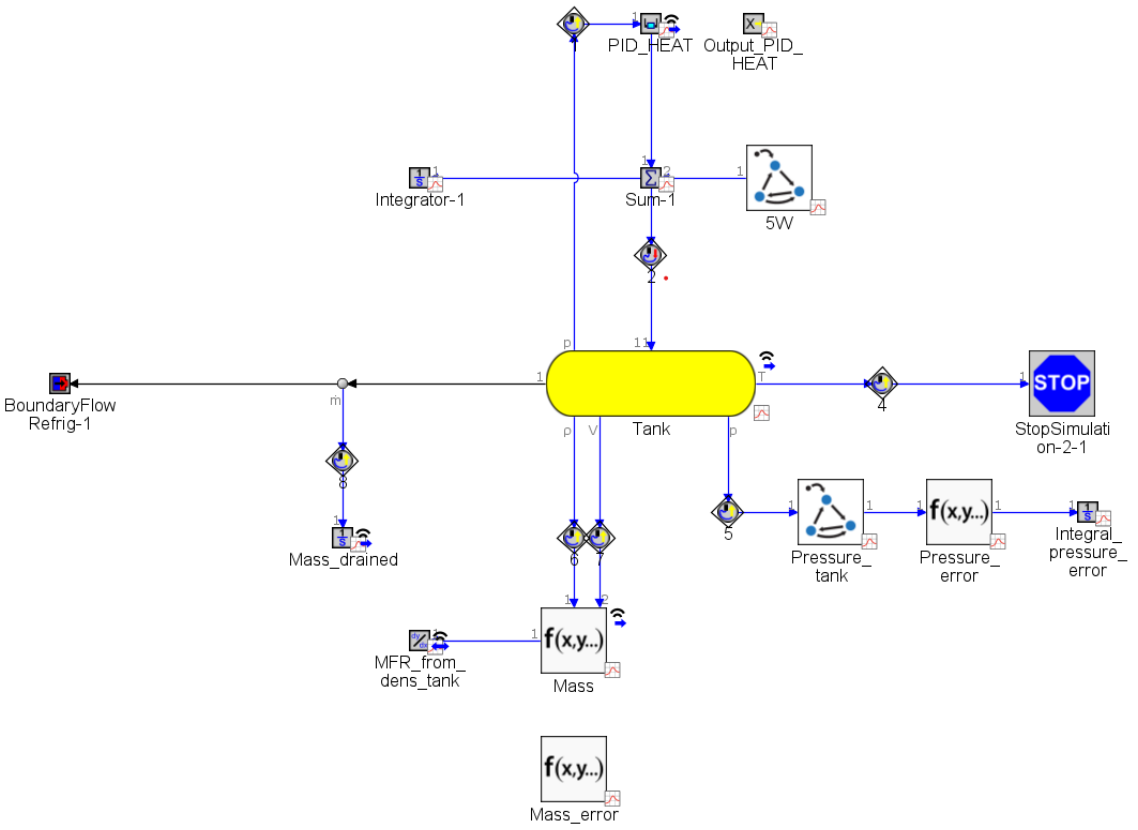

Figure 4.3: defuelling validation model in GT-SUITE

4.2.1 System Description

The defuelling validation model is intentionally kept simple, since its only purpose is to reproduce the discharge behaviour described by Stops et al. [23]. It consists of a single tank element connected to a BoundaryFlow that extracts hydrogen at a fixed rate. A single tank component is sufficient here because the tank starts in a

single dense supercritical state: the initial pressure is above the critical pressure of hydrogen ($p_{\mathrm{crit}} \approx 12.96$ bar), so the fluid is a single phase with no separate vapour volume to be modelled at the beginning of the simulation, unlike in the refuelling case.

The tank geometry and the reference parameters are those already listed in Table 3.3 of Section 3.3, namely a volume of 0.5 m^3, an inner area of 4.0 m^2 and parahydrogen as the working fluid. Hydrogen is drained through the BoundaryFlow at the imposed discharge rate $\dot{M}_{\mathrm{disch}}$, and the simulation is terminated once the tank reaches the temperature corresponding to the ideal stop density $\varrho_{\mathrm{stop}} = 2.4\ \mathrm{kg/m}^3$ at the operative pressure. The rationale for using a temperature-based stop criterion is discussed in Section 4.3.2.

The minimum operative pressure is maintained by an internal heat exchanger whose heat input is regulated by a PID controller, visible in Figure 4.3 as the `PID_HEAT` block; its output is added to the constant 5 W heat leak through the `Sum` block before being applied to the tank. The tuning of this controller is described in Section 4.2.2.1.

The remaining components shown in Figure 4.3 are auxiliary monitoring blocks: together they compute the two error metrics used to assess the numerical accuracy of the model, described below.

- `Mass_error`: it evaluates the difference between the mass actually drained from the tank (`Mass_drained`) and the change of mass inside the tank, computed as the variation in density multiplied by the fixed tank volume. This check is necessary because the residual of the continuity equation can have a significant cumulative effect: since the simulation runs over a long physical time (approximately 9 hours), even a very small per-step error can accumulate into a noticeable mass imbalance.

  As shown in Figure 4.4, the choice of the continuity residual tolerance has a strong effect on mass conservation over the long physical duration of the simulation. Loose tolerances (1×10^{-4} to 1×10^{-5}) lead to an accumulated mass error of more than 13 kg by the end of the discharge, which is clearly unacceptable. Tightening the tolerance progressively reduces this error, until it becomes negligible for values of 1×10^{-8} and below. Beyond this point no further improvement in mass conservation is observed, as the curves for 1×10^{-8}, 1×10^{-9} and 1×10^{-10} essentially coincide. With the selected tolerance of 1×10^{-8}, the accumulated mass imbalance at the end of the discharge remained around 38 g, which is negligible compared to the total discharged mass.

At the same time, requiring an increasingly strict residual makes the implicit solver more likely to fail to converge within the allowed iterations during the two-phase transients, consistent with the convergence difficulties already discussed in Section 3.1.2. A continuity residual of 1×10^{-8} was therefore selected as the best compromise between mass conservation accuracy and numerical robustness.

- `Integral_pressure_error`: it measures the deviation of the tank pressure from the target value (6 bar) and integrates it over time, so that the overall ability of the controller to hold the minimum operative pressure can be quantified, and the controller tuned accordingly.

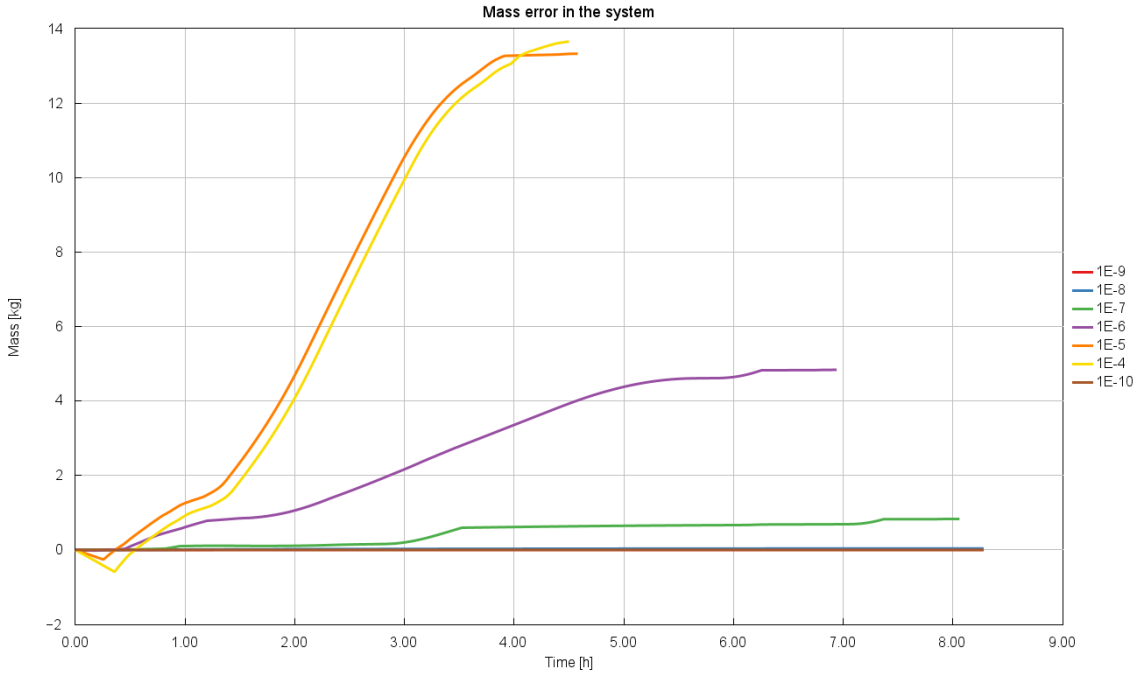

Figure 4.4: Continuity residual sensitivity analysis

4.2.2 Modelling Assumptions

The modelling rationale and the governing equations of the defuelling model have already been presented in Section 3.3. This section focuses only on the assumptions and choices that are specific to the simulation setup in GT-SUITE.
Regarding the end of the discharge, although Stops et al. [23] define it through the ideal stop density $\varrho_{\text{stop}} = 2.4$ kg/m^3, density cannot be measured directly on board a real vehicle, whereas temperature can. The stop condition was therefore set on the tank temperature corresponding to ϱ_{stop} at the operative pressure, namely $T \approx 57$ K, so that the model relies on a practically measurable variable while still reproducing the discharge end-point of the reference.

A further difference with respect to Stops et al. [23], who model the aluminium tank structure as a separate thermal mass ($M_{\mathrm{alu}} = 50$ kg) with its own energy balance, concerns the treatment of the solid structure: in the present model the tank is assumed adiabatic and the solid thermal mass is not resolved explicitly. This choice is motivated by several considerations. It is first of all in line with the general aim of keeping the validation model as simple as possible.

In addition, during discharge the PID controller actively regulates the heat injected into the tank in order to maintain a constant pressure. The heat exchanged with the wall, which initially shares the hydrogen temperature and gradually warms up as the pressure is held constant, would in principle be a correct contribution to include, but its influence is minor: any such heat would simply be compensated by the controller adjusting its own heat input. Moreover, the wall contribution is small compared to the heat added by the PID, because the hydrogen is extracted slowly. The process is not a fast transient, so the wall has enough time to warm up and remain close to the hydrogen temperature. The solid structure is instead accounted for in the more detailed two-tank model used to reproduce the real discharge behaviour, described in Section 4.3.

Finally, treating the tank as adiabatic simplifies the handling of convection and radiation, which, as reported in the reference, together amount to approximately 5 W of heat leak; in this case it is therefore not necessary to characterise the thermal properties of the tank materials.

4.2.2.1 PID Calibration

During discharge the tank pressure is kept at the minimum operative value $p_{\mathrm{min}} = 6$ bar by the internal heat exchanger, whose heat input is set by the `PID_HEAT` controller. The controlled variable is therefore the tank pressure, and the manipulated variable is the heat injected into the hydrogen; the controller output is then added to the constant 5 W heat leak through the `Sum` block before reaching the tank.

Tuning was carried out manually, following an incremental approach. A first estimate was obtained using only the proportional gain, which provides the main response to the pressure deviation. With proportional action alone, however, the pressure stabilised slightly below the target, leaving a residual steady-state offset. An integral gain was then introduced to remove this offset and bring the pressure to settle exactly on the 6 bar target. The derivative gain was kept at zero, since the discharge is a slow process without abrupt pressure changes, so a derivative action would mainly amplify numerical noise without improving the response. The controller therefore operates effectively as a PI controller.

To prevent non-physical values, the controller output was bounded between 0 and 1000 W. The lower limit reflects the fact that the internal heat exchanger can only add heat to the hydrogen, not remove it, while the upper limit acts as a saturation safeguard, chosen as a plausible, non-exaggerated value rather than from a detailed sizing of the heat exchanger, which was outside the scope of this work. In all the simulations carried out, the heat input remained well below this upper bound, so the saturation was never reached and the chosen limit had no effect on the results.

Controller performance was assessed through the integral of the absolute pressure error (IAE) introduced in Section 4.2.1, a standard cumulative metric for control performance. Using the absolute value avoids any cancellation between positive and negative deviations, so a flat curve corresponds directly to a negligible instantaneous error. As shown in Figure 4.5, the integrated error rises during an initial transient and then stays essentially flat at about 0.041 bar $\cdot$ s for most of the discharge, reaching a final value of roughly 0.056 bar $\cdot$ s over the whole process ($\approx$ 8.3 h). The long plateau corresponds to a negligible instantaneous pressure deviation, confirming that the PI controller holds the 6 bar target without any appreciable steady-state offset.

The steps visible in the curve correspond to the changes of thermodynamic regime that the hydrogen undergoes during discharge. Three transitions can be identified: first, the hydrogen leaves the initial supercritical state and becomes a subcooled liquid (p below p_{crit}), then it crosses from liquid into the saturated liquid–vapour region, and finally it leaves saturation and becomes superheated vapour. The long plateau between these events corresponds to the saturated two-phase region, where the controller holds the pressure with negligible error. At each change of regime the relationship between the injected heat and the resulting pressure changes, so the controller momentarily struggles to hold the target and the error accumulates, consistent with the convergence difficulties of two-phase transients already discussed in Section 3.1.2. Outside these transitions the error does not grow, confirming that the controller performs well throughout the rest of the process.

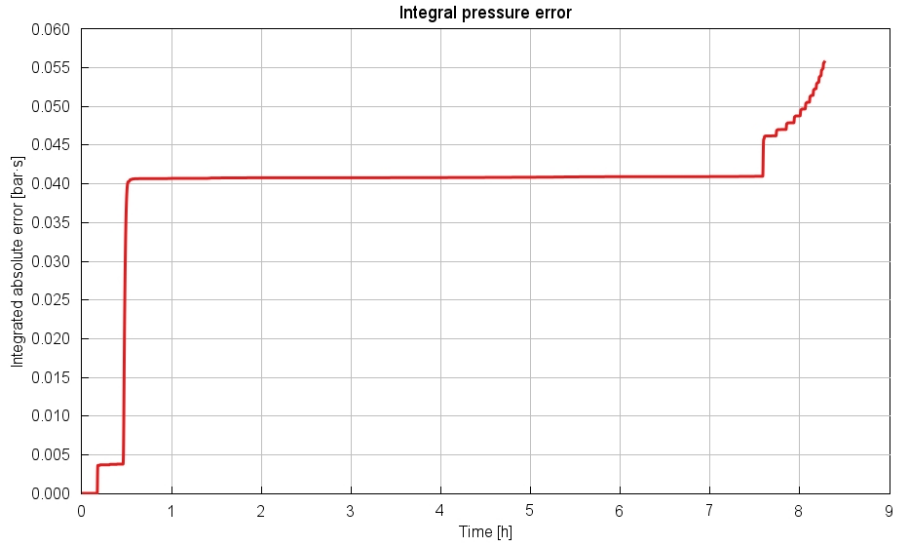

Figure 4.5: Integrated absolute pressure error (IAE) of the PI controller during discharge (continuity residual 1×10^{-8}).

To put this figure into perspective, the final IAE of 0.056 bar $\cdot$ s accumulated over the whole discharge ($\approx$ 8.3 h, i.e. about 3×10^4 s) corresponds to an average absolute pressure deviation of roughly 2×10^{-6} bar. Relative to the 6 bar target, this is of the order of 10^{-7}, confirming that the steady-state pressure error introduced by the controller is entirely negligible.

4.2.3 Initial and Boundary Conditions

The initial and boundary conditions of the defuelling simulation are summarised in Table 4.4. The tank starts from a full, single-phase state at 16 bar and 28.2 K, taken from the reference study [23]. Since the initial pressure lies above the critical pressure of hydrogen, the fluid is in a dense supercritical state, and only the initial temperature and pressure are prescribed: the corresponding density, and all other thermodynamic properties, are evaluated internally by GT-SUITE through REFPROP. The vapour quality is not imposed, as it is not a meaningful parameter for the single-phase initial condition.

The remaining operating parameters, namely the discharge mass flow rate, the minimum operative pressure, the ideal stop density and the constant heat leak, are those already reported in Table 3.3 of Section 3.3 and are repeated here for completeness. The simulation ends when the tank reaches the temperature corresponding to ϱ_{stop}, as discussed in Section 4.3.2.

Table 4.4: Initial and boundary conditions of the defuelling simulation.

Parameter	Value	Unit
Initial State		
Initial tank pressure	16	bar
Initial tank temperature	28.2	K
Initial density (from REFPROP)	62.07	kg/m^3
Hydrogen type	para	–
Operating Parameters		
Discharge mass flow $\dot{M}_{\mathrm{disch}}$	1	g/s
Minimum operative pressure p_{min}	6	bar
Ideal stop density ϱ_{stop}	2.4	kg/m^3
Stop temperature ($\approx$)	57	K
Constant heat leak $\dot{Q}_{\mathrm{leak}}$	5	W

4.2.4 Solver

The solver configuration for the defuelling simulation is essentially the same as the one adopted for the refuelling case, summarised in Table 4.3. The same implicit flow solver and transient thermal treatment were retained, since the same cryogenic two-phase behaviour is involved. Only two settings differ from the refuelling configuration:

- the time step is left to GT-SUITE (`def`), so that it is adjusted automatically during the run depending on the convergence behaviour of the solver. This is appropriate for the defuelling simulation, which spans a much longer physical time (about 8.3 h) than the refuelling event and alternates slow phases with more demanding regime transitions;
- the continuity residual tolerance is tightened from 1×10^{-4} to 1×10^{-8}, for the reasons of long-term mass conservation discussed in Section 4.2.1. All the other convergence tolerances are kept at the values reported in Table 4.3.

4.2.5 Challenges and mitigation strategy

The main challenge of the defuelling simulation was preserving mass conservation over its long physical duration, where even a very small per-step error in the continuity equation could accumulate into a significant mass imbalance. This was addressed by tightening the continuity residual tolerance, as detailed in Section 4.2.1. A secondary difficulty arose at the changes of thermodynamic regime, where the solver occasionally failed to converge within a single time step, and the use of an adaptive time step kept these events from affecting the overall solution.

The manual calibration of the PI controller also proved time-consuming, as the gains had to be adjusted iteratively to hold the target pressure across the different

thermodynamic regimes without introducing oscillations.

Overall, these difficulties are consistent with the known limitations of the 1D modelling approach discussed in Section 3.1.2, and none of them compromised the validity of the results.

4.3 Defuelling

To determine realistic initial conditions for the tank at the start of the refuelling process, a dedicated defuelling model was developed that reflects actual operating conditions. This model builds upon the validated defuelling framework described in Section 4.2, further adapted so that the initial thermodynamic state of the tank is as representative of real-world operation as possible.

4.3.1 System Description

The basic structure of this model is identical to the defuelling validation model described in Section 4.2.1. The two main differences concern the storage system and the thermal treatment of the tank.

First, the storage system is now represented by two tanks of 710 L each, whose geometry and horizontal arrangement, consistent with the configuration used on the truck, are described in Section 3.5. This allows the simulation to reproduce the real hydrogen consumption behaviour during vehicle operation more accurately.

Second, unlike the validation model, the tank wall and insulation are modelled explicitly (aluminium shell and MLI layer), as detailed in Section 3.5, since an accurate description of the wall heat transfer directly affects the predicted initial conditions for the subsequent refuelling.

The hydrogen mass flow rate demanded by the fuel cell was provided by Volvo, based on real consumption data, as a function of time, and was used directly as the discharge boundary condition. The defuelling process was therefore simulated under a realistic, driving-based hydrogen consumption profile.

As in the defuelling validation model, the simulation was terminated on a temperature criterion.

4.3.2 Modelling Assumptions

Most of the modelling choices follow directly from the defuelling validation model of Section 4.2; this section reports only the assumptions specific to the real, two-tank configuration.

The two tanks are drained simultaneously rather than sequentially. To enforce a physically consistent, balanced extraction from both tanks, the upstream layout was kept fully symmetric, with identical pipe lengths and discretisations on the two branches. This prevents one tank from emptying before the other, analogously to

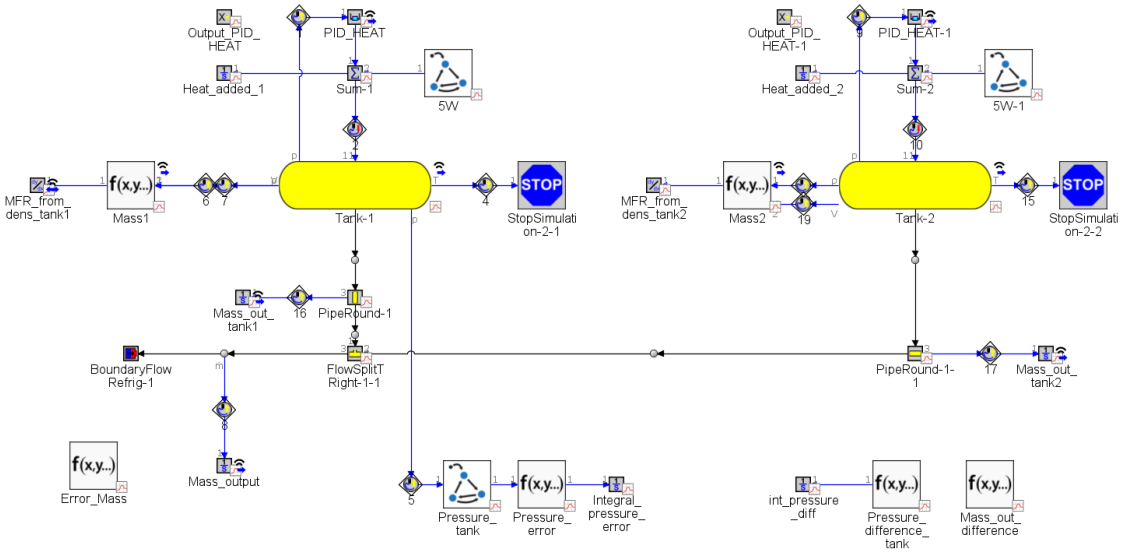

Figure 4.6: defuelling model with two tanks in GT-SUITE

what is discussed for the dual-tank refuelling case in Section 4.4.2.

The pressure of each tank is maintained at the minimum operative value through the internal heat exchanger and PID controller, exactly as in the validation model (Section 4.2.2.1).

The assumption of a single uniform temperature within the tank, which is an inherent limitation of the 1D approach (Section 3.1.2), is considered acceptable in this case. During driving, the continuous motion of the vehicle keeps the hydrogen constantly mixed (sloshing), which promotes thermal homogenisation inside the tank and limits the development of stratification. Under these conditions, representing the tank content with a single average temperature is a reasonable approximation of the real operating behaviour.

4.3.3 Initial and Boundary Conditions

Several initial thermodynamic states of the tanks were analysed, in order to simulate different scenarios corresponding to different conditions at the end of the refuelling. Three cases were considered:

- 16 bar and 28.2 K,
- 16 bar and 29.2 K,
- 16 bar and 30.2 K.

The results of this analysis, together with how the initial conditions for the refuelling system were derived from them, are presented in Section 5.3.

The discharge boundary condition is the time-dependent fuel-cell consumption profile provided by Volvo, introduced in Section 4.3.1, and the minimum operative pressure of 6 bar is maintained through the internal heat exchanger and PID controller, as in the validation model.

A final sensitivity analysis was carried out to determine the most appropriate hydrogen composition to adopt for the simulations, comparing pure parahydrogen, pure orthohydrogen and normal hydrogen (the room-temperature equilibrium composition of 75% ortho and 25% para). The results of this analysis are also reported in Section 5.3.

4.3.4 Solver

The solver configuration is the same as that of the defuelling validation model described in Section 4.2.4, including the adaptive time step and the tightened continuity residual of 1×10^{-8}.

4.3.5 Challenges and mitigation strategy

No new numerical challenges were encountered beyond those already discussed for the defuelling validation model (Section 4.2.5), since the present model shares the same solver configuration and control strategy.

The only aspect specific to the two-tank configuration concerns the distribution of the discharge between the two tanks. Given the flow-sharing behaviour observed in the dual-tank refuelling case (Section 4.4.2), and since investigating the minor differences in the discharge between the two tanks is outside the scope of this thesis, the upstream layout was kept symmetric and consistent with the rest of the system. This simplification ensures a balanced extraction from both tanks without introducing unnecessary complexity that would not affect the objectives of the analysis.

4.4 Refuelling

Following the validation of the refuelling model, the initial conditions of the tanks are extracted from the two-tank defuelling simulation results. Based on these conditions, a refuelling model was developed to simulate the process for the different SoC values resulting from the defuelling end states.

4.4.1 System Description

The model is built upon the reference approach, with several modifications introduced to bring it closer to the in-house configuration.

By modelling the defuelling process for different values of the state of charge (SoC), it was found that the hydrogen remaining in the tank is entirely in the vapour phase, rather than as a two-phase mixture. For this reason, the onboard tank is represented by a single flow-split element corresponding to the vapour hydrogen, instead of the two-element representation used in the validation model. The tank geometry is the same as described in Section 3.5.

As also discussed in Section 3.5, the tanks are modelled in the horizontal configuration used on the truck. The tank wall and insulation are modelled explicitly through their physical properties, rather than with an adiabatic assumption or a prescribed heat flux, since the thermal behaviour of the wall strongly affects the pressure and temperature evolution during refuelling. The aluminium shell and the multilayer insulation layer, together with the rationale for adopting aerospace (NASA) cryogenic tank data, are described in Section 3.5.

4.4.1.1 Integration of the Nozzle Model

To improve the accuracy of the refuelling simulation, the nozzle model developed was incorporated into the final system model.

As described in Section 3.4.3, the nozzle is represented by an equivalent orifice with a forward discharge coefficient that varies as a function of mass flow rate, rather than a fixed constant value. This approach is more physically realistic because, during a typical refuelling event, the mass flow rate changes continuously as the pressure difference between the station and the vehicle tank evolves.

Beyond the pressure drop, the thermal heat leak through the nozzle wall, provided by MANNTEK from their thermal analysis, was also included in the model.
The effect of adding the nozzle model on the overall refuelling behavior was then evaluated by comparing the results with and without the nozzle component. The

complete final model, which includes the station-side boundary conditions, the transfer line, the nozzle model, and the two-element tank representation, is shown in Figure 4.7.

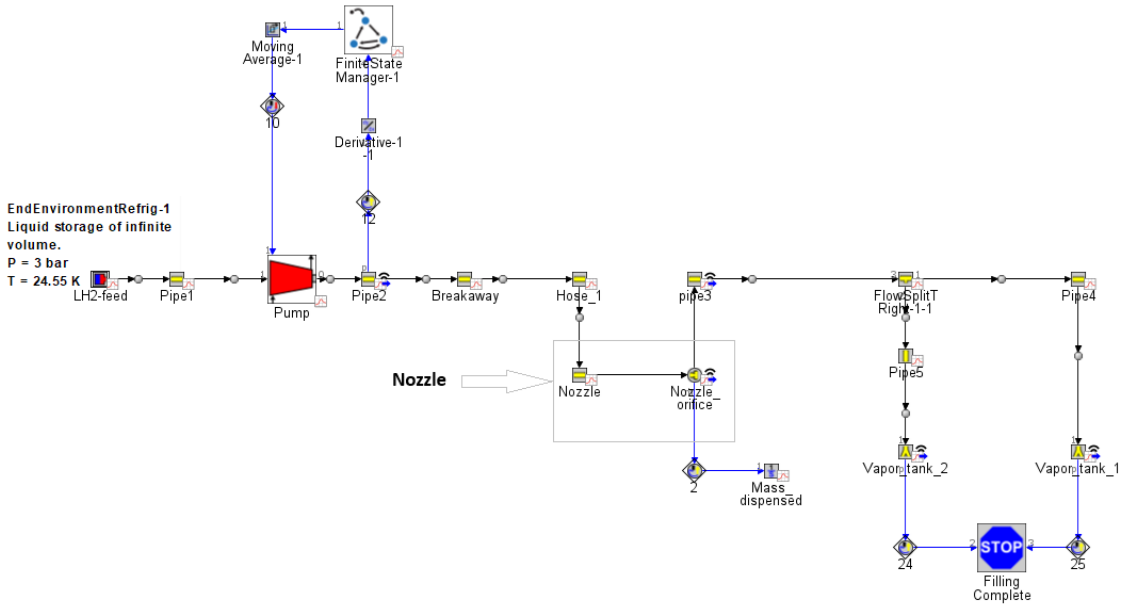

Figure 4.7: refuelling model with detailed nozzle

4.4.2 Modelling Assumptions

Parahydrogen was chosen as the working fluid for this model. The reasoning behind this choice, based on the equilibrium composition of hydrogen at cryogenic temperatures and on the sensitivity analysis of the different hydrogen forms, is presented in Section 5.3.

Furthermore, all the pipes were assigned the same insulation as the tanks, in order to make the model as realistic as possible. This reflects the actual system, where, for instance, the hose is vacuum-insulated so that its outer surface remains safe to handle for the operator performing the refuelling. Modelling the insulation explicitly also allows convection and radiation from the surroundings to be represented more realistically. This is particularly relevant for radiation, which scales with the difference of the fourth powers of the ambient and surface temperatures: without an insulation layer, the outer wall would reach an unrealistically low temperature, producing an excessive temperature difference with the environment and therefore an overestimated radiative heat exchange.

4.4.3 Initial and boundary condition

The initial conditions applied to the system components, including the station tank, pipes, and pump, are the same as those listed in Table 4.2, with the exception of the tank and nozzle, which are defined separately and discussed in the following sections.
The initial conditions of the on-board tanks are set based on the seven different end states obtained from the defuelling simulations, corresponding to SoC values of 4%, 5%, 6%, 7%, 8%, 9%, and 10%, as presented in Section 5.3.

4.4.4 Challenges and mitigation strategy

During the simulation of the dual-tank refuelling scenario with realistic initial conditions derived from the defuelling results, an unexpected filling behavior was observed that needed to be addressed before proceeding with the analysis.
In the initial model, one tank filled completely before the other started to receive a meaningful amount of hydrogen. This kind of sequential filling does not reflect how a real dual-tank system would behave in practice.

In a real system, the way hydrogen is distributed between two parallel tanks depends on the back-pressure difference between them at any given moment. At the start of refuelling, even small differences in the initial condition of each tank, such as a slightly lower pressure in one of them, are enough to direct more flow toward that tank. As that tank fills up and its pressure increases, the flow gradually shifts toward the other tank. This back-and-forth process happens continuously throughout the refuelling event, so both tanks are receiving hydrogen at the same time for most of the process, even if the flow rates are not equal at every moment. In other words, the filling is neither purely simultaneous nor strictly one-after-the-other, but rather a dynamic process that is constantly adjusting based on the pressure state of each tank.

This behavior has a direct impact on how the pressure and temperature inside each tank evolve over time, which in turn affects the overall refuelling performance. To fix the sequential filling issue seen in the initial model, the pipes upstream of both tanks were given the same length and discretizations, creating a fully symmetric model layout. With this setup, the model is able to reproduce the pressure-driven flow sharing between the two tanks in a more physically consistent way. The final configuration is illustrated in Figure 4.8.

It is worth mentioning that this symmetric layout is a simplifying assumption and does not necessarily reflect the actual pipe arrangement in the real vehicle. It was introduced to make sure that the system-level results are not distorted by asymmetric filling behavior, which would add unnecessary complexity and fall outside the

scope of this study.

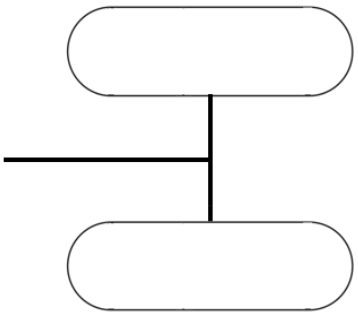

Figure 4.8: Symmetric layout of tank installation

5
Results

In this chapter, the results of the 1D simulations are presented and discussed. First, the refuelling validation process is investigated, including the pressure and temperature behavior of the system during hydrogen filling. Subsequently, the results of the defuelling process are presented and at the end the main result of this thesis which is finding the optimum initial condition of refuelling will be presented.

5.1 Refuelling Validation

The first phase of the refuelling process is the cooldown of the piping and system components, as described in the methodology. During this phase, the State Manager monitors the temperature downstream of the nozzle and triggers the transition to the main refuelling phase once the cooldown criterion is met. As shown in Figure 5.1a, the pipe temperature reaches the threshold value of 25.6 K at approximately 52 s after the start of refuelling, indicating that the cooldown phase is complete. At this point, all pipes in the refuelling system are within the allowable temperature corridor of 23.9-26.5 K specified by the ISO standard. Once the piping has cooled down to this range, the main refuelling phase begins with a target mass flow rate of 111 g/s.

In the Figure 5.1b, the temperature evolution during the first 80 s of the process is presented. Around 10 s, Pipe 2 and the hose, which are located close to the station storage tank, had already cooled down significantly. Pipe 3 reached a temperature below 30 K after approximately 18 s.

Pipes 4 and 6 are located upstream of Tank 1 and Tank 2, respectively. Since Tank 1 is positioned approximately 600 mm farther from the refuelling nozzle than Tank 2, the cooling process in Pipe 4 occurred later than in Pipe 6. However, a noticeable temperature increase can be observed in Pipe 4 around 25 s, where the temperature rises to nearly 38 K. This behavior is attributed to a backflow phenomenon occurring at the onset of the refuelling process.

Due to the difference in pipe lengths and the asymmetric configuration of the two onboard tanks, the tanks did not begin filling simultaneously. Tank 2, which is

closer to the refuelling nozzle, was filled first between approximately 22 and 39 s. Subsequently, Tank 1 started to receive hydrogen at around 39 s; this transition is reflected by the sudden temperature drop observed in Pipe 4. After this point, the flow distribution gradually stabilized, and both tanks were filled simultaneously. As a result, the temperatures in the piping network approached a steady-state cooling behavior for the remainder of the refuelling process.

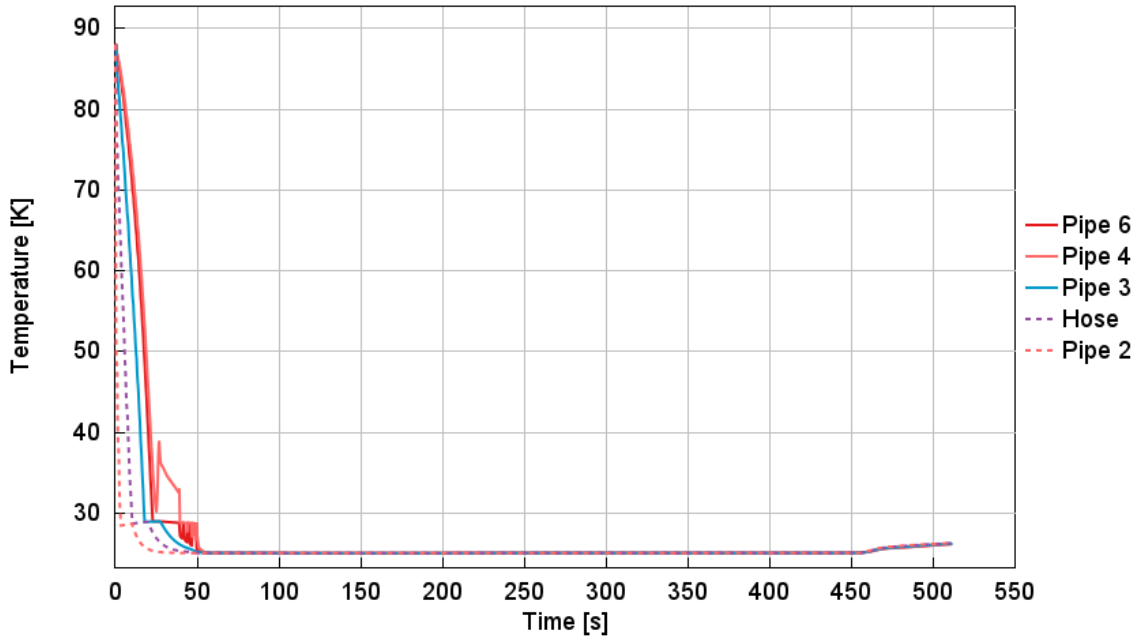

(a) Full refuelling time

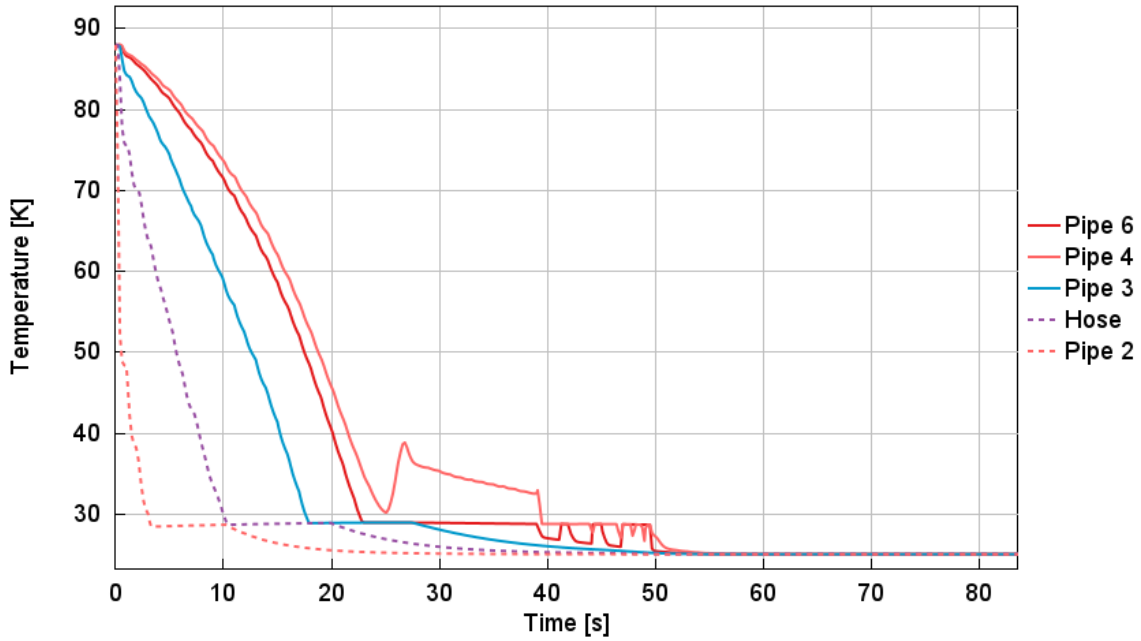

(b) First 80 s

Figure 5.1: Pipes temperature during refuelling

Figure 5.2 shows a comparison of the tank pressure between the reference study and the current 1D model throughout the refuelling process. As can be seen, the total

refuelling time predicted by the present model is in good agreement with the reference. Furthermore, the overall trend of pressure variation during the filling process follows a similar pattern in both models, which suggests that the 1D approach is capable of capturing the general thermodynamic behavior of the system despite its inherent simplifications.

At the beginning of the liquid hydrogen filling process, the incoming cryogenic liquid enters a tank where the pressure is lower than the saturation pressure of the inlet fluid. Under these conditions, a portion of the liquid instantly vaporizes upon entry, a phenomenon known as flash vaporization. As described by Li et al. [13], this effect must be accounted for at the initial filling stage, since it causes a sudden rise in both pressure and temperature inside the tank. This initial spike can be observed in both the 1D and 3D models at the start of the process.

However, the spike appears sharper in the 3D CFD reference than in the 1D GT-SUITE model. This difference can be explained by a well-known limitation of lumped-parameter models: as shown by Melideo et al. [14], 1D models calculate average thermodynamic values across the entire tank volume and cannot capture local variations in temperature or pressure. In a 3D CFD simulation, flash vaporization creates high-pressure and high-temperature zones near the inlet jet that are spatially resolved. In the 1D model, however, the same energy is spread uniformly throughout the tank, which smooths out the pressure response and makes the initial spike less sharp [36].

After this initial phase, the pressure in the 1D GT-SUITE model remains nearly constant, and even shows a slight decrease in some intervals, throughout most of the filling process. This behavior differs from the gradual pressure rise observed in the 3D CFD reference and requires a dedicated explanation.

In the 3D CFD simulation, the ullage gas is not constrained to remain on the saturation curve. As the incoming liquid progressively reduces the ullage volume, the trapped gas undergoes compression and can reach a superheated state, with a pressure higher than the saturation pressure corresponding to the liquid temperature. This ullage compression is the primary mechanism responsible for the slow and steady pressure rise seen in the reference model [37].

In the 1D GT-SUITE model, however, the ullage was defined with a quality of unity, effectively locking the vapor phase onto the saturation curve at all times. As a result, the pressure remains directly tied to the saturation temperature of the fluid, and the compression of the ullage gas is not captured independently. Instead of rising gradually, the pressure stays nearly constant, or even drops slightly, as the cooler incoming liquid hydrogen shifts the average fluid temperature downward

along the saturation curve. This is a known limitation of lumped-parameter 1D models, as they assume thermodynamic equilibrium between phases and cannot resolve the superheating of the ullage gas that drives the gradual pressure increase observed in 3D CFD simulations [14].

The sharp pressure rise observed near $t \approx 470$ s occurs when the tank becomes completely full of liquid. At this point, there is no vapor space left to accommodate the incoming fluid, and the system shifts from a compressible two-phase state to an essentially incompressible liquid-full condition, which leads to a sudden pressure spike.

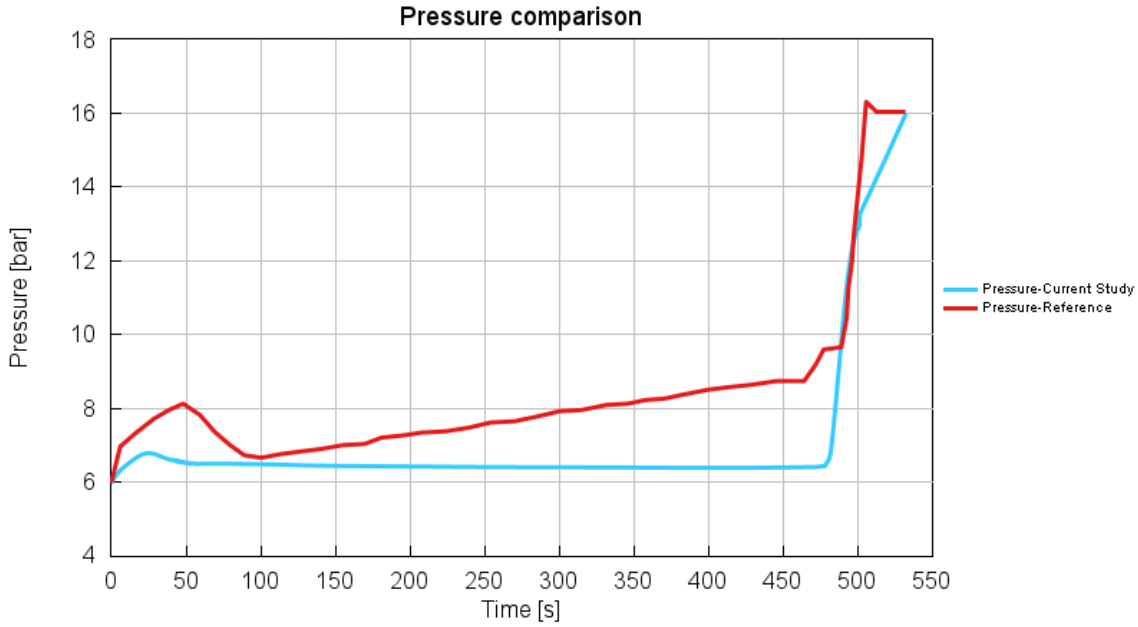

Figure 5.2: Pressure comparison between reference study and current study

Figure 5.3 compares the temperature at the top of the tank between the reference and the current study. As with the pressure plot discussed earlier, the initial temperature peak is caused by flash vaporization, which occurs within the first 50 seconds of the refuelling process.

Following this, the temperature remains nearly constant, which is consistent with the constant pressure behavior observed between $t = 50$ s and $t \approx 470$ s. Finally, the temperature rise at the end of the process is driven by the sharp pressure increase that occurs once the tank reaches a liquid-full condition.

The mass-averaged temperature is calculated as the weighted average of the temperatures of the liquid and vapor phases based on the mass of each of these phases.

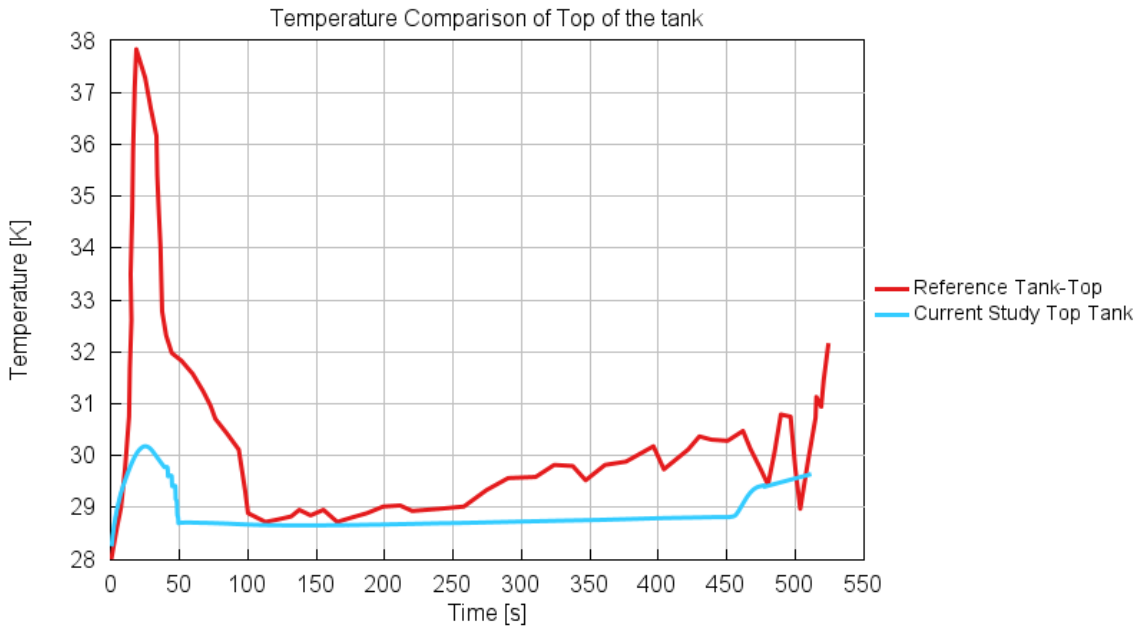

Figure 5.3: Temperature comparison between reference study and current study at top of the tank

The initial temperature decrease observed in the 3D reference model in the early to mid-stages of the refuelling process can be attributed to the gradual increase in the mass of the cold liquid hydrogen entering.

With the continuous entry of liquid hydrogen, the mass contribution of this fluid to the average temperature calculation increases, and as a result, the weighted average temperature value gradually falls below the initial temperature of the tank. The phenomenon of thermal stratification in the 3D simulation leads to this effect being more severe in the 3D simulation.

In this case, the cold liquid hydrogen accumulates in the lower part of the tank, while the warmer vapor remains in the upper part, resulting in a non-uniform temperature distribution inside the tank that directly affects the mass-average temperature value [14].

In contrast, the 1D model is unable to represent the phenomenon of thermal stratification. The assumption of homogeneous mixing in this model causes the incoming cold fluid to be distributed immediately throughout the entire tank volume. As a result, the tank temperature response is smoother and more gradual, and there is no significant decrease below the initial tank temperature.

Additionally it should be mentioned that mean error between the current data and

reference data is 5.13% and the maximum one is 20.78% which is related to flash vaporization period of refuelling.

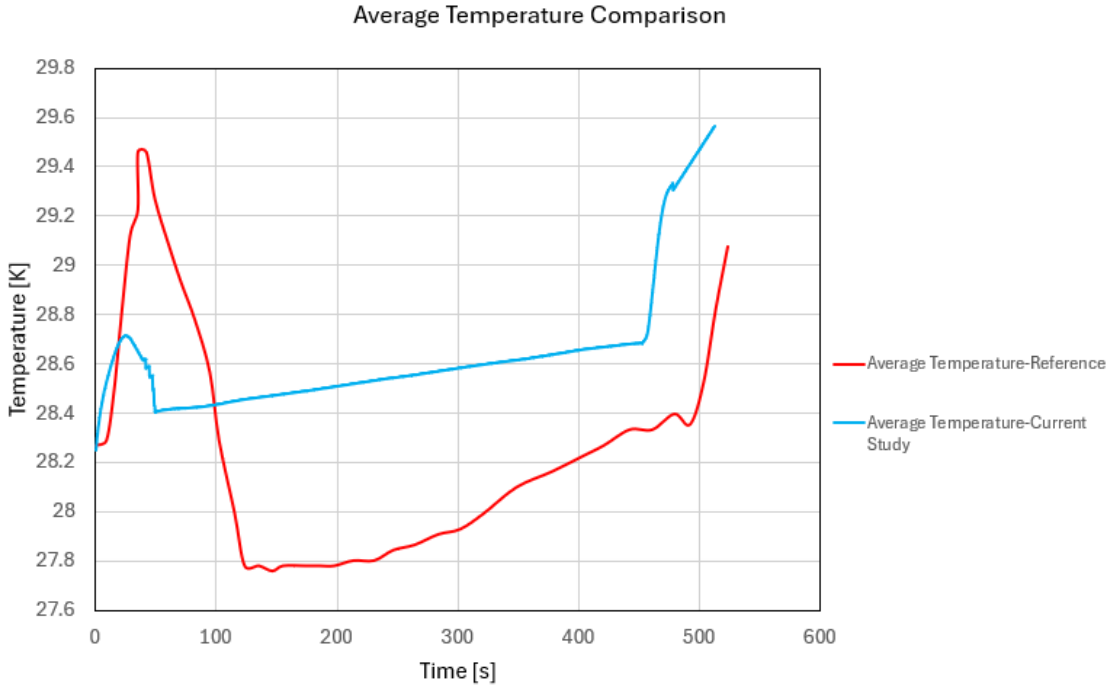

Figure 5.4: Average Temperature comparison between reference study and current study

Figure 5.4 shows a comparison between the mass-averaged temperature of the current 1D model and the average temperature reported in the reference study. The mass-averaged temperature is calculated as the weighted mean of the liquid and vapor temperatures with respect to their masses, making it a more representative parameter for thermal comparison than a simple average, since it accounts for the contribution of each phase based on how much mass it contains.

As can be seen, the model follows the same general trend as the reference throughout the refuelling process. However, a larger discrepancy is visible during the early stage of filling, which is consistent with the reasons discussed earlier, namely, the inability of the 1D model to capture flash vaporization-induced local temperature peaks and thermal stratification effects that are resolved in the 3D CFD reference. Beyond this initial phase, the two results converge well, and the relative error between them ranges from 0.25% to 2.56% for the majority of the process, which indicates that the 1D model produces results that are in reasonably good agreement with the reference data.

5.2 Defuelling Validation

The defuelling results are presented in the density-temperature plane rather than as time histories. This choice follows the reference study of Stops et al. [23], where the same representation is adopted, allowing a direct comparison between the two models. Beyond consistency with the reference, a time-independent representation conveys the discharge process more clearly than a time-based one: it traces the actual thermodynamic path followed by the fluid as the tank empties, independently of how fast the process develops.

Pressure, on the other hand, is held fixed at 6 bar by the PID controller and therefore carries little additional information when plotted explicitly; its constancy is already apparent from the trajectory itself, most visibly in the saturation region, where the curve becomes vertical because a constant pressure imposes a constant temperature. Temperature and density are thus the two quantities that most strongly govern the discharge and, at the same time, characterise it most meaningfully, which is why they are chosen as the axes of the diagram.

5.2.1 Density-Temperature Trajectory

Figure 5.5 illustrates how the fluid density varies with temperature throughout the defuelling process. The red line (Article) represents the results from the zero-dimensional reference study, while the blue line (GT SIM) corresponds to the 1D model developed in this work. As shown, the two sets of data are in excellent agreement across the entire process, confirming that the 1D model can accurately reproduce the thermodynamic behaviour of defuelling. For reference, the saturation lines for both the liquid and vapour phases are displayed as dashed lines.

The process begins in a subcooled state, where the fluid condition is located to the right of the liquid saturation line. As defuelling proceeds, the system moves towards the saturation curve under a constant pressure constraint of 6 bar, which is required to maintain a stable supply to the fuel cell. Upon reaching the saturation curve, the density decreases at a nearly constant temperature and pressure as the liquid gradually evaporates, until only gaseous hydrogen remains in the tank. Beyond this point, as hydrogen consumption continues, the heat input to the tank increases to maintain the 6 bar pressure, causing the temperature of the remaining hydrogen gas to rise. This behaviour is reflected in the low-density, high-temperature region of the curve, where both lines extend towards the right side of the figure.

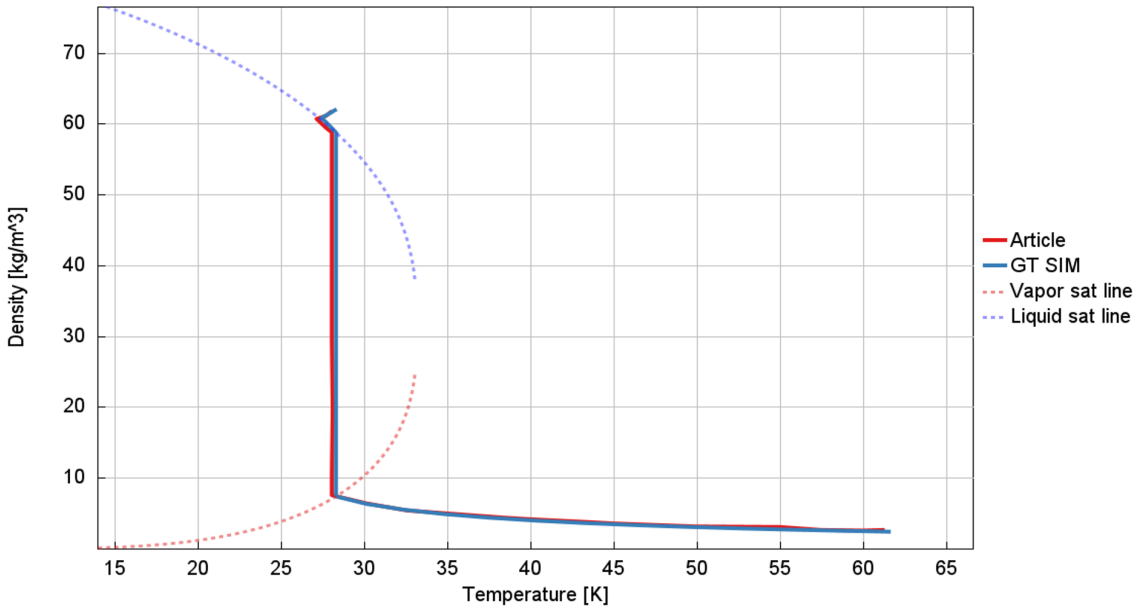

Figure 5.5: Density against temperature during defuelling

5.2.2 Heat Input from the PID Controller

The Heat diagram in Figure 5.6 shows the behaviour of the PID controller output (green line, GT SIM) during the defuelling process, compared with the results of the reference study shown by the red and blue lines. The green line represents the amount of heat injected into the system by the PID controller, the red line (Article vap) corresponds to the vapour outlet condition in the reference study, and the blue line (Article liq) to the liquid outlet condition. It should be noted that the constant heat leakage of 5 W applied to the system is not included in this representation; only the controller output is shown.

In the initial phase of the simulation, the controller produces a relatively strong transient response in order to reach the target pressure of 6 bar, which includes a jump in thermal power. This behaviour is due to the initial conditions of the system and the need to quickly bring the tank to a stable control regime. After this stage, the PID output decreases rapidly and enters a more stable region.

In the continuation of the process, until the middle of the discharge, the thermal power injected by the controller (green line) has a relatively slow and increasing trend that is consistent with the gradual decrease in the mass inside the tank and the change in the thermodynamic conditions of the fluid. In this range, the system is mainly in the liquid region and then close to the saturated region, and the controller can keep the pressure within the target range with limited fluctuations.

When the system enters the saturation region, the controller output departs from the single-phase reference behaviour. As already noted, this departure is expected, and the way the two reference curves in Figure 5.6 are constructed clarifies why it should not be read as a modelling error. These two curves represent limiting cases: the heat that must be supplied to hold the target pressure if the discharged stream were entirely vapour or entirely liquid. In GT-SUITE the quality of the extracted stream cannot be prescribed independently, since the fluid leaving the tank carries the same quality as the bulk content; the discharge therefore consists of a mixture of both phases rather than a single one. Seen in this light, the fact that the model output (green line) remains bounded between the liquid and vapour references throughout the two-phase stage is a strong indication of physically correct behaviour: the heat demand falls, as it should, between the two theoretical limits.

In the final stage of the process, once the system leaves the saturation dome and only superheated vapour remains, the heat input rises sharply. This is the expected consequence of the progressive depletion of mass inside the tank: as less fluid is available, holding the 6 bar set point becomes increasingly demanding, and the controller must supply a rapidly growing amount of energy to compensate. The steep rise at the end of the trace reflects this regime rather than any instability in the control loop.

Taken together, these results show that the PID controller kept the tank pressure within the target range throughout the defuelling process and tracked the energy demand of the system consistently across the successive thermodynamic regimes.

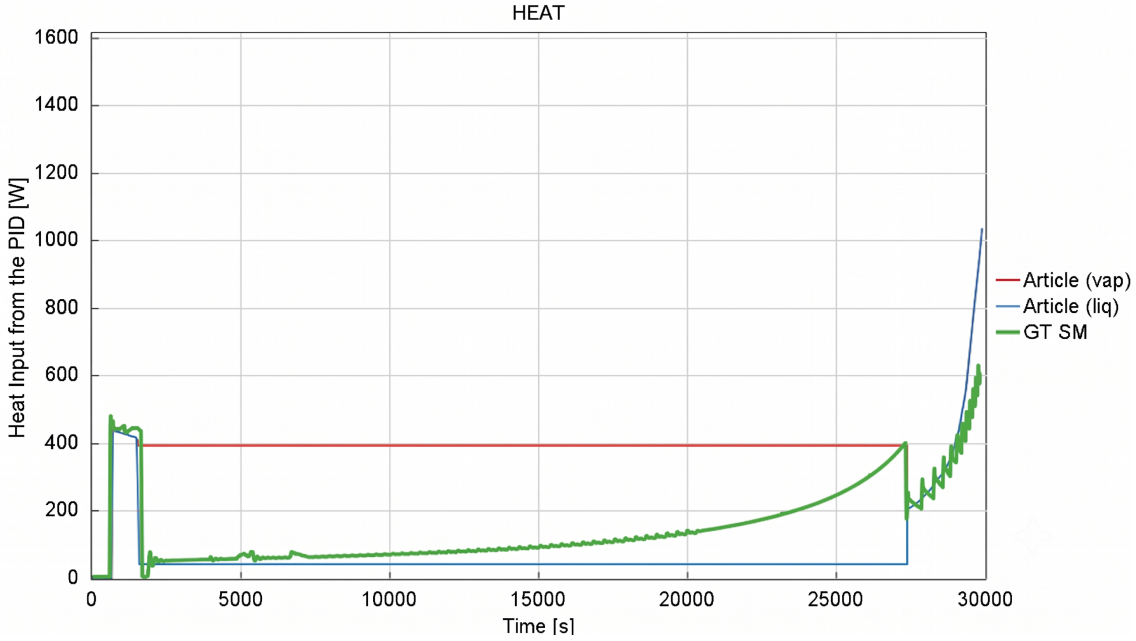

Figure 5.6: Heat input to the tank from the PID controller during the defuelling process

5.3 Defuelling

Figure 5.7 shows the density-temperature trajectory of the hydrogen contained in the tank during defuelling for three different initial temperatures, namely 28.2 K, 29.2 K and 30.2 K. Each of these temperatures corresponds to a different initial density and therefore to a different mass of hydrogen initially stored in the tank.

In the early stages of the discharge the three cases are essentially coincident, following the same path as the fluid evolves from the dense liquid-like state towards the two-phase region. Above approximately 77 K, however, the curves begin to separate, as the thermodynamic path in the final stage of the discharge becomes dependent on the initial state and can no longer be specified unambiguously without prescribing the initial temperature. For this reason 77 K is taken as the upper limit for extracting the data used to define the initial conditions of the defuelling simulations, restricting the extraction to the region where the three trajectories coincide.

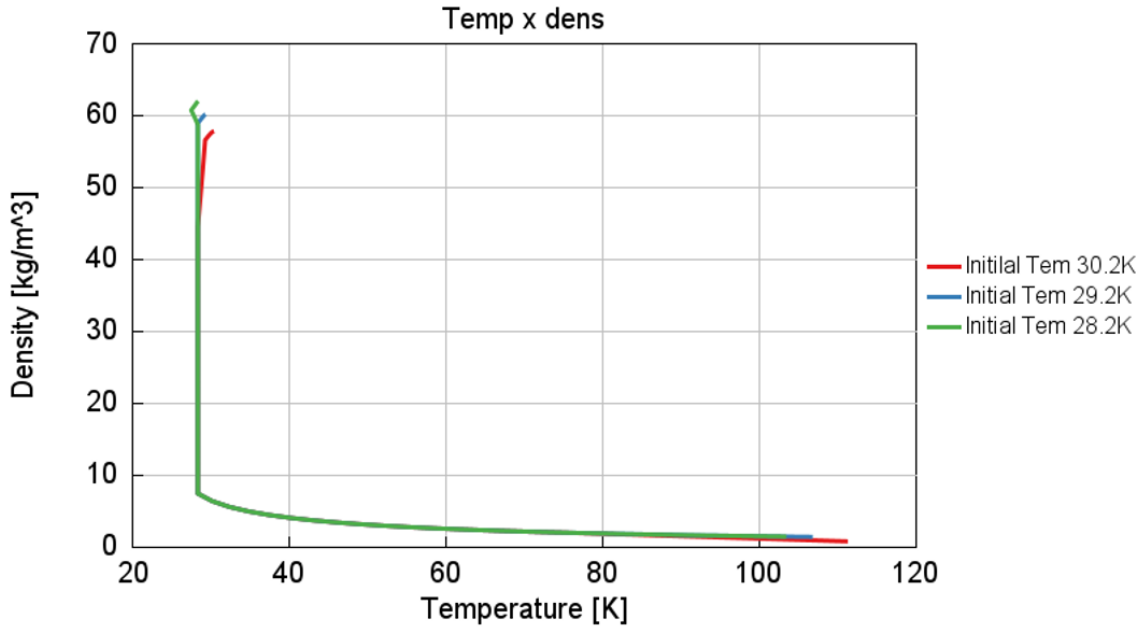

Figure 5.7: Density-temperature profile during the defuelling process for three different initial temperatures

The State of Charge (SoC) is evaluated directly from the fluid density read from the simulation: combining the local density with the fixed tank volume of 710 L yields the instantaneous hydrogen mass, and the SoC is then obtained as the ratio of this mass to a fixed reference mass, evaluated at the baseline density of 62 kg/m^3.

The analysis described above, like the rest of the defuelling study, was carried out as-

suming pure parahydrogen. This assumption rests on the temperature dependence of the hydrogen isomeric equilibrium: hydrogen exists as a mixture of two nuclear-spin isomers, orthohydrogen and parahydrogen, whose equilibrium proportions vary with temperature [38]. At room temperature the mixture settles at the fixed 75:25 ortho-to-para ratio known as normal hydrogen, whereas as the temperature decreases the equilibrium shifts towards the para form, until at cryogenic temperatures parahydrogen becomes almost entirely dominant, as shown in Figure 5.8. Since the fluid remains within this temperature range throughout storage and defuelling, the ortho content is expected to be negligible.

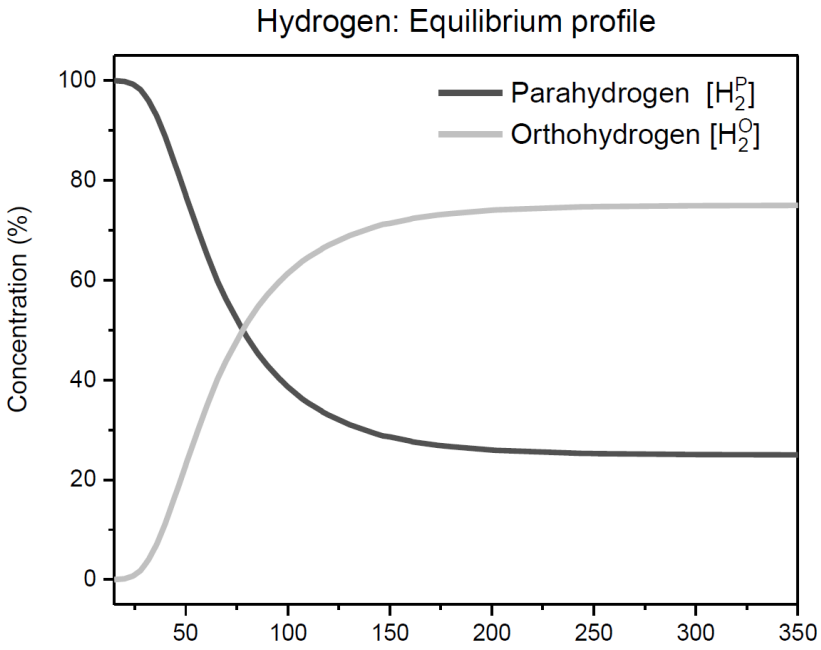

Figure 5.8: Equilibrium concentration of orthohydrogen and parahydrogen as a function of temperature. Adapted from [39]

To verify that this assumption does not affect the results, the fluid behaviour was compared across the three isomers directly in the simulation. The density-temperature curves computed for pure parahydrogen, pure orthohydrogen and normal hydrogen (Figure 5.9) are practically superimposed over the entire defuelling range, separating only in the final low-density tail, while the initial tank temperatures evaluated at matched SoC and pressure (Table 5.1) differ between the three isomers by no more than about a tenth of a kelvin. These results confirm that the choice of isomer has no appreciable effect on the defuelling behaviour, and the fluid is therefore modelled as pure parahydrogen throughout the present work.

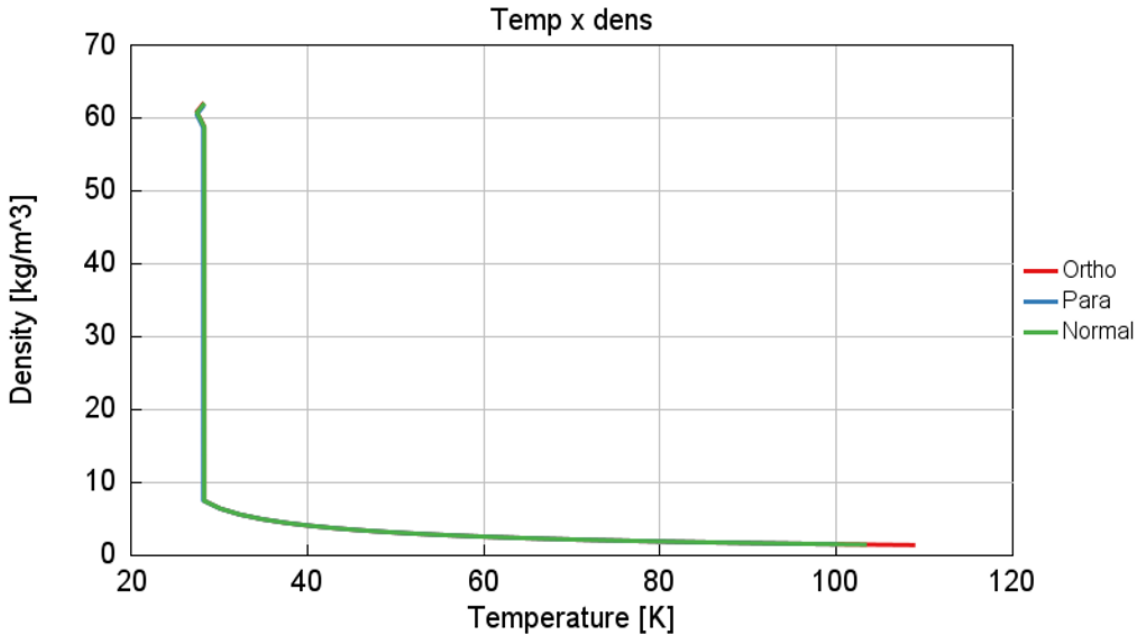

Figure 5.9: Density-temperature profile during defuelling for parahydrogen, orthohydrogen, and normal hydrogen at $P = 6$ bar

Table 5.1: Initial tank temperature at different SoC values for parahydrogen, normal hydrogen, and orthohydrogen at $P = 6$ bar.

		Hydrogen Type		
SoC [%]	**P [bar]**	**Parahydrogen T [K]**	**Normal hydrogen T [K]**	**Orthohydrogen T [K]**
4	6	60.29	60.16	60.21
5	6	49.42	49.37	49.44
6	6	42.57	42.42	42.54
7	6	37.79	37.85	37.84
8	6	34.55	34.53	34.54
9	6	32.15	32.14	32.16
10	6	30.44	30.46	30.47

5.4 Refuelling

The results of the in-house refuelling simulations under different initial conditions, which are themselves obtained from the defuelling simulations, are presented in this chapter.

5.4.1 Final Density graph

The Figure 5.10 shows the final density at the end of refuelling for different initial tank conditions. It can be observed that higher initial temperature leads to higher final density.

To support this result, additional calculations have been performed, which are presented in Table 5.2. The refuelling process is assumed to be isobaric. The initial mass is calculated based on the initial density and a tank volume of 0.71 m^3, and the initial energy is subsequently determined. Using the enthalpy at the final state, the enthalpy difference is calculated, and the corresponding energy change is obtained based on the initial mass. The thermal heat transfer from the tank wall to the fluid is also taken into account, since higher initial temperatures result in a warmer tank wall, which contributes additional energy to the system. The cumulative energy from both contributions is extracted from the GT-SUITE results.

To better understand the effect of initial conditions on the final state of the tank after refuelling, two cases with different State of Charge (SoC) values, 4% and 10%, are compared, assuming the same final reference state of $T = 28$ K and $P = 6$ bar.

The final density inside the tank is determined by an energy balance between two thermal masses: the residual hydrogen already present in the tank at the start of refuelling, and the tank wall itself. In the case with 10% SoC, the initial temperature is approximately 30 K, and the residual hydrogen mass is roughly 2.5 times greater than in the 4% SoC case. Cooling this larger residual mass down to the same final state requires approximately 393.6 kJ of additional energy to be absorbed from the incoming liquid hydrogen, which raises the final temperature of the stored hydrogen.

In the 4% SoC case, on the other hand, the tank wall temperature is initially around 60 K, significantly warmer than in the 10% SoC case. This warmer wall returns approximately 201.6 kJ of thermal energy back into the hydrogen during refuelling. However, since the residual hydrogen mass is much smaller, the overall thermal load on the incoming liquid hydrogen is lower, resulting in a lower final temperature and therefore a higher final density.

As a result, the 10% SoC case ends up with a higher final temperature and a lower

final density compared to the 4% SoC case, with a net energy difference of approximately $393.6 - 201.6 = 192$ kJ. This is consistent with the trend observed in Figure 5.10, where lower SoC values correspond to higher final densities after refuelling. This behavior indicates that the thermal influence of the residual hydrogen mass is more dominant than that of the tank wall, making it the primary factor governing the final thermodynamic state of the tank after refuelling. That said, both contributions are significant and act in competing directions, the residual hydrogen mass tends to lower the final density, while the tank wall heat return tends to raise it.

Table 5.2: Thermodynamic properties for different SoC values

Parameter	**SoC 4%**	**SoC 10%**
Initial Temperature (K)	30.44	60.29
Initial Pressure (bar)	6	6
Initial Enthalpy (kJ/kg)	495.39	857.12
Initial Density	6.18	2.48
Initial Mass (kg)	4.39	1.76
Vapor Enthalpy (kJ/kg)	452.67	452.67
Liquid Enthalpy (kJ/kg)	105.39	105.39
Initial Energy (kJ)	2172.84	1508.27
Final Temperature (K)	28	28
Final Pressure (bar)	6	6
Final Point Enthalpy (kJ/kg)	103.17	103.17
Δh (kJ/kg)	392.22	753.95
Energy (kJ)	1720.33	1326.72
Cumulative Energy Loss (kJ)	408.19	609.80

Based on these findings, the optimum initial condition corresponds to a 4% SoC, as it provides 3.55 kg more usable hydrogen in total, specifically, 0.9 kg more hydrogen at the end of the refuelling process and 2.65 kg more usable hydrogen before returning to the refuelling station. This means that under the 4% SoC condition, the vehicle can return to the refuelling station with only 1.8 kg of hydrogen remaining in the tank. In contrast, under the 10% SoC condition, the vehicle must return with approximately 4.45 kg still remaining, meaning that a significantly larger amount of hydrogen is left unused at the end of each drive cycle.

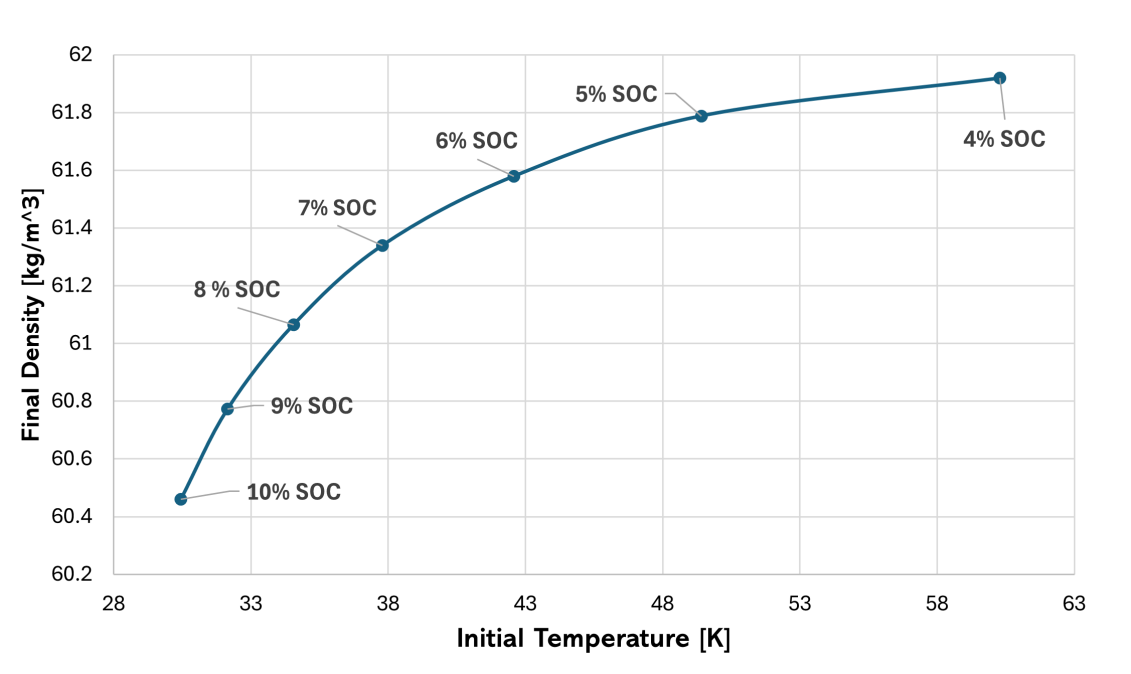

Figure 5.10: Final density for different initial tank conditions

A final test was carried out to confirm the interpretation given above, namely that the final density is governed by two competing thermal masses: the hydrogen already present in the tank at the start of refuelling and the thermal mass of the tank wall. If the wall is removed from the energy balance, the difference in final density between the extreme cases should grow, since it would then be driven solely by the residual hydrogen mass. To test this, the refuelling simulation was repeated with the tank wall set as adiabatic, so that the wall no longer exchanges heat with the fluid.

The outcome, shown in Figure 5.11, confirms the expected behaviour. With an adiabatic wall the final density is higher at every initial temperature than in the standard case, and the gap between the 4% and 10% SoC cases widens from about 1.46 kg/m^3 to about 1.93 kg/m^3. The increase is largest at the higher initial temperatures, where the wall was warmest and therefore returned the most heat to the incoming hydrogen, and almost vanishes at the lowest temperature, where the wall was already close to the fluid temperature. This is precisely what the two-factor interpretation predicts: once the opposing heat return from the wall is removed, the residual-mass effect acts unopposed and the spread between high- and low-SoC cases grows.

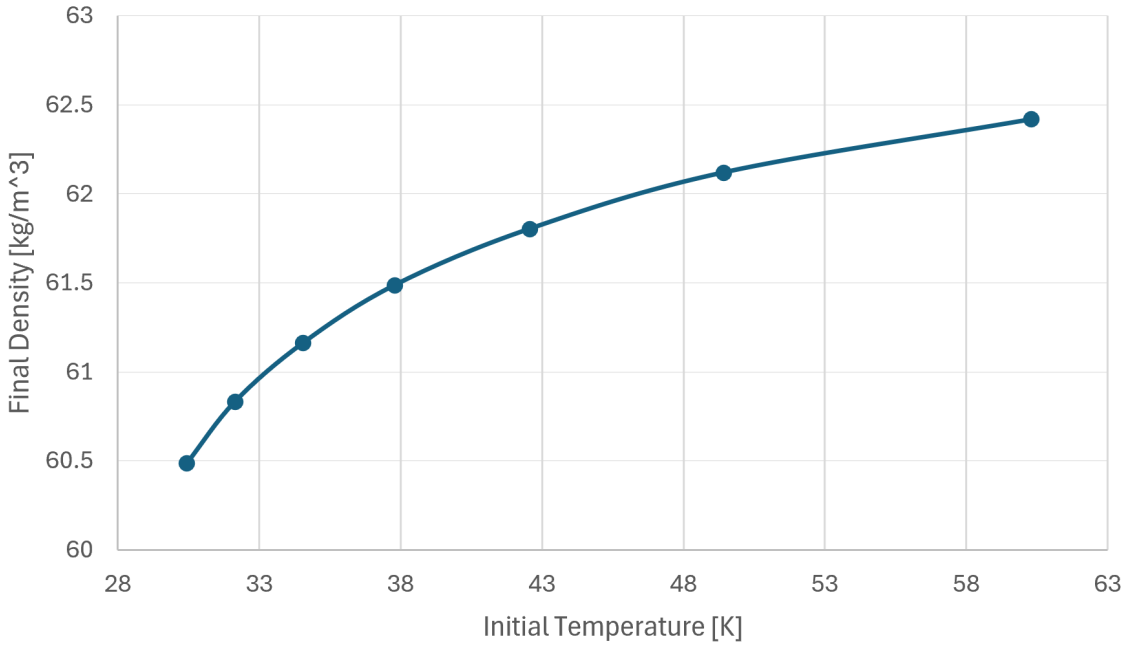

Figure 5.11: Final density for different initial tank conditions with an adiabatic tank wall

5.5 Nozzle

In order to identify the parameters that have a significant influence on the refuelling system, a sensitivity analysis was carried out on two nozzle parameters: the **heat leak** and the **forward discharge coefficient**.
For the heat leak, the value was varied from 10 W to 60 W to examine its effect on the system response. However, as shown in Figure 5.12, the model output was not noticeably affected by this change, indicating that the 1D model is not sensitive to the nozzle heat leak. This behavior is expected, given that 1D lumped-parameter models assume homogeneous mixing and do not resolve local thermal gradients. As a result, the heat transferred through the nozzle wall is distributed instantly across the entire fluid volume, making its effect negligible compared to the dominant energy terms in the system. This suggests that while heat leak may play a role in reality, the current modelling approach does not have sufficient thermal resolution to capture its influence accurately.

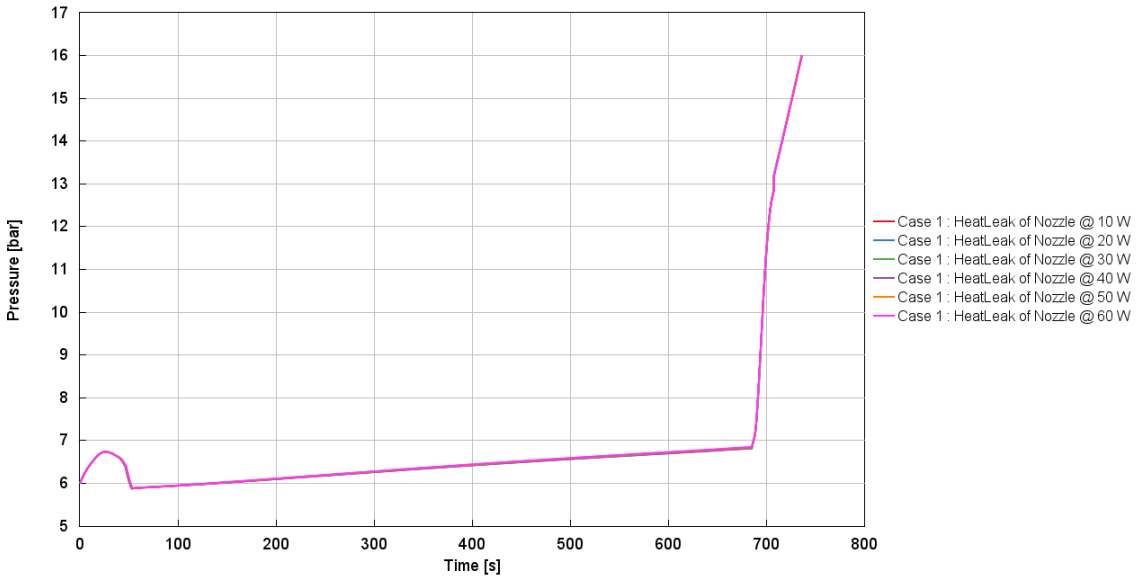

Figure 5.12: Effect of heat leak of the nozzle on the pressure inside the tank

As shown in Figure 5.13, the forward discharge coefficient (FWD) has a relatively small influence on the pressure evolution inside the tank during the refuelling process. In this sensitivity study, the baseline FWD value was progressively reduced by multiplying it by factors of 0.05, 0.10, 0.20, 0.30, 0.40, and 0.50, corresponding to reductions of 95%, 90%, 80%, 70%, 60%, and 50%, respectively.
As the results show, the pressure profiles for most cases overlap closely with the baseline, and a noticeable difference only appears when the FWD is reduced by

95%, that is, when the coefficient is brought to nearly zero. Even in this extreme case, the maximum observed difference in the final stored liquid hydrogen mass is approximately 2.23 kg compared to the baseline. Given that this deviation only occurs under a near-zero discharge coefficient, a condition that is physically unrealistic in practice, it can be concluded that the 1D refuelling model is not highly sensitive to the FWD. The parameter has a limited effect on the overall system performance within any realistic operating range.

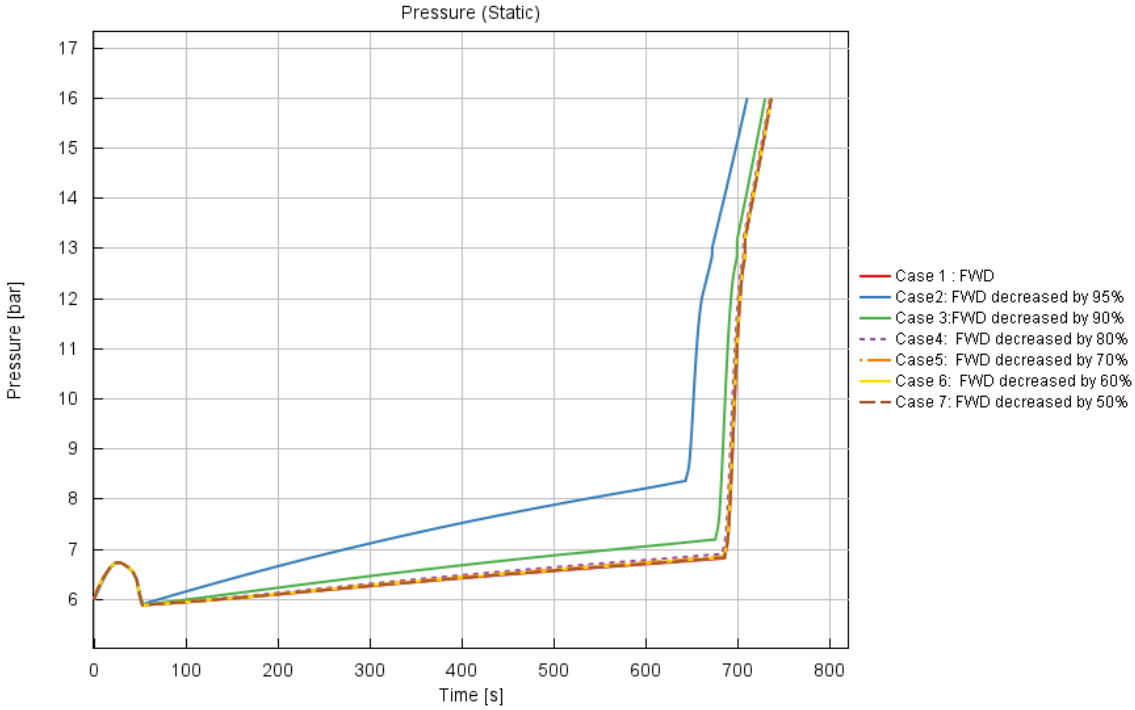

Figure 5.13: Effect of decreasing the FWD of the nozzle on the pressure inside the tank

As shown in Figure 5.14, the final amount of liquid hydrogen stored in the tank decreases as the FWD is reduced. Relative to the baseline case, the largest reduction in the final stored mass is approximately 2.23 kg; however, this deviation only appears once the FWD has been reduced by about 95%, that is, when the coefficient is brought close to zero. Since such a condition is not physically realistic, it can be concluded that the 1D refuelling model is only marginally sensitive to the FWD within any realistic operating range.

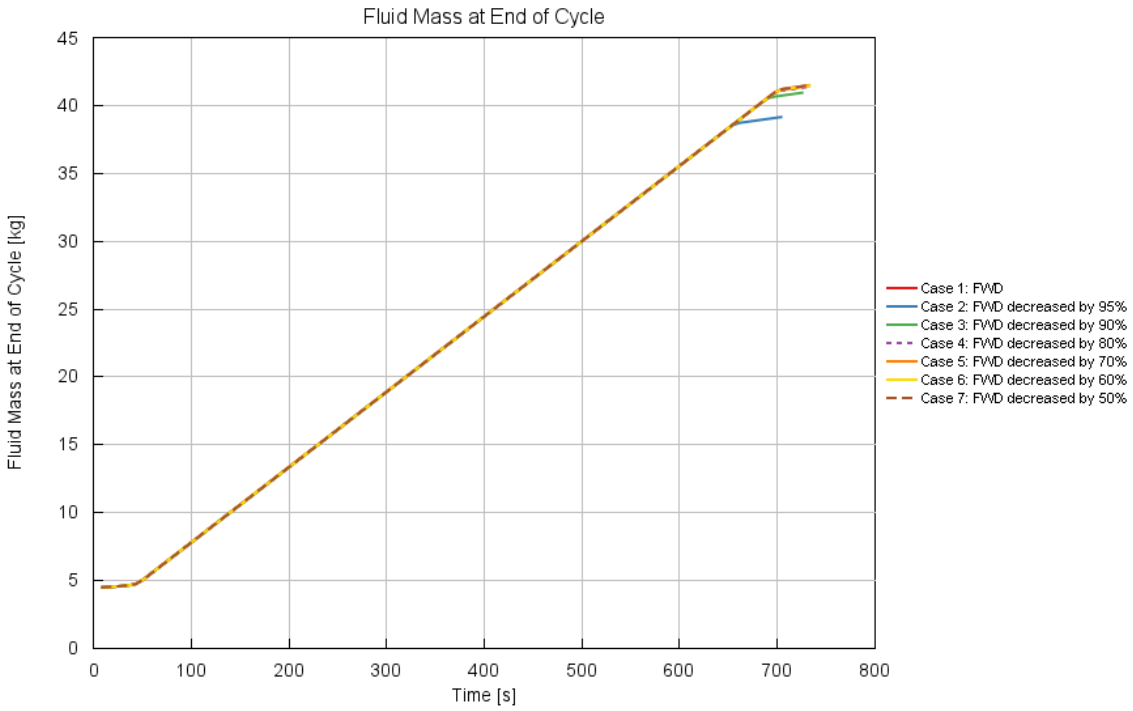

Figure 5.14: Effect of decreasing the FWD of the nozzle on the mass inside the tank

6

Conclusion

This thesis investigated the refuelling and defuelling of subcooled liquid hydrogen storage for heavy-duty trucks through one-dimensional system modelling in GT-SUITE, with the aim of identifying the initial tank conditions that maximise the usable hydrogen mass and the parameters that most influence the process. The refuelling system was first modelled and validated against a three-dimensional CFD reference; the defuelling process was then modelled to determine the thermodynamic state and State of Charge at the start of refuelling; and a sensitivity analysis was finally carried out on the nozzle to assess which parameters govern the system response.

The validation confirmed that a 1D approach reproduces the overall thermodynamic behaviour of the system reliably, while remaining subject to the well-known limitations of lumped-parameter models. In the refuelling validation the model did not capture the early flash-vaporization transient accurately, which is responsible for the largest local deviation from the reference (a maximum temperature error of 20.78% confined to that initial phase); this is an inherent consequence of the homogeneous-equilibrium assumption, which spreads the inlet energy uniformly across the tank and cannot resolve the local peaks, the thermal stratification, or the ullage compression that a 3D CFD simulation captures. What the 1D model does reproduce correctly, however, is precisely what is needed to validate it: the overall pressure and temperature trends and the final state of the process, with a mean temperature error of 5.13% and a relative error between 0.25% and 2.56% over the bulk of the filling. In the defuelling validation the agreement was excellent: the PID controller held the tank pressure at the 6 bar set point throughout the discharge, and its heat output remained bounded between the pure-liquid and pure-vapour reference limits, confirming that the modelled two-phase behaviour is physically consistent. The central engineering finding concerns the role of the initial conditions. Because the tank pressure is fixed by the fuel-cell demand, the initial tank temperature, and hence the residual State of Charge, becomes the dominant factor governing the final stored mass. Comparing a residual SoC of 4% with one of 10% towards the same final state showed that the lower SoC is preferable: per tank it yields about 3.55 kg more usable hydrogen in total, made up of roughly 1 kg more stored at the end of refuelling and about 2.65 kg more usable before the vehicle must return to the sta-

tion. Since the truck carries two tanks, these figures double at vehicle level, to about 7.1 kg of additional usable hydrogen per drive cycle. This advantage arises because the thermal influence of the residual hydrogen mass outweighs the heat returned by the warmer tank wall, the two contributions acting in opposite directions with a net energy difference of roughly 192 kJ in favour of the lower-SoC case, which carries less residual hydrogen to be cooled to the final state. The role of the tank wall was further isolated by repeating the refuelling with an adiabatic wall. Removing the wall from the energy balance eliminated its heat contribution to the fluid and widened the spread in final density between the two cases, confirming that the wall exerts a non-negligible effect of opposite sign to the residual-mass term, rather than a marginal one. This outcome is consistent with the two-factor interpretation put forward in Section 5.4, in which the final density results from the balance between the residual hydrogen mass and the heat returned by the tank wall, and it confirms that reasoning.

Although a difference in final density of this order may appear modest, it is not negligible from an operational standpoint. The density difference translates, through the fixed tank volume, into a difference in stored mass, and across the two tanks of the vehicle the total usable hydrogen gain of about 7.1 kg per drive cycle corresponds, at a representative heavy-duty consumption of about 7 kg per 100 km, to roughly 101 km of additional driving range available before refuelling. Over the planning of a truck mission this is a meaningful margin, and it accumulates over every drive cycle.

It should be stressed, however, that the optimum identified here corresponds to the lowest SoC actually simulated, around 4%, and not necessarily to the true maximum. Lower SoC values were not investigated, for the reasons discussed earlier in Section 5.3, so while the optimum is expected to lie close to this condition, its exact location cannot be stated with certainty. What can be stated is the underlying trend: as the initial temperature increases, the heat returned by the tank wall becomes progressively more dominant, and once this contribution overtakes the residual-mass effect the final density is expected to stop rising and eventually fall. The flattening of the final-density curve towards the higher initial temperatures is already consistent with the approach to such a turning point.

The sensitivity analysis on the nozzle must be read on two distinct levels. At the system scale that is the subject of this thesis, neither the nozzle heat leak nor the forward discharge coefficient has an appreciable effect on the refuelling response: varying the heat leak between 10 W and 60 W left the tank pressure essentially unchanged, and the forward discharge coefficient affected the final stored mass only when reduced by about 95%, an essentially closed-valve condition with no physical relevance. Within any realistic operating range, therefore, the refuelling outcome is insensitive to both parameters at system level. This conclusion, however, applies

only to the global picture. The analysis was not refined around the nozzle itself, and a system-level 1D model, with its homogeneous-mixing assumption and absence of local thermal resolution, cannot capture the local effects that the nozzle certainly produces in reality. Resolving those effects would require a dedicated, finer-scale analysis of the component, which lies outside the scope of the present system-level study.

Bibliography

[1] European Environment Agency (2024) Sustainability of Europe's mobility systems-Climate. Available at: https://www.eea.europa.eu/en/analysis/publications/sustainability-of-europes-mobility-systems-2025/climate.

[2] Syré, A. M. and Göhlich, D. (2023) Decarbonization of Long-Haul Heavy-Duty Truck Transport: Technologies, Life Cycle Emissions, and Costs.

[3] Linstrom, P. J. and Mallard, W. G. (eds.) NIST Chemistry WebBook, NIST Standard Reference Database Number 69, National Institute of Standards and Technology, Gaithersburg MD. Available at: https://webbook.nist.gov.

[4] Leitão, A. B. V., Bringhenti, C., Tomita, J. T., Silva, F. J. S., Xisto, C., Grönstedt, T. (2025) A review of hydrogen aircraft propulsion systems: recent advances and environmental perspectives. *International Journal of Hydrogen Energy*, 176, 151489.

[5] General Motors. (2025) Retro Rides: The 1966 GM Electrovan Fuel Cell Vehicle. *General Motors News*. Available online: `https://news.gm.com/home.detail.html/Pages/topic/us/en/2025/apr/0429-Retro-Rides-1966-GM-Electrovan-fuel-cell-vehicle.html`.

[6] Alstom (2022) Alstom's Coradia iLint Successfully Travels 1,175 km Without Refueling its Hydrogen Tanks. Available at: https://www.alstom.com/press-releases-news/2022/9/alstoms-coradia-ilint-successfully-travels-1175-km-without-refueling-its

[7] Stolten, D., Grube, T. and Lohmar, J. (2024) Subcooled Liquid Hydrogen Technology for Heavy-Duty Trucks, World Electric Vehicle Journal, 15(1), 22.

[8] Pizzutilo, E., Acher, T., Reuter, B., Will, C. and Schäfer, S. (2024) Communication: Subcooled Liquid Hydrogen Technology for Heavy-Duty Trucks.

[9] Kuroki, T., Nagasawa, K., Peters, M., Leighton, D., Kurtz, J., Sakoda, N., Monde, M. and Takata, Y. (2021) Thermodynamic modeling of hydrogen fueling process from high-pressure storage tank to vehicle tank. International Journal of Hydrogen Energy, 46(42), pp. 22004-22017.

[10] Wang, B., Huang, Y., Li, P., Sun, P., Chen, Z. and Wu, J. (2022) Numerical Simulation on the Thermal Dynamic Behavior of Liquid Hydrogen in a Storage Tank for Trailers, Case Studies in Thermal Engineering, 39, 102380.

[11] Abedi, H., Xisto, C., Jonsson, I., Grönstedt, T., and Rolt, A. (2022) Preliminary Analysis of Compression System Integrated Heat Management Concepts Using LH2-Based Parametric Gas Turbine Model. *Aerospace*, 9(4), 216.

[12] Adler, E. J. and Martins, J. R. R. A. (2024) Liquid Hydrogen Tank Boil-Off Model for Design and Optimization. Journal of Thermophysics and Heat Transfer, 38(4), pp. 1-15.

[13] Li, X., Wei, Q., Yu, L., Zhang, X., Zou, Y., Zhu, Y., Peng, Y., Wang, D., Zhu, Z., Chen, Z., Zhao, Y., Tu, C. and Bao, F. (2025) Numerical Study of Liquid Hydrogen Internal Flow in Liquid Hydrogen Storage Tank. Preprints.org, doi:10.20944/preprints202510.0049.v1.

[14] Melideo, D., Baraldi, D., De Miguel Echevarria, N. and Acosta Iborra, B. (2019) Effects of some key-parameters on the thermal stratification in hydrogen tanks during the filling process. International Journal of Hydrogen Energy, 44(26), pp. 13569-13582.

[15] Fesmire, J. E. (2006) Aerogel insulation systems for space launch applications, Cryogenics, 46(2–3), pp. 111–117. https://doi.org/10.1016/j.cryogenics.2005.11.018

[16] Hastings, L. J., Hedayat, A. and Brown, T. M. (2004) Analytical Modeling and Test Correlation of Variable Density Multilayer Insulation for Cryogenic Storage, NASA Technical Memorandum, NASA/TM-2004-213175, NASA Marshall Space Flight Center.

[17] Fesmire, J. E., Augustynowicz, S. D. and Scholtens, B. E. (2007) Robust Multilayer Insulation for Cryogenic Systems. NASA Kennedy Space Center / Sierra Lobo Inc., Technical Report.

[18] Choi, Y., Kim, J., Park, S., Park, H. and Chang, D. (2022) Design and analysis of liquid hydrogen fuel tank for heavy duty truck. International Journal of Hydrogen Energy, 47(32), pp. 14687-14702.

[19] Lemmon, E. W., Bell, I. H., Huber, M. L. and McLinden, M. O. (2018) NIST Standard Reference Database 23: Reference Fluid Thermodynamic and Transport Properties — REFPROP, Version 10.0, National Institute of Standards and Technology. Available at: https://doi.org/10.18434/T4JS3C

[20] Leachman, J. W., Jacobsen, R. T., Penoncello, S. G. and Lemmon, E. W. (2009) Fundamental Equations of State for Parahydrogen, Normal Hydrogen, and Orthohydrogen, *Journal of Physical and Chemical Reference Data*, 38(3), pp. 721–748. Available at: https://doi.org/10.1063/1.3160306

[21] Gamma Technologies (2023) GT-SUITE Overview. Available at: https://www.gtisoft.com/gt-suite-applications

[22] Molkov, V., et al. (2024) Liquid Hydrogen Refuelling at HRS: Description of SLH2 Concept, Modelling Approach and Results of Numerical Simulations. International Journal of Hydrogen Energy. Available at: https://www.sciencedirect.com/science/article/pii/S0360319924046044

[23] Stops, L., Siebe, D., Stary, A., Hamacher, J., Sidarava, V., Rehfeldt, S. and Klein, H. (2024) Generalized thermodynamic modeling of hydrogen storage tanks for truck application. Cryogenics, 139, p. 103826. Available at: https://doi.org/10.1016/j.cryogenics.2024.103826

[24] ISO/TC 197 (2025) Liquid Hydrogen — Land Vehicle Fuelling Protocol. ISO/FDIS 13984:2025(en), Final Draft International Standard, International Organization for Standardization (ISO).

[25] Gamma Technologies LLC (2019) Set-Up and Validation of an Integrated Engine Thermal Model in GT-SUITE for Heat Rejection Prediction. SAE Technical Paper 2019-24-0078. Available at: https://doi.org/10.4271/2019-24-0078

[26] Gamma Technologies LLC (2020) Thermal Management of Electrified Vehicle by Means of System Simulation. SAE Technical Paper 2020-28-0033. Available at: https://doi.org/10.4271/2020-28-0033

[27] Gamma Technologies LLC (2019) Modeling Fuel Tank Draining/Sloshing in a Typical Transiently Accelerating Vehicle using GT-SUITE for Reliable Tank Designing. SAE Technical Paper 2019-01-1262. Available at: https://doi.org/10.4271/2019-01-1262

[28] Lemmon, E.W., Bell, I.H., Huber, M.L. and McLinden, M.O. (2018) NIST Standard Reference Database 23: Reference Fluid Thermodynamic and Transport Properties (REFPROP), Version 10. National Institute of Standards and Technology. Available at: https://doi.org/10.18434/T4/1502528

[29] Hamacher, J., Stary, A., Stops, L., Siebe, D., Kapp, M., Rehfeldt, S. and Klein, H. (2023) Modeling the thermodynamic behavior of cryo-compressed hydrogen tanks for trucks. Cryogenics, 135, p. 103743. Available at: https://doi.org/10.1016/j.cryogenics.2023.103743

[30] Sdanghi, G., Maranzana, G., Celzard, A. and Fierro, V. (2019) Review of the current technologies and performances of hydrogen storage materials.

[31] Munson, B. R., Okiishi, T. H., Huebsch, W. W. and Rothmayer, A. P. (2013) Fluid Mechanics, 7th ed., Wiley.

[32] Pacific Northwest National Laboratory (2024) Vacuum-Jacketed Piping, H2Tools Hydrogen Best Practices. Available at: `https://h2tools.org/bestpractices/hydrogen-system-components/liquid-piping-systems/vacuum-jacketed-piping`

[33] MannTek AB (2024) Innovations in Coupling Solutions and Hydrogen Fueling. Available at: `https://www.manntek.se/innovations-in-coupling-solutions-and-hydrogen-fueling/`.

[34] MannTek AB (2024) MannTek plays a role in the building of the first sLH_2 refueling station. Available at: `https://www.manntek.se/first-slh2-refueling-station/`

[35] Gamma Technologies LLC (2025) Cryogenic Fluid and Thermal Systems. Available at: https://www.gtisoft.com/cryogenic-fluid-and-thermal-systems-2/

[36] Sakowski, B. A., Yamashita, K. G. and Baker, M. C. (2023) Liquid Hydrogen Tank Chill and No-Vent Fill Prediction Using Computational Fluid Dynamics, Cryogenic Engineering Conference and International Cryogenic Materials Conference (CEC/ICMC), Honolulu, Hawaii, July 9–13, 2023. NASA Glenn Research Center, NASA/TM-2023-009593.

[37] Simonovski, I., Baraldi, D., Melideo, D., Acosta-Iborra, B. (2015) Thermal simulations of a hydrogen storage tank during fast filling. International Journal of Hydrogen Energy, 40(35), pp. 11960–11969.

[38] Flynn, T.M. (2005) Cryogenic Engineering. 2nd ed., Marcel Dekker, New York.

[39] Karlsson, E. (2017) Catalytic Ortho- to Parahydrogen Conversion in Liquid Hydrogen. Master's Thesis, Lund University, Faculty of Engineering (LTH), Lund, Sweden. ISRN LUTFD2/TFMT–17/5056–SE.

Declaration of Generative AI and AI-assisted technologies in the writing process

During the preparation of this work, the authors used Claude (developed by Anthropic) to assist with text drafting and language refinement. After using this tool, the authors thoroughly reviewed and edited the content as needed and take full responsibility for the content of the publication.

Department of Mechanics and Maritime Sciences
CHALMERS UNIVERSITY OF TECHNOLOGY
Gothenburg, Sweden
www.chalmers.se

CHALMERS
UNIVERSITY OF TECHNOLOGY